APPENDICES & REFERENCES

Appendix A. *The* Fundamentals *of Lynx* Science Performance

A.1 Source Confusion Limit and Angular Resolution Requirements

In very crowded fields, telescopes suffer from source confusion caused by significant fluctuations in the background induced by a large number of unresolved and/or undetected sources. Confusion manifests itself as significant centroid shifts and as large fluctuations in the flux of detected sources on top of purely statistical noise. The effects become severe and uncontrollable at flux levels at which images contain 1/50 to 1/15 sources per beam[627]. For PSF $\gtrsim 1''$, source confusion is the main limiting factor preventing X-ray telescopes from reaching the flux levels needed to detect $z = 10$ black hole seeds (§1.1.3) or resolve cores of young star forming regions in the Milky Way (§3.1).

The main parameter controlling the source confusion is the number of sources per one PSF beam near the detection threshold. The effective solid angle of the beam is defined as $\Omega_b = \int \mathrm{PSF}\, d\Omega$, where the PSF is normalized to 1 at its peak (Condon [628]). The *Lynx* PSF here is assumed to be Gaussian. This is appropriate, e.g., in cases when angular resolution is limited by small misalignments of a large number of mirrors. This is indeed expected to be one of the main contributors to the *Lynx* PSF. For a Gaussian PSF, the beam solid angle is $\Omega_b \approx 1.13 \times \mathrm{FWHM}^2 \approx 1.18 \times \mathrm{HPD}^2$, where HPD is the 50% power diameter of the PSF. Effects of confusion become strong at levels below

$$b = q^2/(3-\gamma) \text{ beams per source,} \qquad \text{(A.1)}$$

where γ is the differential slope of the $\log N - \log S$ distribution and $q \approx 5$ is the "quality factor" [628].

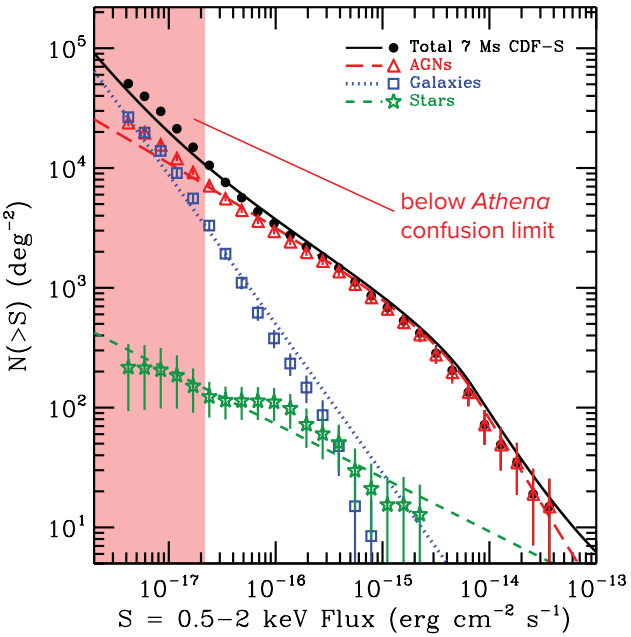

Fig. A.1— *Chandra* $\log N - \log S$ distribution observed in the 7 Msec deep survey (reproduced from [95]). Extrapolation of this function to low fluxes is used to compute *Lynx* confusion limits. Shaded region shows fluxes below the anticipated *Athena* confusion limit (5″ PSF, HPD).

We now need to estimate γ near the flux limits appropriate for *Lynx*. The $\log N - \log S$ distribution observed in the deepest *Chandra* surveys shows an upturn very near the flux limit achieved in its 4 Msec surveys (Lehmer et al. [629]). This upturn is now very clearly observed in the 7 Msec pointings ([95], reproduced in Fig. A.1), and is associated with the integrated flux of X-ray binaries in $z \lesssim 3$ galaxies. This dominant source component is modeled in Lehmer et al. Their model is reliable and well-constrained because it describes sources originating in relatively low-redshift galaxies via a well-known process (XRB activity

associated with star formation) and can be calibrated using a well-established distribution of star formation rates in the not-so-distant Universe. Therefore, extrapolations of the Lehmer et al. model to low fluxes can be used to compute the effect of source confusion.

The results are shown in Fig. A.2. A steep slope of the $\log N - \log S$ function below $f_x = 10^{-17}$ erg s^{-1} cm^{-2} corresponds to a quickly increasing confusion flux limit as the PSF degrades. For sub-arcsecond PSFs, confusion limits are below the sensitivity target in the *Lynx* deep surveys. However, already for a 2″ PSF, the confusion limit is an order of magnitude higher than the target. Such levels of angular resolutions are unacceptable. The confusion limit for *Athena* (5″ PSF) is above the sensitivity levels achieved in the 4 Msec *Chandra* survey, and is a factor of ~ 200 above the *Lynx* sensitivity targets.

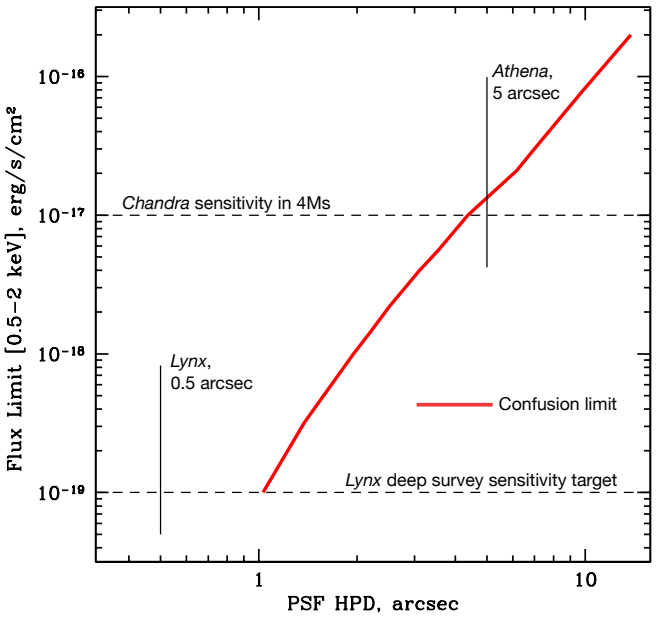

Fig. A.2— Confusion limit in the 0.5–2 keV band as a function of angular resolution for a Gaussian PSF.

A.2 XRBs in High-*z* Galaxies

The main science goal for deep surveys with *Lynx* is detection of black hole seeds in $z \approx 10$ galaxies (§1.1), which have relatively low mass and L_X. Therefore, a possible contamination of X-rays flux from massive black holes by the integrated emission of X-ray binaries in the host galaxy should be considered.

Highest-z galaxies detected by *Hubble* are compact, < 1 kpc half-light radius [630], which corresponds to < 0.5″ angular diameter at $z = 10$. Such galaxies will be barely resolved with *Lynx* if at all. The X-ray spectrum of XRBs is expected to be softer than that of the BH seeds (see below), which will serve as an additional discriminator. However, the safest approach is to limit the analysis to X-ray fluxes sufficiently above the floor set by the XRB emission.

A key point to note here is that we expect a strong correlation between near-IR (NIR) magnitude of high-z galaxies and the integrated flux of their XRBs. The total flux of high-mass X-ray binaries (which will dominate the total XRB emission [391]) reflects the on-going star formation in the host galaxy. The observed NIR magnitude also reflects star formation, because at $z = 10$, the observer-frame NIR corresponds to the UV emission in the source rest frame (e.g., $\lambda = 1.65$ μm corresponds to 1,500 Å at $z = 10$).

At low redshifts, a strong correlation between the star formation rate and the XRB flux is indeed observed [631, 632], $L_X \propto$ SFR. This correlation is well understood, and can be successfully derived from the population synthesis models (e.g., [391]). The specific X-ray output, L_X/SFR, depends on the high-mass end of the stellar IMF and on the metallicity of the stellar population. At low

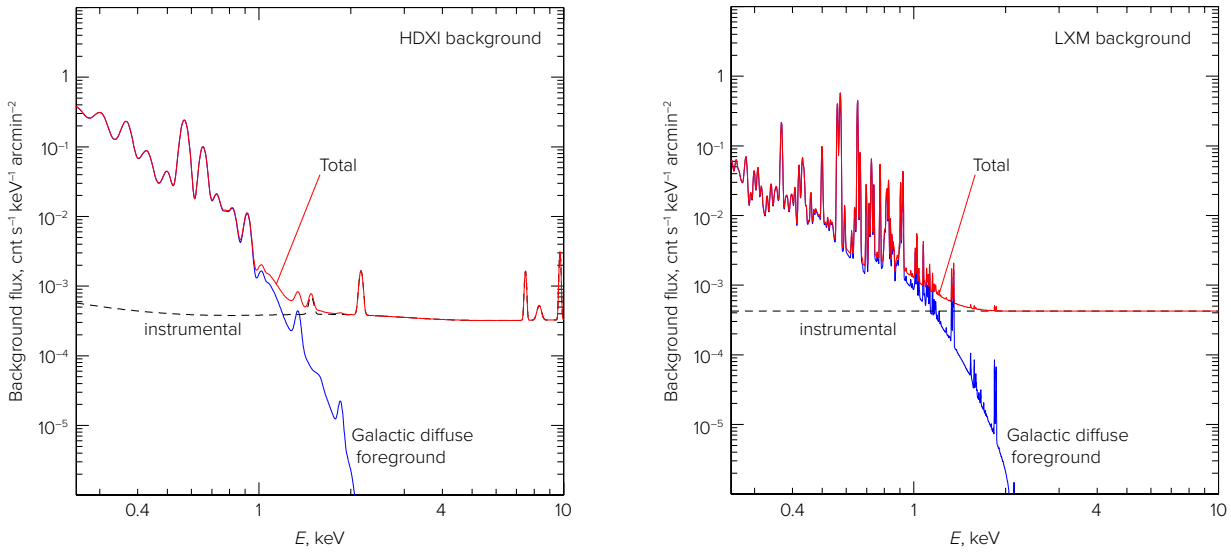

Fig. A.3— Predicted spectra of diffuse backgrounds for the *Lynx* HDXI and LXM instruments. Backgrounds are normalized to a solid angle of 1 arcminute^2 on the sky (for the 10-m focal length, 1 arcmin^2 = 0.0846 cm^2). Below ~ 1.5 keV, the background is dominated by the diffuse Galactic foreground (a model from Hickox & Markevitch [640] is used here). This signal is astrophysical in origin, and varies proportionally to the telescope effective area. The instrumental background is dominated by secondary X-rays produced by charged particles. For HDXI, it is assumed to be identical to the *Chandra* ACIS-I background. For LXM, predictions for the *Athena* XIFU instrument are adopted.

redshifts, this has indeed been seen [631–637], L_X [2–10 keV]/SFR = 4×10^{39} erg s^{-1} $M_\odot^{-1}$ yr, which is in a good agreement with predictions of the population synthesis models of Fragos et al. [391]. This model generically predicts that the L_X/SFR ratio increases almost ten-fold for low-metallicity stellar populations expected in high-z galaxies. Therefore, the adopted value of the X-ray luminosity of XRBs in high-z galaxies is 4×10^{40} erg s^{-1} for each $M_\odot$ yr^{-1} of star formation. Using Kennicutt's relation between UV luminosity and star formation rate [638], corrected for lower metallicities following Madau & Dickinson [136], we have:

$$f_{\rm XRB,\,0.5–2\,keV} = 1.0 \times 10^{-19}\,{\rm erg\ s^{-1}\ cm^{-2}}\ 10^{0.4\,(30-{\rm m})},$$

where m is the apparent galaxy magnitude in the band that corresponds to the rest-frame wavelength 1,500 Å. The coefficient here is computed for an X-ray spectrum with cutoff at $E \approx 6$ keV, as observed at low redshifts [394, 639]. Note that, in this case, one expects virtually no source photons detected above ~ 1 keV. This is in strong contrast with the power-law spectra expected for the black hole seeds. Therefore, the presence of the spectral cutoff can be established even for relatively faint sources and used as a discriminator between the XRBs and black hole seed emission.

To conclude, there is a natural X-ray flux "floor" set by the XRB emission, and the level of this floor depends on the depth of the counterpart OIR survey. For the m ≈ 30 surveys expected from *JWST* and *WFIRST*, the XRB floor is around $f_x = 10^{-19}$ erg s^{-1} cm^{-2}, which represents a natural target for the deep surveys with *Lynx* aimed at detection of black hole seeds in the early Universe. This X-ray flux level corresponds to the XRB emission from galaxies with a 5 $M_\odot$ yr^{-1} star formation rate at $z = 10$. For objects with *a priori* known locations, *Lynx* can reach down to $f_x \approx 5 \times 10^{-20}$ erg s^{-1} cm^{-2} in a ~ 4 Msec survey (Fig. A.5 below), which corresponds to SFR ~ 2 $M_\odot$ yr^{-1}.

A.3 Faint Point Source Detection and Sensitivity Projections

Reaching $f_x \sim 10^{-19}$ erg s^{-1} cm^{-2} flux limits (two orders of magnitude below the sensitivity of deepest *Chandra* observations) is obviously a challenge. As discussed above, source confusion will not be a limiting factor for *Lynx* at these flux levels. Instead, the main limiting factor for *Lynx* is the diffuse background, which is both astrophysical and instrumental in origin. The expected background is discussed below, followed by a summary of the faint source detection approach projected for *Lynx*, as well as results of Monte-Carlo simulations of detection thresholds as a function of exposure time.

A.3.1 Expected *Lynx* background

In its deepest exposures, *Lynx* will resolve close to 100% of the cosmic X-ray background originating from discrete X-ray sources. Therefore, only truly diffuse background components need to be considered. The first component is the instrumental background, dominated by the secondary X-rays generated by charged particles interacting with the detector itself and detector housing. For the LXM instrument, this component can be substantially reduced by employing an anti-coincidence shield, as designed for the *Athena* XIFU instrument. The instrumental background predictions developed for the *Athena* XIFU [641] were adapted for the LXM instrument. For the HDXI, the particle-induced background per unit area was assumed to be identical to that of the *Chandra* ACIS-I detector.

Below ~ 1.5 keV, the background will be dominated by emission of the Milky Way halo. Its spectrum and intensity has been measured with *ROSAT* [642], *XMM-Newton* [643], and with *Chandra* by Hickox & Markevitch [640]. All of these results are consistent, but for *ROSAT* and *XMM-Newton* it is a challenge to separate the truly diffuse Galactic foreground from the residual cosmic X-ray background generated by discrete sources that will be detected and masked out in *Lynx* images. Therefore, the Hickox & Markevitch measurements derived from the deepest *Chandra* pointings are used. The results are shown in Fig. A.3. The soft Galactic component follows the same model for the HDXI and LXM instruments, the only differences being the energy resolution of these detectors and a different throughput at the very soft energies.

The shape of the expected *Lynx* background spectrum is very different from that of the typical sources dominated by the power-law continuum. Therefore, source detection can be significantly optimized by choosing the appropriate energy band. For traditional source detection methods operating on single-band images, the most optimal band for *Lynx* is $\approx 0.7 - 2$ keV. This spectral difference can be exploited to further lower the source detection threshold. A next-generation detection procedure is described below. It maximizes information utilized for detection of faint sources and optimally combines data from different energies so that there is no need to restrict detection to, e.g., the 0.7–2 keV band.

A.3.2 Next-generation source detection methods

Images obtained with focusing X-ray telescopes have low background levels, enabling extremely faint detection limits. Sources with only ten, five, or even fewer photos collected over weeks of observing time can be confidently detected. Currently, the standard approaches for X-ray source detection are based on a convolution of single-band images with a filter approximating the telescope PSF [644, 645]. This method is close to, but is not, theoretically optimal for detecting faint sources in images

dominated by Poisson noise. *Lynx* will push limits in sensitivity, and therefore more sophisticated and optimized analysis techniques are required. The derivation of an improved detection filter based on the likelihood function is described below. It can be easily generalized for combining the data from multiple energy bands. This method is close to being theoretically optimal. Compared with traditional approaches, it leads to approximately a factor of two savings in exposure time needed to reach the given sample purity at a given flux threshold in the *Lynx* deep images.

Single-band optimal filter — Source detection can be thought of as a statistical test of whether a source with a positive flux exists at a given location. The goal is to minimize the probability of missing real sources, e.g., because of unnecessary high detection thresholds, while also minimizing a number of "false positives" — statistical fluctuations mistaken as sources with positive flux. The Neyman-Pearson lemma [646] suggests that the likelihood ratio provides the most statistically powerful test in this case.

For faint sources on top of high background and uniform, white noise, a convolution of the image with the PSF is equivalent to performing the likelihood ratio test (c.f. [647]). This is the regime found in optical and NIR images, and the convolution with the PSF has been widely used as a detection filter throughout astronomy. However, X-ray images are in a different regime of statistical noise, and therefore the optimal filter is different, as shown below.

For a Poisson-dominated image noise, the likelihood function can be written as

$$-\ln L = \sum_i \ln\, m_i - \iint m, \tag{A.2}$$

where the sum is over the location of detected photons, and m_i is the image model evaluated at each point i. In the case of a single, isolated point source on top of a uniform background, the model can be written as $m = f \times P + b$, where P is the PSF image ($\iint P = 1$), f is the total source flux, and b is the background brightness. Substituting this into eq. (A.2), we have

$$-\ln L = \sum_i \ln\left(f\, P_i + b\right) \;-\; B \;-\; f,$$

where $B = \iint b$. The likelihood ratio test is equivalent to analyzing the difference in the log-likelihoods computed for models with and without the source,

$$\Delta \ln L = \sum_i \ln\left(f\, P_i + b\right) - \sum_i \ln b - f = \sum_i \ln\left(f\, P_i/b + 1\right) \;-\; f. \tag{A.3}$$

The first term in this equation is a convolution kernel that can be thought of as the optimal detection filter,

$$\Phi = \ln\left(\frac{f}{b}\, P + 1\right). \tag{A.4}$$

Filter Φ is the optimal filter for searching for sources with flux f on top of a uniform background b. In the limit of very faint sources, where $f \to 0$, it reduces to the expected shape of the PSF itself, $\Phi \approx P$.

That the filter shape depends on the flux of the target sources is a complication of little significance. One should simply develop the filter for sources near the target detection threshold and then use it

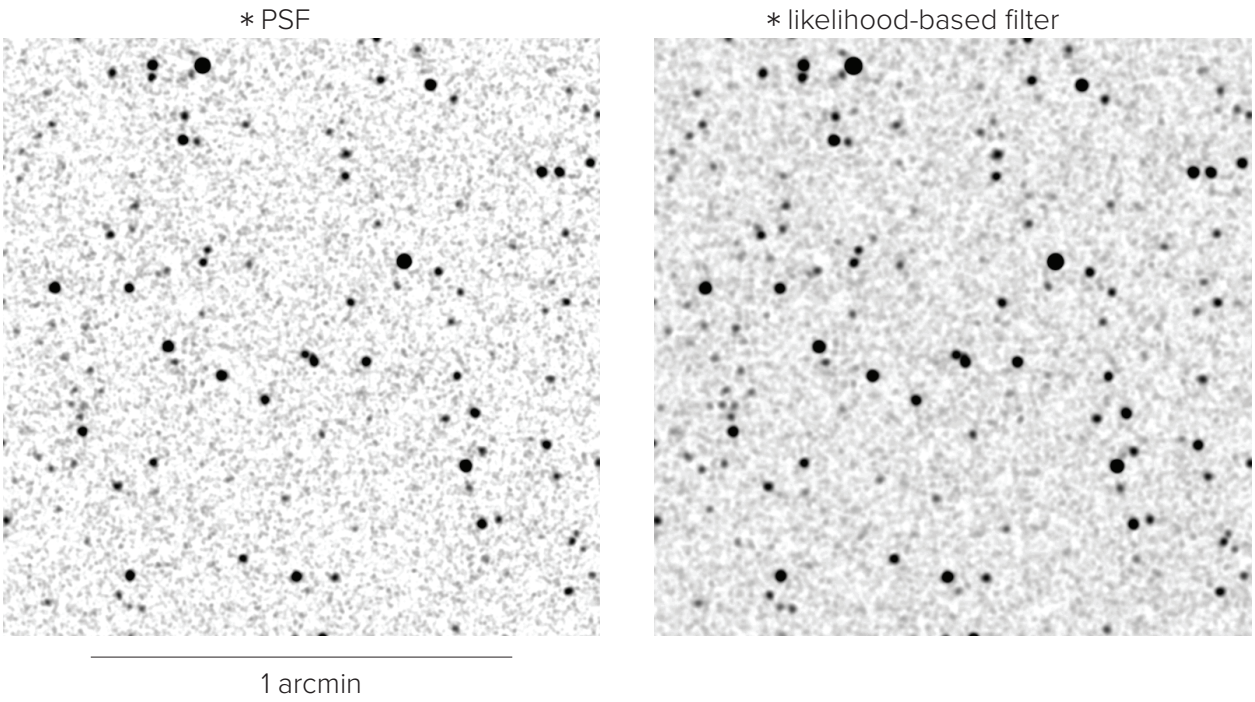

Fig. A.4— Examples of source detection in a 4 Msec *Lynx* HDXI exposure using a traditional detection filter based on convolution with the PSF *(left)*, and the optimal likelihood-based filter given by eq. (A.5). Traditional detection is performed in the optimal single energy band (0.7–2 keV), while the likelihood-based detection uses a broader band, 0.3 – 3 keV. Images are normalized to the same source brightness. The likelihood filter results in a much suppressed level of noise, leading to lower false detection probabilities and the possibility of reaching fainter flux levels for the same exposure time.

for all sources. The filter will be suboptimal for sources far above the threshold, but such sources will be confidently detected in any case.

One possible procedure for setting the target detection thresholds is based on the required sample purity or false detection probability. The thresholds themselves can be established via Monte-Carlo simulations. For real sources with flux f, the convolution with filter Φ produces a peak with an average amplitude

$$C_{\rm peak} = f \iint P \ln\left(f\,P/b + 1\right).$$

$C_{\rm peak}$ can be precomputed for given b and f. The analysis of simulated Poisson images with uniform background b and convolved with filter Φ provides the probability that the level $C_{\rm peak}$ in the convolved image is exceeded by purely statistical fluctuations. The factor f is then increased until that probability is below a pre-defined level. The resulting f serves as the threshold and defines the optimal detection filter.

Extension to multiple energy bands — Since the detection filter in eq. (A.4) is proportional to the log of the likelihood function, it enables an extremely straightforward combination of the data in multiple energy bands in a statistically optimal way: simply adding the convolutions in individual (narrow) energy bands is equivalent to the logarithm of the combined likelihood function,

$$\Delta \ln L = \sum_{i,j} \ln\left(f\,\frac{P_{i,j}\,s_j}{b_j} + 1\right) \tag{A.5}$$

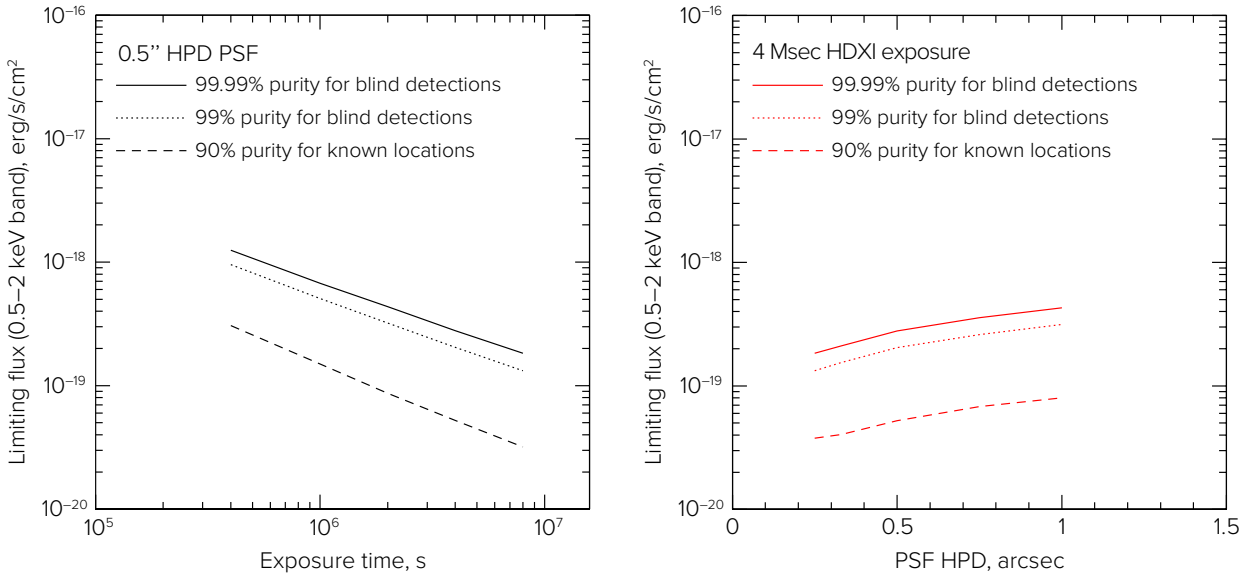

Fig. A.5— *Lynx* limiting sensitivity as a function of exposure time *(left)* and PSF size *(right)*. Detection thresholds are computed for different levels of required sample purity, and different detection modes (blind detections and search around known locations such as high-z JWST galaxies). The limiting fluxes are quoted in the observed 0.5–2 keV energy band, even though the optimal detection is performed over a somewhat wider 0.3–3 keV energy band (see text). A flux limit of 6×10^{-20} erg s^{-1} cm^{-2} achievable for known locations in a 4 Msec exposure for the on-axis 0.5″ PSF corresponds to 5 photons detected in the 0.3–3 keV band.

where the sum is over the detected photon positions i as before and the detected photon energies j, $s(E)$ is the source spectrum, b_j is the background brightness at energy j, $P_{i,j}$ is the PSF evaluated at location i and energy j, and f is the total source flux. Further simplifications to computing the convolution given by eq. (A.5) are possible if, e.g., the PSF is energy independent, but such cases are beyond the scope of this analysis.

The threshold for optimal detection in a wide energy band will depend on the source spectrum. This is a strength of this new technique, since it opens the possibility of searching for specific classes of sources (power-law, strongly absorbed, etc.) in a statistically optimal way.

An example of the likelihood-based optimal detection performance is shown in Fig. A.4. The method leads to a factor of ≈ 10 improvement of sample purity for a given source flux, or nearly a factor of 2 reduction in exposure time needed to achieve the required sample purity for a given source flux. Approximately half of these gains comes from using a more optimal shape for detection filter (eq. (A.4)), the rest coming from a statistically optimal combination of the data from a wider energy band.

A.3.3 Sensitivity projections

Limiting sensitivities computed for the detection of power-law sources with $\Gamma = 2$ in *Lynx* HDXI images with exposures ranging from 400 ksec to 8 Msec are shown in Fig. A.5. The variation of detection thresholds with the PSF size is shown in the right panel of the same Figure. These results show that flux limits ≈ 10^{-19} erg s^{-1} are achievable in the deep *Lynx* exposure for sample purities corresponding to detection around *a priori* known source locations (e.g., high-z *JWST* galaxies). Exceptionally high sample purities (> 99.99% for blind detections) will be achieved for somewhat

higher flux levels, $f_x = (2-3) \times 10^{-19}$ erg s^{-1} cm^{-2}. For reference, a flux level of 10^{-19} erg s^{-1} cm^{-2} in the 0.5–2 keV band corresponds to 8 photons detected in the 0.3–3 keV detection band in a 4 Msec exposure.

As shown in Fig. A.5, flux limits scale with exposure more slowly than $t_{\rm exp}^{-1}$, and they also improve somewhat for smaller PSF sizes. This indicates that the diffuse background is affecting source detection. The background is dominated by the astrophysical component (Fig. A.3) whose intensity scales as the telescope effective area. As a consequence, the exposure times needed to achieve a given flux threshold are approximately inversely proportional to the effective area.

A.4 Considerations for X-ray Gratings

Grating spectrometers are essential instruments for future X-ray missions, and existing technologies provide 50 – 1,500-fold higher throughput compared to current orbiting instruments. The characteristic temperature of galaxies, galaxy clusters, stars, neutron stars, black hole accretion disks, and exploding objects occurs at T > 0.5×10^6 K. At temperatures of 0.5–100×10^6 K, diagnostic emission and absorption lines are from metals (i.e., O, C, Fe, Mg, Si, Ne), and most have energies in the X-ray band. Of these lines, the strong oxygen lines at 10^6 K (O VII Heα and O VIII Lyα, at 21.6Å and 18.9Å) are particularly important because of the oxygen abundance relative to other metals and the variety of environments where they are detected. To measure line profiles and detect faint lines, the resolution must be close to the thermal width, which for the oxygen lines is $54 \times (T_6)^{1/2}$ km s^{-1}, where T_6 is the temperature in units of 10^6 K. This suggests a spectral resolution target of R = 5,000 – 10,000, matching the thermal widths of the oxygen lines for $T = 10^{5.5} - 10^6$ K. A resolving power of 5,000 is therefore used as a requirement for the XGS instrument. At this level, spectral resolution plays an insignificant role on the detectability of faint absorption lines from the CGM and Cosmic Web, because an internal kinematic structure with Δv of at least a few tens of km s^{-1} is expected in these settings (Fig. A.7). Overall, for the nominal XGS design with A = 4,000 cm^2 and R = 5,000, absorption lines with equivalent widths of 0.5–1 mÅ will be detectable, and that the kinematic structure can be measured starting from EW ≈ 2 mÅ.

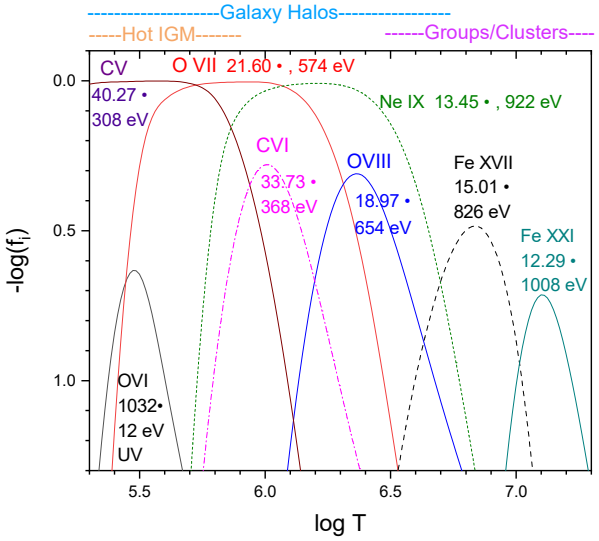

Fig. A.6— Ionization states for strong absorption lines in the CGM around galaxies and groups. Many of the important ions and strong resonance lines are in the soft X-ray band (12.29–40.27 Å⟺ 0.31–1.01 keV), and most are already detected in the MW hot halo. Other ions not shown here, but detectable, are N VI, N VII, S XI, S XII, Si X, Si XI, Fe XIX, and Fe XXII. Approximate temperature ranges of the primary hosts for intergalactic absorption are indicated on top.

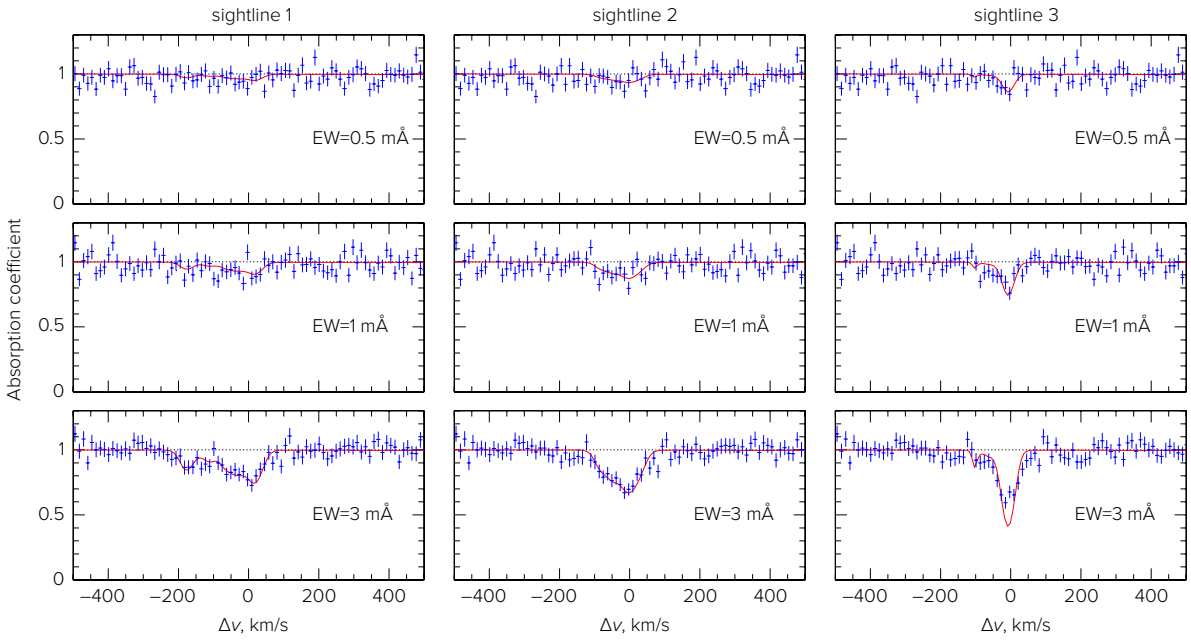

Fig. A.7— Simulated XGS absorption spectra of O VII in the CGM, observed in a 300 ksec *Lynx* pointing at a background AGN with $f_x = 10^{-11}$ erg s^{-1} cm^{-2}. The line profiles were obtained from different sightlines through the EAGLE simulations (see discussion in §A.5 below). The absorption lines were rescaled to integrated equivalent widths of 0.5, 1, and 3 mÅ. Red lines show the intrinsic line profiles. Simulated spectra (blue data points) contain effects of spectral resolution (R = 5,000) and Poisson noise. Only sightline 3 contains a sufficiently narrow line for which the instrumental spectral resolution becomes apparent.

A.5 Sensitivity projections for CGM and Cosmic Web

The assessment of the feasibility of observing the CGM is based on analyzing mock observations generated from several modern numerical simulations of galaxy formation, including EAGLE, FIRE, MUFASA, Illustris-TNG, and Agertz & Kravtsov zoom-in simulations. These simulations generally reproduce the observed stellar populations but use different numerical models, subgrid physics, and prescriptions for feedback. These outputs provide a representative range of predictions of what *Lynx* can see in the galactic halos (Fig. A.8).

All of these simulations lead to a consistent picture. Galaxy halos are the brightest in the soft X-ray band, $E < 0.7$ keV, because of their low temperatures. However, the emission is dominated by a small number of bright spectral lines (notably, O VII and O VIII transitions). The contrast of the CGM continuum emission relative to the unavoidable foreground from the Milky Way halo is low, making CGM density measurements in the soft band impossible, except for the very inner radii. At higher energies, $E > 0.7$ keV, the CGM spectrum has a stronger continuum component, and the foreground Milky Way halo emission is much weaker. Therefore, the gas density can be derived using the CGM emission in this energy band. Simultaneous solid detections of the CGM flux in three spectral bands, 0.4–0.7, 0.7–1.05, and 1.05–1.5 keV, are sufficient for ≈ 10% determination of gas density, and ~20% determination of temperature and metallicity. Detections in only two bands constrain a degenerate combination of density, metallicity, and temperature. Detection only in the soft band provides a measure of the O line flux, which is very difficult or even impossible to convert to thermodynamic quantities. Therefore, X-ray observations aiming at a detailed characterization

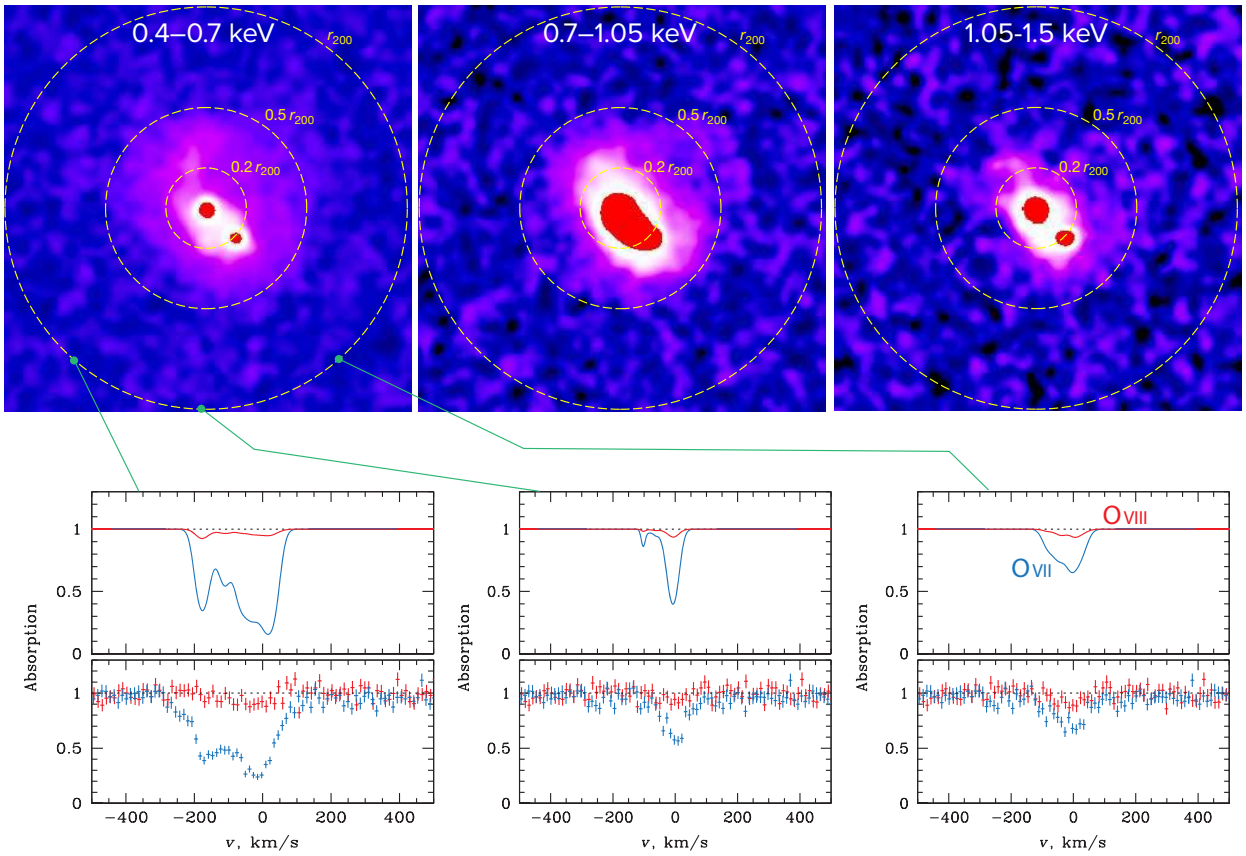

Fig. A.8— Mock *Lynx* observations of a $M_{\rm tot} = 3\times10^{12}\,M_\odot$ galaxy at $z = 0.03$ generated using an output from the EAGLE simulation. The top panels show 500 ksec HDXI images in three energy bands (the virial radius, r_{200}, corresponds to 9′), including the realistic noise from astrophysical and instrumental backgrounds, detection and removal of background point sources, etc. The CGM can be mapped out to $\sim 0.5\,r_{200}$ in all three bands. The bottom panels show simulated O VII and O VIII absorption spectra (300 ksec XGS observations, $f_{\rm AGN} = 10^{-11}$ erg s^{-1} cm^{-2}) at three arbitrary lines of sight located near the virial radius. Solid lines show the ideal absorption spectra derived from simulation output, including thermal broadening and random velocities, whose data points indicate what *Lynx* will observe with XGS at spectral resolution $R = 5{,}000$. Note the strong variations of absorption spectra for different lines of sight, emphasizing the complex kinematic and multiphase structure of the CGM. *Lynx* will provide very high signal-to-noise measurements of the O VII line, and solid detections of O VIII. A joint analysis of the O VII and O VIII lines will constrain the distribution of random velocities and temperatures in each of the lines of sight.

of the CGM must have the sensitivity for solid detections in all three of the 0.4–0.7, 0.7–1.05, and 1.05–1.5 keV bands. This requirement can be satisfied with *Lynx* to at least half the virial radius in galaxies with mass as low as $\approx 3\times10^{12}\,M_\odot$ (see below).

An alternative approach for measuring CGM temperatures is possible using the LXM, whose spectral resolution is sufficient to separate the O VIII and O VII emission lines in the CGM from those in the MW halo for $z > 0$ galaxies. This increases the CGM contrast in the soft band by a factor of ~10, and the O VIII and O VII lines will be detectable to $\approx 0.5\,r_{200}$ for galaxies with $M_{\rm tot} \approx 3\times10^{12}\,M_\odot$ or higher. Flux ratio in the O VII and O VIII lines is a sensitive temperature indicator, such that a simple detection of both lines constrains the gas temperature to better than 10%. However, solid measurements of the CGM continuum emission in the soft band are still impossible, even with the microcalorimeter spectral resolution. To constrain gas density and metallicity, one needs to detect the CGM emission at $E > 0.7$ keV.

All simulations in our suite show the expected X-ray emission from the CGM of the Milky Way-type galaxies at large radii to be very faint, certainly well below the *Chandra* and *XMM-Newton* limits. Its detection is challenging even for next-generation X-ray missions. The limiting factor is the low expected contrast of the CGM emission relative to the astrophysical and instrumental diffuse backgrounds, which leads to an unavoidable level of systematics. Based on the *Chandra* experience, the systematic uncertainties will be approximately 1% of the foreground/background in the corresponding energy band. In addition, imaging of the CGM at $E \gtrsim 0.7$ keV is severely affected, unless most of the cosmic X-ray background is resolved into discrete sources, for which arcsecond resolution is required (e.g., Figs. A.1 and A.2). Mock simulations of long exposures show that the residual background fluctuations from sources below the *Athena* confusion limit are at least a factor of 10 above the Poisson noise-dominated residual fluctuations for *Lynx*. Moreover, *Athena* mirrors will not be protected from stray light, which will introduce additional large-scale non-uniformities in the background. These two factors will introduce severe fundamental limitations on *Athena*'s ability to map diffuse gas in galactic halos and Cosmic Web filaments. In contrast, *Lynx* will be limited almost exclusively by statistical noise. Mapping the CGM can be accomplished with *Lynx* to at least half the virial radius in galaxies with mass as low as $\approx 3 \times 10^{12}\, M_\odot$. A sample of what *Lynx* can observe in galactic halos is shown in Fig. A.8.

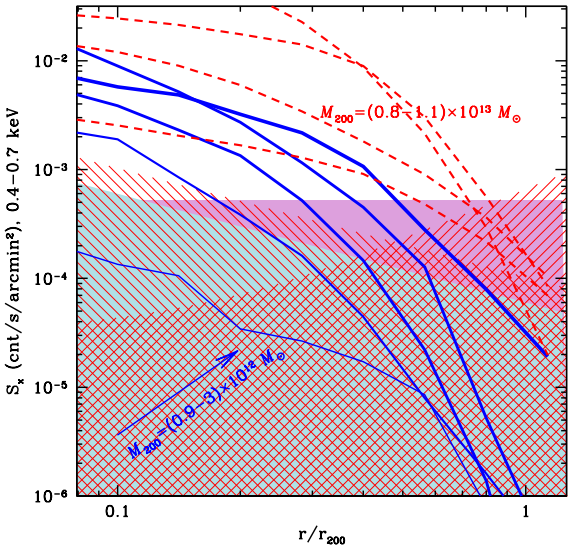

Fig. A.9— Surface brightness profiles of representative simulated galaxies in the 0.4–0.7 keV band, together with the estimated levels of statistical and systematic uncertainties. Solid blue corresponds to a 5 σ level of statistical fluctuations of the *Lynx* background. Solid purple corresponds to 3% of the background, indicative of the level of unavoidable systematics. Red hashed regions indicate uncertainties for *Athena*: residual surface brightness fluctuations (decreasing with radius) and stray light (increasing with radius).

Summary of mock observation analysis for CGM in emission — Figures A.9–A.11 show results from the mock data analysis of the CGM observations with *Lynx* and *Athena*, illustrating the following key findings:

- In the soft band, 0.4–0.7 keV, the sensitivity of *Lynx* and *Athena* is similar. For both observatories, the main limiting factor is low contrast of the observed signal relative to the unavoidable background dominated by the diffuse Milky Way emission.
- At $E > 0.7$, *Athena* is significantly less sensitive than *Lynx* because of the higher level of background fluctuations due to undetected or confused background sources. This sensitivity difference reaches an order of magnitude in the 1–1.5 keV band. *Athena* stray light is another important limiting factor for these studies.
- At 500 ksec, *Lynx* statistical uncertainties are similar to the level of unavoidable systematics. Therefore, the nominal soft-band effective area of 2 m^2 of the *Lynx* Design Reference Mission (§6) is a good configuration choice from the point of view of CGM studies.

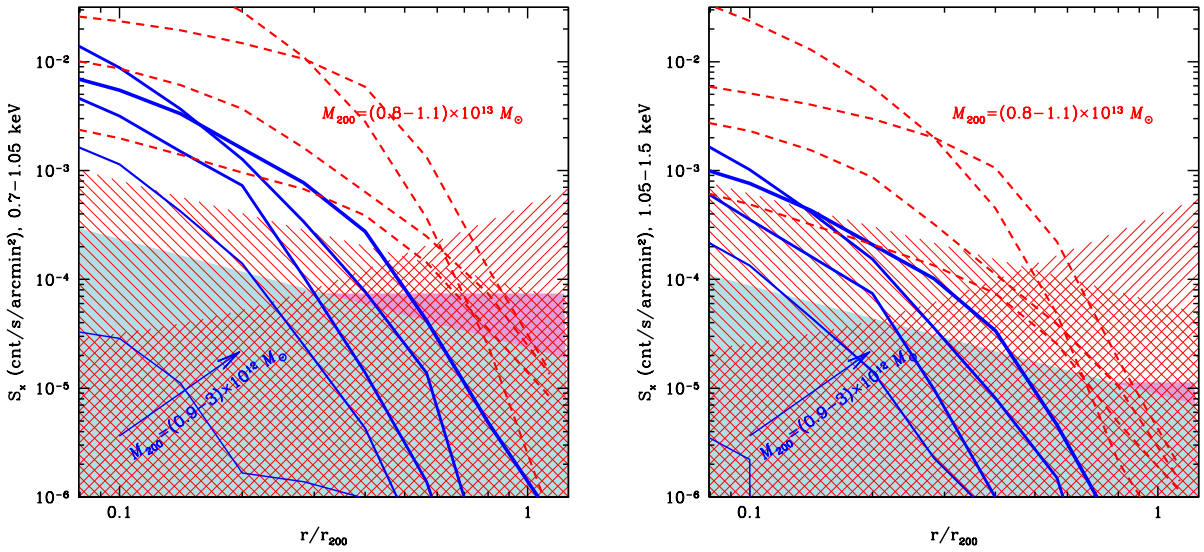

Fig. A.10— Same as Fig. A.9, but for the 0.7-1.05 keV and 1.05-1.5 keV bands (*left and right, respectively*).

- Overall, *Lynx* is capable of providing detailed information on the state of hot gas at half the virial radius for galaxies down to $\approx 3 \times 10^{12}\,M_\odot$. *Athena* is fully sensitive only for $M_{\rm tot} \gtrsim 8 \times 10^{12}\,M_\odot$ galaxies.

Absorption line studies of the CGM — Numerical simulations also enable assessment of how far down in the mass scale the hot CGM can be probed via absorption line studies. EAGLE simulations in particular provide spectral line profiles, including full thermal broadening and kinematic information. Examples of predicted absorption spectra for sight lines at the virial radius of $M_{\rm tot} = 10^{12}\,M_\odot$ galaxies are shown in Fig. A.8. Overall, the mock analysis shows that O VII absorption should be routinely detectable with the XGS in this regime; O VIII is also detectable in many cases. The O VIII/O VII flux ratio is a sensitive temperature diagnostic, so detection of both lines should constrain the CGM temperature rather well. This is an important characteristic of the CGM thermodynamic state, even though the gas density cannot be derived from the oxygen absorption lines.

The kinematic structure of O VII and O VIII is complex, but it can be characterized rather well in the stronger detection cases, opening a door to a new diagnostic of the hot CGM in L^* galaxies. Because of the complex, non-Gaussian structure of the line-of-sight velocity distribution, proper characterization of the lines requires a spectral resolving power at least matching the expected thermal width of the oxygen lines, $R \approx 5{,}000$.

To assess how many absorption line measurements of the CGM halos are possible with *Lynx*, the RASS-6dFGS catalog of bright AGN [648] was used as a representative sample of appropriate background sources. The probability of intercepting each sight line with a CGM absorption system at a given fraction of the virial radius depends on the AGN redshift and galaxy mass. The mass is relevant because it strongly affects the number density of galaxies (via the dark matter halo mass function, $dn/dM \sim M^{-2}$, for low M), and because the impact parameter scales with mass as $r \propto M^{1/3}$. Integrating the mass function [649] and folding in AGN redshifts and fluxes, a 5 Msec survey of 80 X-ray bright AGN should yield ~ 30 measurements of absorption line systems near the virial radius of galaxies with $M_{\rm tot} = 10^{12}\,M_\odot$, with data quality similar to that shown in Fig. A.8. Many more

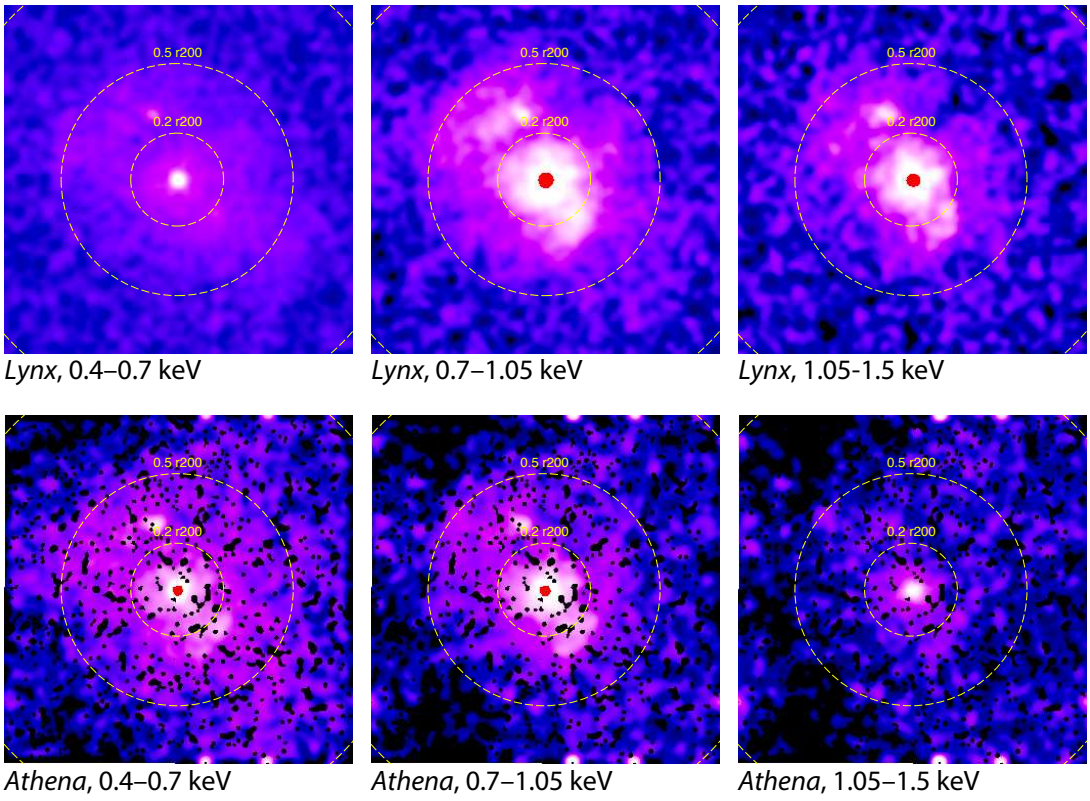

Fig. A.11— Simulated 500 ksec observation of an EAGLE galaxy with $M_{\rm tot} = 8 \times 10^{12}\, M_\odot$ with the *Lynx* HDXI *(top)* and *Athena* WFI *(bottom)* detectors. Each panel is 20 arcminute on a side. The color scale in all panels is normalized to the individual level of noise.

detections in the same sample of AGN are expected from higher-mass systems and from the Cosmic Web filaments [195]. Such a survey can be substantially optimized by measuring galaxy redshifts near the AGN sightlines in advance of the X-ray observations.

Detectability of Cosmic Web in emission — *Lynx*' ability to detect and remove discrete X-ray sources contributing to the cosmic X-ray background, and its low instrumental background (relative to astronomical signals), enable detection of extremely low surface brightness structures. This capability can be exploited for detection of hot gas in the Cosmic Web filaments converging on galaxy clusters. On the largest angular scales (appropriate for the mapping of the Cosmic Web), the limiting factor for *Lynx* will be systematic 1%-level background uncertainties, as shown in Figs. A.9–A.10. A possible observing scenario is to select a rich supercluster at $z \sim 0.1$ and survey a 10 deg^2 region around it with 100 ksec HDXI pointings. The point source sensitivity in each pointing will exceed that of the 7 Msec *Chandra* deep field, so the cosmic X-ray background will be nearly completely resolved into sources. Detectable surface brightness in the 0.7–1.5 keV band is only a few counts per 100 ksec per arcmin^2. Mock X-ray brightness maps derived from numerical simulations clipped to this limit show that *Lynx* will be capable of mapping the Cosmic Web in emission (see Fig. 4.7). Assuming a $\approx$ 1 Mpc line-of-sight depth appropriate for the expected size distribution of Cosmic Web filaments [401], the brightness limit can be converted to the corresponding gas density threshold. This estimate suggests that *Lynx* will be sensitive to structures with density contrasts of only $\rho/\langle\rho\rangle \approx 50$.

Only a minor fraction of the area in the survey concept described here will be covered by high surface-brightness regions of low-z galaxy clusters. The majority of the area will be suitable for, e.g., traditional AGN and distant galaxy cluster surveys, in addition to studies of the low-z Cosmic Web filaments. Such a survey is therefore multi-purpose and can constitute one of the *Lynx* "Legacy" fields (§4.4.1).

B. *Lynx* Trade Studies

The *Lynx* mission concept development depends upon quantitative and qualitative assessments and comparisons with respect to performance, cost, schedule, and risk of identified realistic alternatives to achieving the *Lynx* scientific goals. These trade studies are an integral part of the decision-making activities performed by the *Lynx* team throughout the course of this study.

This section outlines the mission-level, optics, science instrument, and spacecraft trade studies undertaken by the *Lynx* team in order to achieve the most acceptable technical solutions among viable alternatives. The purpose of this section is to document the trades undertaken as well as their outcomes to enable traceability. The following entries list the candidate choices, the selection criteria used, and the evaluation leading to the trade choice. References given point to the locations in the body of this report that are relevant to the given trade.

B.1 Mission-Level Trades

B.1.1 Configuration Architecture

Candidates:

- *Chandra*-like with spacecraft bus forward encircling *Lynx* Mirror Assembly (LMA), with mirror focused on a choice of focal plane cameras and insertable grating spectrometer (**SELECTED**)
- Distributed spacecraft bus components
- Simultaneous use of gratings and focal plane detectors via multiple mirror modules

Selection Criteria:

- Thermal control and stability
- Heritage
- Structural integrity and robustness for launch
- Assembly, Integration, and Test (AI&T) flow
- Efficiency of instrument use

Evaluation:

Grazing-incidence X-ray telescope payloads with two reflections will be somewhat longer than their focal lengths with mass distributed primarily at both ends of the optical bench. Thermal management favors the location of the spacecraft bus at the optics end of the optical bench. Therefore, like *Chandra*, the *Lynx* design places the spacecraft bus surrounding the LMA to ensure tight control of the mirror temperature and gradients. All previous high-resolution X-ray telescopes — namely *Einstein*, *ROSAT*, *XMM/Newton*, and *Chandra* — have used this configuration. Use of heritage gives confidence that the Observatory can be designed to meet structural and thermal requirements. The configuration allows the spacecraft to be developed, assembled, and tested independently of and in parallel to the optics and science instruments. Many scientific objectives do not require the use of simultaneous gratings or

multiple focal plane cameras. Therefore, a grating array fixed in the optical path or a secondary X-ray optics to simultaneously illuminate multiple instruments were rejected because they would significantly increase the time (decrease the efficiency) necessary to meet all the scientific objectives. This trade study was performed by the *Lynx* engineering team.

Reference: §6.4 Design of Spacecraft and Subsystems, Figure 6-4

B.1.2 Orbit

Candidates:

- Sun-Earth L2 (SE-L2) (SELECTED)
- High-Earth orbit, *Chandra*-like ellipse
- Drift-away orbit, Spitzer-like
- Lunar resonant, Transiting Exoplanet Survey Satellite- (TESS-) like
- Lunar Distant Retrograde Orbit (LDRO)
- Low-Earth Orbit (LEO)

Selection Criteria:

- Observing efficiency (must be capable of 85%)
- Lifetime (must not be limited to less than 20 years)
- Delta-V to achieve and maintain orbit (desired to be minimal)
- Radiation dose (desired to be minimal)
- Thermal environment (desired to be most stable)

Evaluation:

The LEO option did not meet efficiency requirements and was eliminated. Table B.1 shows the evaluation of the other candidates. "A" scored as 1.0, "B" as 0.75, and "C" as 0.5. The SE-L2 and TESS/lunar resonant were the top two candidates.

SE-L2 was chosen based on its smaller delta-V — which results in less mass for propellant and propellant tanks — and for the lack of eclipses, which results in simpler operations and a reduced number of batteries and lower battery mass. The *Lynx* engineering team performed the trade study, and the decision was made by the Science and Technology Definition Team (STDT).

Reference: §6.7.1 Launch to Orbit – Cruise, Commissioning, and Checkout

Table B.1. *Lynx* orbit trade.

	Total Score	Science Observing	Launch Vehicle	Delta-V	Duration	Thermal	Comm	Environment	Serviceability
Max Points	100	15	10	15	10	15	15	15	5
SE-L2	91	A	A	A	A	A	B	B	B
Drift-away	81	A	A	A	C	A	C	B	C
LDRO	84	A	A	C	A	B	A	B	B
CTO	73	B	B	B	A	C	A	C	C
TESS	86	A	A	B	A	B	A	B	C

B.1.3 Launch Vehicle

Candidates:
- Launch Services Program- (LSP-) defined heavy-class (SELECTED)
- Space Launch System (SLS)
- SLS co-manifested payload
- Intermediate-class (as defined by LSP)

Selection Criteria:
- Mass capability meets or exceeds *Lynx* Observatory estimate
- Fairing geometry meets or exceeds *Lynx* Observatory estimate

Evaluation:
While details of the Launch Vehicle (LV) fleet available at the time of *Lynx*'s anticipated launch is highly uncertain, total Observatory mass and geometry comparison to anticipated LV mass and fairing size capabilities are central to mission cost and payload architecture. A trade study assessing heavy-class, SLS (alone or as co-manifested payload), and intermediate-class LV options was performed by the *Lynx* engineering team in accordance with NASA's LSP and SLS program recommendations.

Given the mass and volume of the as-presented *Lynx* Observatory and the LSP-provided guidelines for payload mass to SE-L2 and payload volume for LVs in the 2030s, the *Lynx* study selected the "heavy-class" LV as the baseline for all structural, propulsion, and orbital mechanics design analyses.

The feasibility of launching the *Lynx* Observatory as a co-manifested payload on the SLS is also appealing, and design scenarios for meeting SLS co-manifested requirements have been considered as well. Launching as a co-manifested payload significantly reduces the cost of LV services (WBS 08), as the LV cost is assumed to be a "contributed" cost. However, as a co-manifested payload, launch availability is reduced, and propulsion requirements to SE-L2 are increased.

The LSP-provided mass to SE-L2 and payload volume of the "intermediate-class" launch vehicle for the 2030s is not sufficient to carry the as-presented *Lynx* Observatory. Although a larger *Lynx*-specific payload shroud could be designed for the intermediate-class vehicle and/or an Extended Optical Bench (EOB) could be designed to be compatible with the LSP-provided intermediate-class payload volume, significant payload mass reductions would be required to utilize this as-provided vehicle class.

Reference: §6.5 Launch Vehicle

B.2 Optics

B.2.1 *Lynx* Mirror Assembly Trade

Candidates:
- Silicon monocrystalline meta-shell (SELECTED)
- Slumped glass adjustable via piezoelectric elements
- Full-circumference shells

Selection Criteria:

- Optical performance must meet science requirements for area, energy range, and angular resolution over a defined Field of View (FOV)
- Highest technology readiness
- Best demonstrated performance
- Credibility of roadmap to reach required on-orbit performance
- Minimal mass and cost
- Credibility of cost estimate

Evaluation:

The *Lynx* STDT, recognizing that a credible and feasible path to maturing the LMA was crucial to a compelling and executable *Lynx* mission concept and—following deliberations within the *Lynx* Optics Working Group (OWG) and Study Office and corroborated by a *Lynx* Interim Report Red Team recommendation—commissioned a trade study in January 2018 to recommend a reference mirror design that demonstrates a technological path to realizing the science envisioned by the STDT. The trade study was specifically chartered to provide a recommendation for one Design Reference Mission (DRM) concept for the mirror assembly architecture to focus the design for the Final Report and identify any feasible alternates.

The *Lynx* Mirror Architecture Trade (LMAT) Working Group represented scientific and technical leadership across academia, NASA, and industry, including international participation. Using public evaluation criteria, this community working group conducted an open science, technical, and programmatic evaluation in a series of meetings from February through July of 2018. The team reached a broad consensus on the recommendation and the basis for the recommendation after amassing over 650 pages of documents and committing over 5,000 manhours of study and deliberations.

The study used the Kepner-Tregoe decision analysis method facilitated by Gary Blackwood of the Jet Propulsion Laboratory (JPL). The process began with agreeing on evaluation criteria and their weights (Figure B.1), followed by documenting descriptions of the technology options, evaluating these options against the criteria, reaching consensus on the evaluation, documenting potential risks and opportunities, and finally making a recommendation that accounted for these risks and opportunities. Leading evaluation criteria that drove the recommendation were the current and near-future demonstrated performance and technology development plans. Relative simplicity of mirror assembly production process and test as well as relative impact of technical accommodation to the spacecraft were also discriminating factors.

The LMAT recommended the Silicon Meta-shell Optics as the DRM concept mirror assembly architecture to focus the design for the Final Report. The Full Shell Optics and Adjustable Segmented Optics technologies were determined to be feasible alternates. The Silicon Meta-shell Optics technology was deemed the most mature with the shortest path to achieving Technology Readiness Level 5 (TRL 5) by Key Decision Point A (KDP-A) and TRL 6 by Preliminary Design Review (PDR). It uses the shortest mirrors, which leads to improved off-axis Point Spread Function (PSF) performance relative to the other designs, but also requires the largest quantity of mirror elements to be produced, aligned, and bonded, resulting in the longest estimated production schedule. Full Shell Optics, conversely, has potentially the shortest schedule (fewest mirror shells) but was deemed most challenging to produce very thin high-quality mirrors of large diameter. The Adjustable Segmented Optics design was determined

to have a short production and installation schedule due to the relaxed figure error tolerances afforded by adjustability, but the many steps in the process had yet to be demonstrated and the application of actuated control at the system level was deemed likely to adversely affect the A&IT schedule.

MUSTS										
	Science	Per definitions / analysis of SET								
M1	Optical performance will meet requirements flowing down from Science Trace Matrix					Y		Y		Y
	Technical	Per definitions / analysis of TET								
M2	Credible roadmap from today's status to predict flight on-orbit performance					Y		Y		Y
M3	Performance modeling tools related to current results are demonstrated to be credible					Y		Y		Y
M4	Repeatable fabrication process based on current status					Y		Y		Y
M5	Credible error budget					Y		Y		Y
M6	Expected to survive launch					Y		Y		Y
	Programmatic	Per definitions / analysis of PET								
M7	Show a credible plan to meet TRL 4-6					Y		Y		Y
M8	Produce the mirror assembly within the Program schedule allocation					Y		Y		Y
WANTS		**Key**	**Driving**	**Weights**						
	Technical	Per definitions / analysis of TET								
W1	Highest predicted technology readiness at Astro2020 by March 2020	K	D	12	7	small-significant	7	small-significant	10	BEST
W2	Relative demonstrated performance	K	D	12	4	**SIGN./VL**	4	**SIGN./VL**	10	BEST
W3	Relative credibility of roadmaps from today's status to predict flight on-orbit performance (reflected M2)	K	D	12	5	SIGN. DIFFERENCE	5	SIGN. DIFFERENCE	10	BEST
W4	Relative simplicity of mirror assembly production process and test	K	D	10	8	small difference	10	BEST	10	BEST
W11	Relative complexity and accuracy of ground calibration of mirror assembly	K	D	6	8	small difference	10	BEST	10	BEST
W13	Relative impact of technical accommodation (cost, mass,	K	D	10	8	small difference	5	SIGN. DIFFERENCE	10	BEST
	Technical Sub total					400		402		620
	Programmatic									
W12	Relative cost and credibility of grass-roots cost estimate of the mirror assembly through delivery	K		10	10	WASH	10	WASH	10	WASH
W18	Best assessment of the schedule to mirror assembly delivery (reflects M8)	K	D	6	8	small difference	10	BEST	8	small difference
	Programmatic Sub Total			100		148		160		148
	Final Total				548		562		768	SELECTED

Figure B.1. Kepner-Tregoe *Lynx* Mirror Assembly Trade study outcome. Evaluation criteria as determined by science, technology, and programmatics teams (SET, TET, and PET, respectively) were classified as Musts and Wants. The three technologies evaluated were (last three columns; left to right) Adjustable Segmented, Full Shell, and Silicon Meta-shell Optics. All three technologies met the Must criteria and were deemed feasible.

Reference: §6.3.1.1 LMA Design Overview, §7.2 Optics Development Overview

B.2.2 Other Optics Trades

B.2.2.1 High Energy Effective Area

Candidates:

- Primary configuration (SELECTED)
- Modification with extended capability for mirror effective area above 10 keV and to LXM for Quantum Efficiency (QE) at these energies, including potential use of multilayer optics coating

Selection Criteria:
- Science return for cost

Evaluation:
The possibility of enhancing *Lynx* science capabilities by extending the performance range to higher X-ray energies has been discussed by the STDT. This may be a Phase A trade to enable additional science beyond the current *Lynx* science requirements. The STDT carried out the science trade, while the LXM instrument lead estimated the cost impact to this instrument. No assessment was made of the cost or schedule impacts to the mirror development before this modification was tabled.

Reference: §6.3.4.1 LXM Design Overview

B.2.2.2 LMA Fabrication

Candidates: (CHOICE PENDING STUDIES TO BE COMPLETED)
- Number of parallel lines for each process step
- Degree of automation for each process line

Selection Criteria:
- Length of schedule
- Cost of production equipment
- Cost of labor
- Risk of schedule slip

Evaluation:
The manufacturability and production of the mirror components has been recognized as a risk, and a study to identify areas to reduce the overall development schedule and cost for this portion of the project will be performed by the *Lynx* study office. The trade has been undertaken by *Lynx* study office personnel, industry partners, and the Silicon Meta-Shell Optics technical lead.

Reference: §8.3 Risks and Risk Mitigation

B.3 Science Instruments—LXM

B.3.1 Pixel Array Types

Candidates:
- 1-arcsecond pixels, 5-×-5-arcmin FOV, 3 eV-resolution (SELECTED – MAIN ARRAY)
- 0.5-arcsecond pixels, 1-×-1-arcmin FOV, 2 eV resolution (SELECTED – ENHANCED MAIN ARRAY)
- 1-arcsecond pixels, 1-×-1-arcmin FOV, 0.3 eV resolution (SELECTED – ULTRA-HIGH-RESOLUTION ARRAY)
- 5-arcsecond pixels, 20-×-20-arcmin FOV, 1 eV resolution Extended Array
- 0.5-arcsecond pixels, 20-×-20-arcsecond FOV, 1.5 eV resolution High-Resolution Inner Array

Selection Criteria:
- Satisfy science objectives
- Minimal cost, risk, complexity

Evaluation:
Three-pixel array types (the Main Array, Enhanced Main Array, and Ultra-High-Resolution array) span the scientific needs of *Lynx*. The trades of various focal plane arrays and subarrays necessary to carry out *Lynx* science objectives was discussed by STDT, including a face-to-face meeting in January 2018 where it was decided that three of the original five array types are necessary to cover all the important *Lynx* science objectives while simplifying the demands on the instrument. The trade study was conducted by the Instrument Working Group in conjunction with the STDT.

Reference: §6.3.4 *Lynx* X-ray Microcalorimeter

B.4 Science Instruments—HDXI

B.4.1 Focal Plane Field of View

Candidates:
- 22-arcminute diameter (SELECTED)
- 46-arcminute diameter

Selection Criteria:
- Satisfy science requirements
- Minimize cost, complexity
- Minimize mass, power

Evaluation:
The LMA PSF degrades slowly with off-axis distance, but certain scientific enhancements may be possible if the High Definition X-ray Imager (HDXI) detector FOV extends beyond that needed to meet the *Lynx* grasp requirement for sub-arcsecond resolution. This trade was made by the STDT in consultation with the *Lynx* Instrument Working Group and their recommendations.

Reference: §6.3.2.1 HDXI Design Overview

B.4.2 Sensor Architecture (Phase A selection)

Candidates:
- Hybrid Complementary Metal-Oxide Semiconductor (CMOS)
- Monolithic CMOS
- Digital Charge-Coupled Device (CCD) with CMOS readout

Selection Criteria:
- Low-energy response
- High-energy response
- Readout noise and energy resolution

Evaluation:
Three technologies were identified by the *Lynx* Instrument Working Group as candidates for meeting the scientific requirements for the HDXI. These technologies differ primarily in their architecture, but not in their functionality; each has demonstrated proof of concept. At present, each of these technologies

individually meets some, but does not simultaneously meet all, of the *Lynx* HDXI requirements, and each is assessed at TRL 3 for *Lynx* by the most recent Physics of the Cosmos (PCOS) Technology Review Board. Each technology requires similar resources from the spacecraft, and all three have similar development paths. The development plan assumes, during the course of pre-Phase A activities, a downselection to two technologies will precede a final downselection prior to Phase A.

Reference: §6.3.2.1 HDXI Design Overview, §7.3.1 High-Definition X-ray Imager

B.5 Science Instruments—XGS

B.5.1 Gratings Architectures

Candidates:
- Critical-Angle Transmission (CAT) gratings (SELECTED)
- Off-Plane Gratings (OPG)

Selection Criteria:
- Meets science requirements per the *Lynx* STDT
- Evidence of a repeatable fabrication process
- Ease of accommodation in the Observatory
- Shows a clear instrument-level requirements flowdown to grating elements
- Launch survivability

Evaluation:
The two technologies identified by the *Lynx* Instrument Working Group both meet the required effective area, energy resolution and bandwidth requirements, and are acceptable grating architecture choices. A trade study following the Kepner-Tregoe process was conducted with evaluation criteria, weights, and scores developed through consensus. The X-ray Grating Spectrometer (XGS) technologies were evaluated on science and technology criteria (not cost or schedule). Both technologies were deemed feasible and capable of meeting science and technical requirements (both are currently at TRL 4). The CAT grating was deemed to require less alignment precision, less contamination control, and less stringent thermal control.

Reference: §6.3.3.1 XGS Design Overview, §7.3 Instrument Development Overview

B.6 Spacecraft

B.6.1 Star Camera

Candidates:
- Single camera, internally redundant (SELECTED)
- Dual co-aligned cameras
- Dual offset cameras

Selection Criteria:
- Serve for real-time pointing control

- Serve for ground aspect reconstruction
- Redundancy
- Minimum mass, power

Evaluation:
Dual-offset cameras give the best measurement of roll angle; however, the measurement accuracy required to reconstruct 0.5-arcsecond images means that a very small, 2-deg2 FOV allows enough lever arm to measure roll to the accuracy needed. Star cameras should be aligned with the X-ray telescope to obtain the best measurement of celestial location. Failure of the glass optical elements or of the structural support is non-credible. Therefore, only one co-aligned star tracker is necessary and sufficient.

Reference: §6.4.2 Guidance, Navigation, and Control

B.6.2 Pointing Stability

Candidates:
- Precision gyros and reaction wheels (SELECTED)
- Control moment gyros

Selection Criteria:
- Mass and cost
- Hold to 0.17 arcseconds per second stability
- Stay within 10 arcseconds of target
- Mission heritage

Evaluation:
Control moment gyros are very massive and expensive. They can give much greater stability than is required, since the Observatory counts each single X-ray photon and can reconstruct an image via post facto knowledge of where the telescope was pointing.

Reference: §6.4.2 Guidance, Navigation, and Control

B.6.3 Data Storage

Candidates:
- Consultative Committee for Space Data Systems- (CCSDS-) compliant packets (SELECTED)
- Fixed format (e.g., time division multiplexed)

Selection Criteria:
- Flexibility for variable data rates
- Contemporary standard

Evaluation:
Time-Division Multiplexing (TDM) forces a fixed maximum data rate and results in large blocks of "zeroes" telemetered for weak sources. CCSDS packets allow mission planning to interleave observations, resulting in counting rates requiring much higher-than-average telemetry balanced by low-rate observations.

Reference: §6.4.6 Command and Data Handling

B.6.4 Antenna

Candidates:
- Phased array (SELECTED)
- Gimbaled antenna

Selection Criteria:
- Power to support communication at SE-L2
- Impact on pointing

Evaluation:
Both antennas can provide needed db margin for communications. Phased array avoids vibrations from the use of gimbaled antenna.

Reference: §6.4.6 Command and Data Handling

B.6.5 Safe Mode Control

Candidates:
- Independent control processing electronics and firmware (SELECTED)
- Redundant computer

Selection Criteria:
- Robust against single failures
- Robust spacecraft safing while unknown anomalies are diagnosed
- Minimize hardware, complexity, mass, and power

Evaluation:
Redundant computers, which are included already to protect against computer hardware failure, are subject to single-point failure due to running the same software. Independent control processing electronics run different software, which is concentrated on fewer tasks just to stabilize the vehicle in power-positive configuration.

Reference: §6.4.5 Avionics and Flight Software

B.6.6 Observatory and OBA Thermal Control

Candidates:
- Active control, cold-biased with heaters (SELECTED)
- Passive control, heat pipes, and Multilayer Insulation (MLI)

Selection Criteria:
- Robust control at all pitch angles, 45° to 175°
- Maintain required thermal environment for possible 20-year mission

Evaluation:
Development of a detailed integrated thermal model of the Observatory, including the thermal control of the LMA and Optical Bench Assembly (OBA), was performed by a *Lynx* study office-industry

partnership. A separate OBA trade comparing passive and active thermal control options concluded that the use of heat pipes and MLI alone (a purely passive control system) could not maintain the required limit on gradients at all pitch angles due to the variation of the heat input to one side of the bench.

Reference: §6.4.4 Thermal

B.6.7 Thermal Coverings

Candidates:
- Ag-Teflon MLI, with offset Si-coated Kapton shield (SELECTED)
- Second-surface quartz mirrors (Optical Solar Reflectors)
- Si-Kapton MLI
- Ag-Teflon MLI

Selection Criteria:
- Stability over 20 years in L2 environment
- Low value of absorptance: 0.1 to 0.3, low α/ε ratio.
- Low mass

Evaluation:
Quartz mirrors were eliminated as a significant mass penalty. Ag-Teflon was eliminated due to the significant increase in α to values >0.5. Si-coated Kapton is relatively stable, but starts with α>0.3 andα/ε >0.5. Ag-Teflon shielded by Si-coated Kapton provides the desired thermal environment and stability.

Reference: §6.4.4 Thermal

B.6.8 Communications Trade

Candidates:
- Ka-band (SELECTED for telemetry downlink
- X-band (SELECTED for command uplink and status downlink
- S-band
- Optical

Selection Criteria:
- Conservatively meet *Lynx* data volume and data rate estimates
- High flight heritage; low obsolescence risk

Evaluation:
A trade study performed by the *Lynx* engineering team, with guidance from NASA/Space Communications and Navigation (SCaN) experts on future Deep Space Network (DSN) communications capabilities, was concluded and reported in April 2017. *Lynx* bandwidth requirements do not require capabilities beyond the data rates provided by Ka-band. Ka-band for data return (downlink) and X-band for low-rate command uplink and status downlink were selected for *Lynx*. Optical (laser) communications TRL was deemed too low to use in the design but is a promising technology that may be considered for future analysis.

Technology for long-distance space-based laser communications was demonstrated in NASA's 2013 Lunar Laser Communication Demonstration (LLCD), the space terminal which flew on the Lunar Atmosphere and Dust Environment Explorer (LADEE) spacecraft. Using a (gimballed) 10-cm satellite-based telescope (which is the analog of an antenna in the optical regime), a 0.5-W laser transmitter, and a ground station comprised of four 40-cm telescopes, LLCD demonstrated error-free data transmission at a rate of 622 Mbps from lunar orbit.

In the near future, NASA plans two more laser communications demonstrations, and, on the timescale of *Lynx*, laser communications would be a feasible option. Moreover, with its orbit about SE-L2, unlike missions to the Moon or Mars, *Lynx* would always be viewed in the nighttime sky, significantly reducing demands on the ground station in terms of thermal loading from the Sun and noise introduced by the sky brightness.

From the science perspective, there are two complementary benefits to considering higher data rates. First, the same volume of data could be downlinked in a much shorter time. Feasible data rates could be 5× or higher than the current baseline, enabling additional time for science observations. Alternately, larger volumes of data could be downlinked in the same amount of time. Doing so could enable new observational possibilities, particularly in the time domain. Table B.2 summarizes the *Lynx* radio frequency-based baseline telecommunications, LLCD, the two near-term NASA laser communications demonstrations, and an illustrative extrapolation to the SE-L2 distance of *Lynx*. The illustrative *Lynx* with laser communications is not meant to suggest a specific implementation (as there is ample trade space to consider), but only illustrate that much higher data rates could be achieved for *Lynx*.

Table B.2. Comparison of the *Lynx* baseline telecommunications, near-term NASA laser communications, and an illustrative *Lynx* case.

System	Data Rate (Mbps)	Range (x106 km)	Flight Terminal Aperture (cm)	Transmitter Power (W)	Ground Station
Lynx baseline Ka-band radio	22	1.5	N/A	N/A	DSN 34 m antenna
LLCD	620	0.5	10	1	0.8 m telescope
Optical to Orion (O2O)[1]	80	0.5	10	1	0.4 m telescope
Deep Space Optical Communications (DSOC)[2]	20	150	22	4	5 m telescope
Illustrative *Lynx* w/Laser Communications	32,000	1.5	22	4	2 m telescope

[1] O2O system is scheduled to be included on the Orion crew capsule of Exploration Mission-2 (EM-2), with a planned launch in 2022. It will have an architecture similar to LLCD, but will use more commercially built subsystems, notably the space modem and the ground detectors. Because the Orion data transmission requirements (80 Mbps) are lower than those for the LLCD, only a single 40-cm ground telescope is planned.
[2] DSOC system is manifested on the Psyche Discovery mission, with a planned launch in 2022. The requirements include demonstrating laser communications over ranges comparable to the distance to Mars, but, as an illustration of capability, DSOC will provide approximately 10 Mbps at ranges of 1 au.

Reference: §6.4.6 Command and Data Handling

B.6.9 Orbital Insertion

Candidates:
- Parking orbit (SELECTED)
- Direct insertion

Selection Criteria:
- Launch window flexibility
- Maximal payload mass

Evaluation:
A direct insertion allows for greater payload mass at the expense of fewer launch opportunities and shorter launch windows. A circular parking orbit allows more flexibility in targeting the outgoing transfer trajectory. Analysis showed a modest mass increase of 2%–3% in payload mass was possible (but not guaranteed) by direct insertion and that the performance may not increase due to range safety considerations. Direct ascent maneuvering designed to expand the launch window could further decrease performance, and the direct injection burns could exceed the burn-time limit of the engines. The parking orbit was chosen because the modest possible increase in mass from the direct ascent was outweighed by the flexibility of the parking orbit. The trade study was performed by the *Lynx* engineering team with consultation with the NASA LSP.

Reference: §6.4.1 Propulsion

B.6.10 Optical Bench Assembly

Candidates:
- Fixed optical bench (SELECTED)
- Extendable optical bench

Selection Criteria:
- Launch vehicle fairing accommodation
- Structural stability
- Stable length. Sensitivity to thermal changes.
- Minimal mechanisms and risk

Evaluation:
The OBA is a precision metering system with tight tolerances. Epoxy fiber composites can be laid out to have very small coefficients of thermal expansion, allowing excursion of several degrees Celsius to still be within the mirror assembly depth of focus. However, depending upon LV fairing constraints, the 10-m focal length *Lynx* payload may need to be accommodated using a one-time extendable (rather than fixed-length) OBA. Consideration of an extendable bench may facilitate LV flexibility with modest impacts on mass and cost. Due to a lowered center of gravity when stowed, the payload will experience reduced launch loads with the EOB. To a first order, the EOB option was considered feasible; however, further detailed analysis with the engineering team and industry partners is required to fully assess this option. Conversely, a fixed OBA eliminates the extra mechanism and deployment operation that would be required by an EOB. Additional mechanisms and deployments add risk.

Reference: §6.3.6 Optical Bench Assembly, §6.5 Launch Vehicle

B.6.11 Placement of Optical Axis on Selected Instrument

Candidates:
- Moveable focal plane assembly (SELECTED)
- Moveable mirror

Selection Criteria:
- Precision of locating the optical axis on the focal plane camera
- Mass and complexity of required mechanisms.
- Thermal control and stability of mirror on-orbit
- Structural integrity and mass distribution
- Ground calibration and verification

Evaluation:
An early appraisal of the distribution of mass within the *Lynx* Observatory indicated that, similar to *Chandra*, structural integrity would be maintained within reasonable mass budgets for a moveable instrument platform. Qualified mechanisms and motors could implement either choice. Ground verification of the moveable mirror positioning accuracy and the integrity of the optics in all required positions were considered a risk in view of gravity effects. Thermal control and stability were considered to be more tractable if the mirror maintains an identical configuration with respect to its surroundings. In view of the precision required to achieve sub-arcsecond angular resolution, a translating table affixed to the Integrated Science Instrument Module (ISIM) is baselined by the *Lynx* engineering team and associated instrument teams.

Reference: §6.3.5 Integrated Science Instrument Module

C. *Lynx* Model-Based Systems Engineering

The *Lynx* team plans to follow well-established systems engineering policies and processes and will implement them using state-of-the-art tools and methodology. The team has started implementing those new tools during the *Lynx* Study Phase.

The *Lynx* Study Office has partnered with the University of Alabama in Huntsville on the development of the Model-Based Systems Engineering (MBSE) tool for the *Lynx* X-ray Observatory. The objectives of the *Lynx* Observatory model during the Study Phase are to provide requirement traceability framework for the identification of relationships between science and mission goals to engineering design decisions, model the WBS, and identify the logical interfaces between the physical elements.

As the *Lynx* project advances into pre-Phase A, the *Lynx* model will expand to include all applicable systems engineering products and tasks such as formal system requirements, requirements logical decomposition and allocation to lower level elements, error budgets and analysis results showing current calculations and margins to those budgets, traceability, interface management, configuration management, define and track Measures of Effectiveness (MOEs), Measures of Performance (MOPs), and Technical Performance Measures (TPMs) as appropriate and will link these systems engineering products to design solutions. This allows rapid and efficient technical management, assessment, and decision analysis as the design matures. As the *Lynx* project moves into the verification and validation phase, the *Lynx* model will be used to track compliance to requirements to ensure that the Observatory will be able to fully enable science goals.

The systems engineering processes performed by the model are illustrated using Systems Modeling Language (SysML) diagrams. The Study Phase requirements traceability diagrams show the relationship between the three types of requirements identified: science traceability, mission traceability, and Ground Rules and Assumptions (GR&A). A freeform diagram captures the schema for the traceability from science goals to the GR&A. Bridge requirements were created to help narrow the gap in the relationship between GR&A with their respective mission traces. These requirements are written in the form of a "shall statement" and provide clarity as to how a specific GR&A can trace to a broader mission capability. Stereotypes were created and are used on all requirements to differentiate between the three types. Lastly, a generic table was generated to illustrate the trace between a requirement and all of its associated requirements. Other generic tables capture GR&A without a trace relationship to the mission traceability requirements for visibility of traceability for the systems engineering team.

All of the WBS elements were modeled as blocks, and their associated hierarchical decomposition is illustrated on multiple Block Definition Diagrams (BDDs). The *Lynx* WBS is composed of the organizational tasks as well as the end product hardware. The MBSE tool enables the visualization of the structural hierarchy of the elements and allows for the identification of interfaces among the elements illustrated in an Internal Block Diagram (IBD). Item flows such as data being passed or how the path power is distributed among the subsystems are just a few examples that are visually enabled by IBDs. MBSE usage in the *Lynx* project facilitates the communication between members of the team by the visual presentation of data that is dynamically presented from various views versus document based-exchange.

An online demonstration of the *Lynx* MBSE model can be accessed via the link below.

https://drive.google.com/drive/folders/1Xr_G1Kv8ZgW1MvEDQG84ZGtSJiyFq5OO?usp=sharing

1. Highlight all folders/files.
2. Right-click.
3. Select Download All (the download may take some time).
4. Once downloaded to your computer, unzip the file.
5. Enter the folder and open *Lynx*HTML

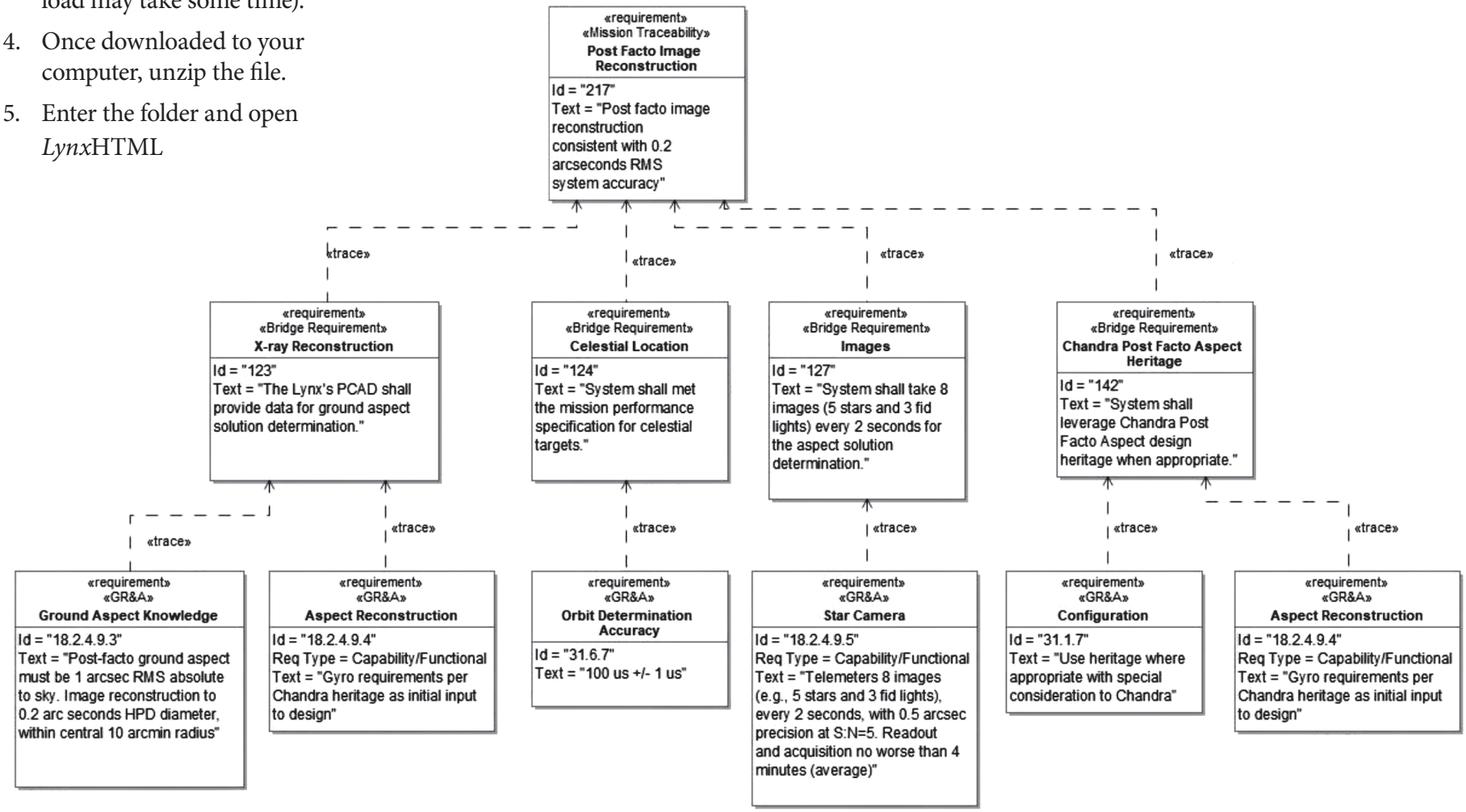

Figure C.1. Requirement trace example from *Lynx* MBSE tool.

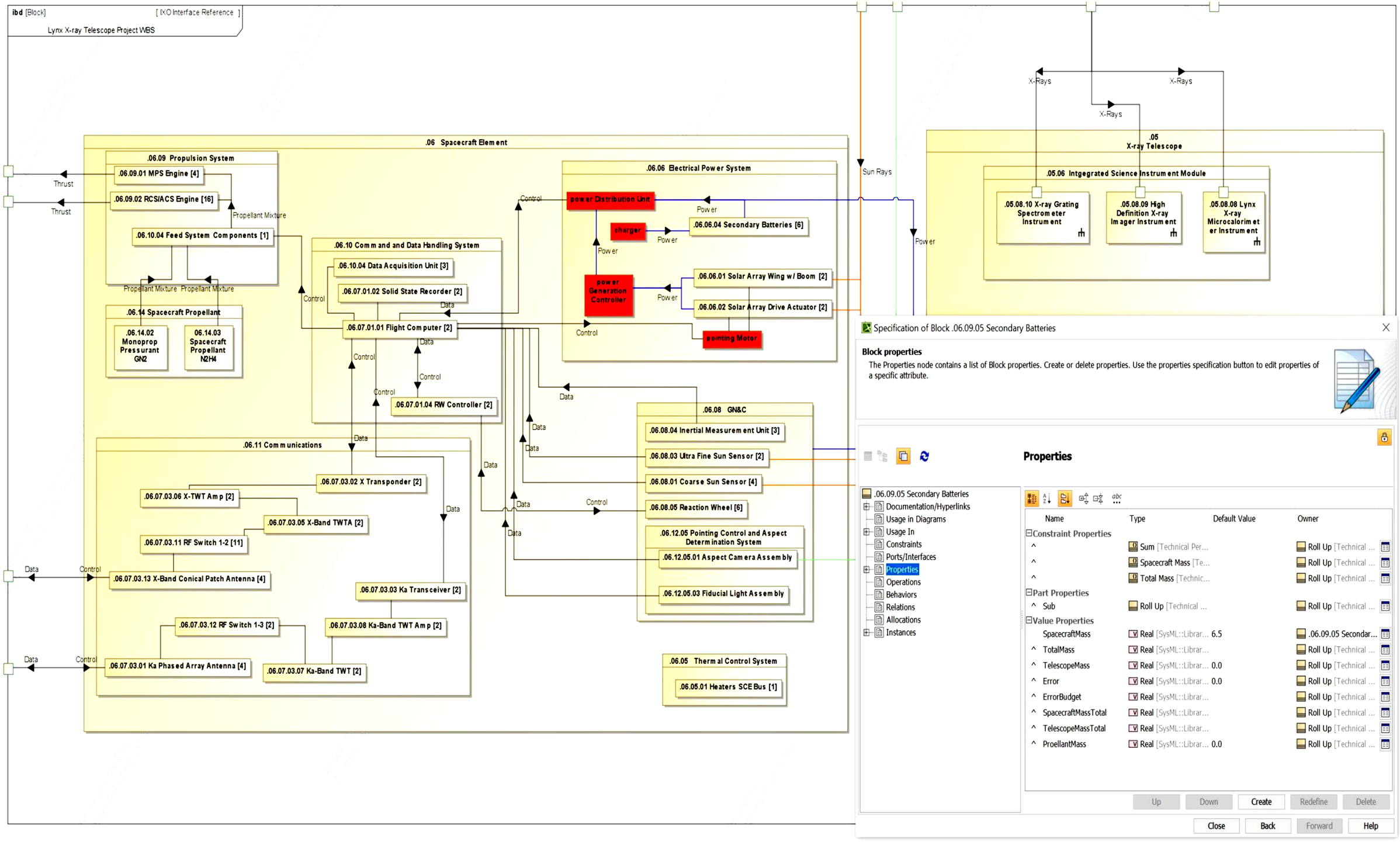

Figure C.2. Diagram from the *Lynx* MBSE tool showing IBD and the ability to display engineering data for each element in the diagram (example mass from the MEL).

D. Master Equipment List/Power Equipment List

Table D.1. *Lynx* Master Equipment List for the DRM.

WBS1	WBS1 Desc	WBS2	WBS2 Desc	WBS3 Desc	WBS5	WBS5 Desc	Basic Mass (kg)	MGA (kg)	Predicted Mass (kg)	TRL	Example Model, Manufacturer, and Part No. if available
09	X-ray Telescope (XRT)	05.06	*Lynx* Mirror Assembly (LMA)	X-ray Mirror Modules	05.06.07.04	X-ray Mirror Modules Optical Elements (segments, modules)	888.92	222.23	1,111.15		
					05.06.07.05	X-ray Mirror Modules Meta-Shell Forward / Aft Ring Structure	59.19	14.80	73.99		
					05.06.07.06	X-ray Mirror Modules Spider Structure	308.00	77.00	385.00		
				LMA Thermal Control	05.06.08.01	LMA MLI	3.42	0.68	4.11	9	
					05.06.08.02.01	LMA Pre-Collimator Assembly	118.82	29.71	148.53		
					05.06.08.02.02	LMA Post-Collimator Assembly	182.84	45.71	228.55		
					05.06.08.03	Spider Heaters	20.00	4.00	24.00	9	
				LMA Contamination Control Door Assemblies	05.06.09.01.01	FCD Structure	21.34	5.34	26.68		
					05.06.09.01.02	FCD Motor	15.40	3.85	19.25	9	Moog Type 7 Rotary Actuators
					05.06.09.01.03	FCD Motor Mount	12.00	3.00	15.00		
					05.06.09.01.04	Forward Door Hold Down Mechanisms (Launch Locks)	4.20	1.26	5.46	9	NEA Model 9106B
					05.06.09.02.01	Aft Contamination Door (ACD) Structure	21.60	5.40	27.00		
					05.06.09.02.02	ACD Motor	15.40	4.62	20.02	9	Moog Type 7 Rotary Actuators
					05.06.09.02.03	ACD Motor Mount	12.00	3.00	15.00		
					05.06.09.02.04	Aft Door Hold Down Mechanisms (Launch Locks)	4.20	1.26	5.46	9	NEA Model 9106B
				LMA Barrel Assembly	05.06.10.01	Barrel Structure	163.30	40.83	204.13		
					05.06.10.02	Subsystem Ring	28.67	7.17	35.84		
					05.06.10.03	LMA Flexures	2.20	0.55	2.75		
		05.06 Total					**1,881.51**	**470.40**	**2,351.90**		
		05.07	X-ray Gratings Array (XGA)	XGA Elements (gratings, facets)	05.07.06	XGA Elements (gratings, facets)	15.23	3.81	19.04		
				XGA Grating Array Structure (GAS)	05.07.07	XGA Grating Array Structure (GAS)	22.28	5.57	27.85		
				Grating Array Motor	05.07.08	Grating Array Motor	15.40	4.62	20.02	9	Moog Type 7 Rotary Actuators
				Grating Array Motor Mount	05.07.09	Grating Array Motor Mount	12.00	3.00	15.00		
				Gratings Array Structure Hold Down Mechanisms (Launch Locks)	05.07.10	Gratings Array Structure Hold Down Mechanisms (Launch Locks)	4.20	1.26	5.46	9	NEA Model 9106B
		05.07 Total					**69.11**	**18.26**	**87.36**		
		05.08	Optical Bench Assembly (OBA)	Magnetic Broom	05.08.05	Magnetic Broom	28.00	7.00	35.00		
				OBA TCS	05.08.06.01	OBA Heaters	50.00	10.00	60.00	9	
					05.08.06.02	OBA MLI	71.27	14.25	85.53	9	
					05.08.06.03	OBA OSR Support Structure	-	-	-	TBD	
					05.08.06.04	Observatory Sunshade	44.40	22.20	66.60	5	
				OBA Structure	05.08.07	OBA Structure	407.84	101.96	509.80		
		05.08 Total					**601.51**	**155.41**	**756.93**		
		05.09	Integrated Science Instrument Module (ISIM)	ISIM TCS	05.09.06.01	TTA Heaters	2.22	0.44	2.67	9	
					05.09.06.02	ISIM Heaters	8.76	1.75	10.51	9	
					05.09.06.03	TTA MLI	5.06	1.01	6.08	9	
					05.09.06.04	ISIM MLI	19.96	3.99	23.95	9	
					05.09.06.05	Radiator, LXM Cryostat	5.33	1.07	6.39	4 (TRL 9 are available)	
					05.09.06.06	Radiator, LXM Cryocooler	2.32	0.46	2.78	4 (TRL 9 are available)	
					05.09.06.07	Radiator, LXM Electronics 1	10.91	2.18	13.09	4 (TRL 9 are available)	
					05.09.06.08	Radiator, LXM Electronics 2	12.57	2.51	15.09	4 (TRL 9 are available)	
					05.09.06.09	Radiator, HDXI Detector Assembly	7.82	1.56	9.39	4 (TRL 9 are available)	
					05.09.06.10	Radiator, HDXI DEU	2.78	0.56	3.34	4 (TRL 9 are available)	
					05.09.06.11	Radiator, XGD Assembly	5.73	1.15	6.88	4 (TRL 9 are available)	
					05.09.06.12	Radiator, XGD DEU	2.31	0.46	2.77	4 (TRL 9 are available)	
					05.09.06.13	Radiator, Mounting Plate XGD	11.52	2.30	13.82	9	
					05.09.06.14	Subsystem Cold Plates and Survival Heaters	64.33	12.87	77.20	9	

Table D 1. *Continued*

WBS1	WBS1 Desc	WBS2	WBS2 Desc	WBS3 Desc	WBS5	WBS5 Desc	Basic Mass (kg)	MGA (kg)	Predicted Mass (kg)	TRL	Example Model, Manufacturer, and Part No. if available
				ISIM Structural System	05.09.07.01	ISIM Box	98.07	24.52	122.59		
					05.09.07.02	Translation Table Assembly (TTA)	75.26	18.82	94.08		
					05.09.07.02.02	LXM Struts	5.06	1.27	6.33		
					05.09.07.02.03	LXM Strut Fittings	4.95	1.24	6.19		
					05.09.07.02.04	Translation Table Hold Down Mechanisms (Launch Locks)	1.02	0.31	1.33	9	
					05.09.07.03.01	Horizontal TTA mechanisms	129.00	38.70	167.70		
					05.09.07.03.02	Vertical TTA Mechanisms	19.80	5.94	25.74		
					05.09.07.04	Mounting Plate XGD	58.65	14.66	73.31		
					05.09.07.05	XGD Fine Focus Motor w/ Tilt Offset	7.00	2.10	9.10		
					05.09.07.01	ISIM Box	98.07	24.52	122.59		
				Lynx X-ray Microcalorimeter (LXM) Instrument	05.09.08.05	LXM Electronics System (includes avionics)	145.94	36.48	182.42		
					05.09.08.07	LXM Thermal Control System (heat pipes)	72.00	18.00	90.00		
					05.09.08.08	LXM Miscellaneous Hardware (includes GSE stays)	24.13	6.03	30.16		
					05.09.08.09	LXM Harnesses	33.78	8.44	42.22		
					05.09.08.10	LXM Instrument Deck Assembly	28.34	7.09	35.43		
					05.09.08.11	LXM Dewar Assembly	163.75	40.94	204.69		
				High Definition X-ray Imager (HDXI) Instrument	05.09.09.07	HDXI Thermal Interface Material	0.25	0.06	0.31		
					05.09.09.08	HDXI Miscellaneous Hardware	3.81	1.14	4.95		
					05.09.09.09	HDXI Harnesses	9.70	3.01	12.70		
					05.09.09.10	HDXI Detector Assembly (DA)	51.60	16.00	67.60		
					05.09.09.11	HDXI Detector Electronics Unit (DEU)	15.02	3.30	18.32		
				X-ray Gratings Detector (XGD) Instrument	05.09.10.07	XGD Assembly	19.24	5.19	24.43		
					05.09.10.08	XGD Detector Electronics Unit (DEU)	38.77	8.14	46.91		
		05.09 Total					**1,166.76**	**293.70**	**1,460.47**		
05 Total							**3,718.89**	**937.77**	**4,656.66**		
06	Spacecraft Element (SCE)	06.07	SCE Structural System	Spacecraft Bus	06.07.01	Spacecraft Bus	361.84	90.46	452.30		
				Interface Struts (OBA/Bus/LMA)	06.07.02.01	Struts	94.34	23.59	117.93		
					06.07.02.02	Strut Fittings	27.48	6.87	34.35		
				Secondary Structures	06.07.03	Secondary Structures	238.78	59.70	298.48		
				Sunshade Door Assembly (SDA)	06.07.04.01	Sunshade Door	32.95	8.24	41.19		
		06.07 Total					**755.40**	**188.85**	**944.24**		
		06.08	SCE Thermal Control System	Heaters, SCE Bus	06.08.01	Heaters, SCE Bus	36.11	7.22	43.33	9	
				Multilayer Insulation (MLI), SCE Bus	06.08.02	Multilayer Insulation (MLI), SCE Bus	44.74	8.95	53.68	9	
				Radiator SCE Bus	06.08.03	Radiator SCE Bus	78.90	15.78	94.68	4 (TRL 9 are available)	
				SSD MLI	06.08.04	SSD MLI	13.73	2.75	16.47	9	
				Heaters, Propulsion Tanks	06.08.05	Heaters, Propulsion Tanks	0.50	0.10	0.60	9	
				MLI, Propulsion Tanks	06.08.06	MLI, Propulsion Tanks	2.50	0.50	3.00	9	
		06.08 Total					**176.47**	**35.29**	**211.76**		
		06.09	SCE Electrical Power System (EPS)	Solar Array Wing (with Boom)	06.09.01	Solar Array Wing (with Boom)	109.00	27.25	136.25	9	
				Solar Array Drive Actuator	06.09.02	Solar Array Drive Actuator	10.00	2.50	12.50	9	
				Integrated Power Electronics	06.09.03	Integrated Power Electronics	59.00	14.75	73.75		
				Secondary Distribution	06.09.04	Secondary Distribution	10.40	2.60	13.00		
				Secondary Batteries	06.09.05	Secondary Batteries	39.00	9.75	48.75		
				Cabling	06.09.06	Cabling	137.00	68.50	205.50		
				Solar Array Deployment Mechanism	06.09.07	Solar Array Deployment Mechanism	10.40	2.60	13.00	9	
		06.09 Total					**374.80**	**127.95**	**502.75**		

Table D 1. *Continued*

WBS1	WBS1 Desc	WBS2	WBS2 Desc	WBS3 Desc	WBS5	WBS5 Desc	Basic Mass (kg)	MGA (kg)	Predicted Mass (kg)	TRL	Example Model, Manufacturer, and Part No. if available
		06.10	SCE Command and Data Handling (C&DH) System	Flight Computer	06.10.01	Flight Computer	22.00	1.10	23.10	8	JPL, Uses BAE Systems RAD750 SBC
				Safe Mode Electronics Unit	06.10.02	Safe Mode Electronics Unit	17.80	2.67	20.47	6	TBD/Custom
				Solid State Recorder	06.10.03	Solid State Recorder	14.00	0.42	14.42	9	EADS Astrium CORECI
				Data Acquisition Unit	06.10.04	Data Acquisition Unit	9.54	0.48	10.02	9	L3 Cincinnati Electronics, DTP-503 Telepak
				MPS Controller	06.10.05	MPS Controller	14.00	2.10	16.10	6	TBD/Custom
				RCS Controller	06.10.06	RCS Controller	14.00	2.10	16.10	6	TBD/Custom
				RW Controller	06.10.07	RW Controller	14.00	2.10	16.10	6	TBD/Custom
				LMA Heater Controller	06.10.08	LMA Heater Controller	23.00	3.45	26.45	6	TBD/Custom
				SC/OBA/ISIM Heater Controller	06.10.09	SC/OBA/ISIM Heater Controller	19.00	2.85	21.85	6	TBD/Custom
				Avionics / Propulsion Heater Controller	06.10.10	Avionics / Propulsion Heater Controller	24.00	3.60	27.60	6	TBD/Custom
				Translation Table Controller	06.10.11	Translation Table Controller	4.00	1.00	5.00	6	PI USA, C-884.6DC
				Doors/Gratings Controller	06.10.12	Doors/Gratings Controller	10.00	1.50	11.50	8	MOOG/Broad Reach
				Instrumentation and Monitoring	06.10.13	Instrumentation and Monitoring	47.30	11.83	59.13	9	Assortment of sensors, temp, press, strain, etc.
				Avionics Cabling	06.10.14	Avionics Cabling	30.00	7.50	37.50	6	TBD/Custom
				Heater and Temp Sensor Cabling	06.10.15	Heater and Temp Sensor Cabling	105.60	26.40	132.00	6	TBD/Custom
		06.10 Total					**368.24**	**69.09**	**437.33**		
		06.11	SCE Communications	Ka Phased Array Antenna	06.11.01	Ka Phased Array Antenna	10.92	2.18	13.10	8	Messenger X-band MER
				X Transponder	06.11.02	X Transponder	6.40	0.19	6.59	9	General Dynamics SDST
				Ka Transceiver	06.11.03	Ka Transceiver	38.40	1.92	40.32	8	Harris Ka-band SDR
				Ka Diplexer	06.11.04	Ka Diplexer	2.00	0.40	2.40	8	Custom Microwave Inc.
				X-Band TWTA	06.11.05	X-Band TWTA	4.00	0.20	4.20	9	Thales, TH4604C
				X-TWT Amp	06.11.06	X-TWT Amp	5.00	0.25	5.25	8	Thales
				Ka-Band TWT	06.11.07	Ka-Band TWT	4.00	0.20	4.20	9	Thales, TH4626C
				Ka-Band TWT Amp	06.11.08	Ka-Band TWT Amp	5.00	0.25	5.25	8	Thales
				Waveguides	06.11.09	Waveguides	5.10	1.02	6.12	6	TBD/Custom
				RF Combiner	06.11.10	RF Combiner	1.20	0.12	1.32	6	TBD/Custom
				RF Switch 1-2	06.11.11	RF Switch 1-2	6.60	0.66	7.26	8	L3 SW-509 MER
				RF Switch 1-3	06.11.12	RF Switch 1-3	1.20	0.12	1.32	8	L3 SW-509 MER
				X-Band Conical Patch Antenna	06.11.13	X-Band Conical Patch Antenna	2.00	0.20	2.20	6	S-band Surrey MER
				X-Band MGA Array	06.11.14	X-Band MGA Array	0.25	0.05	0.30	8	L3 Narda 640,WR90
				Coax Cabling, Misc	06.11.15	Coax Cabling, Misc	11.00	1.65	12.65	6	TBD/Custom
		06.11 Total					**103.07**	**9.42**	**112.49**		
		06.12	SCE Guidance, Navigation and Control (GN&C) System	Coarse Sun Sensor	06.12.01	Coarse Sun Sensor	0.40	0.06	0.46	9	Adcole Course Sun Sensor
				Ultra Fine Sun Sensor	06.12.02	Ultra Fine Sun Sensor	4.00	0.60	4.60	9	Adcole Fine Sun Sensor
				Inertial Measurement Unit	06.12.03	Inertial Measurement Unit	13.50	2.03	15.53	9	Honeywell, Miniature Inertial Measurement Unit (MIMU)
				Reaction Wheel System	06.12.04.01	Reaction Wheels	45.60	6.84	52.44	9	Rockwell Collins, TELDIX RDR 68-3
					06.12.04.02	Reaction Wheel Drive Electronics	7.50	1.13	8.63	9	Rockwell Collins, TELDIX RDR 68-3
					06.12.04.03	Reaction Wheel Isolation System	24.00	3.60	27.60	9	Rockwell Collins, TELDIX RDR 68-3
				Pointing Control and Aspect Determination (PCAD) System	06.12.05.01	Aspect Camera Assembly	42.20	10.55	52.75	9	Ball, CT-601 High Accuracy Star Tracker
					06.12.05.02	Periscope	8.00	1.20	9.20	9	Ball
					06.12.05.03.01	Fiducial Light	0.60	0.09	0.69	9	Ball
					06.12.05.03.02	Fiducial Light Controller Assembly	2.90	0.44	3.34	9	Ball
				Star Tracker System	06.12.06.01	Star Tracker Camera Head (DTU micro ASC)	1.50	0.23	1.73	9	Danish Technical University (DTU)
					06.12.06.02	Star Tracker Double Data Processing Unit (DPU) (Internally Redundant)	1.12	0.17	1.29	9	Danish Technical University (DTU)
		06.12 Total					**151.32**	**26.92**	**178.24**		

Table D 1. *Continued*

WBS1	WBS1 Desc	WBS2	WBS2 Desc	WBS3 Desc	WBS5	WBS5 Desc	Basic Mass (kg)	MGA (kg)	Predicted Mass (kg)	TRL	Example Model, Manufacturer, and Part No. if available
		06.13	SCE Propulsion System	Main Propulsion System (MPS) Engine	06.13.01	Main Propulsion System (MPS) Engine	2.00	0.30	2.30	6	Northrop Grumman MRE-15
				Reaction Control System (RCS)/Attitude Control System (ACS) Engine	06.13.02	Reaction Control System (RCS)/Attitude Control System (ACS) Engine	17.60	2.64	20.24	9	Northrop Grumman MRE-1.0
				Propellant Tanks	06.13.03	Propellant Tanks	60.75	9.11	69.86	5	ATK 80274, modified
				Feed System Components	06.13.04.01	Service Valve	2.55	0.26	2.81	9	Moog C71465-001, Moog C71466-001
					06.13.04.02	Latch Valve	6.50	0.65	7.15	9	Wright Components Inc., 15512-1
					06.13.04.03	Flow Control Orifice	5.46	0.55	6.01		
					06.13.04.04	Filter	1.74	0.17	1.91	9	Vacco F1D10785-01
					06.13.04.05	Pressure Transducer	3.68	0.37	4.05	9	Paine 213-36-450-02
				Miscellaneous Hardware	06.13.05	Miscellaneous Hardware	14.69	3.67	18.37		
		06.13 Total					**114.97**	**17.72**	**132.69**		
		06.14	SCE Propellant	Propellant (N2H4)	06.14.01	Propellant (N2H4)	488.60	-	488.60		
		06.14 Total					**488.60**	**-**	**488.60**		
		06.15	SCE Non Propellant Fluids	Residual Propellant (N2H4)	06.15.01	Residual Propellant (N2H4)	24.40	-	24.40		
				Monoprop Pressurant (GN2)	06.15.02	Monoprop Pressurant (GN2)	23.31	-	23.31		
		06.15 Total					**47.71**	**-**	**47.71**		
		06.16	Payload Adapter	Payload Adapter	06.16.01	Payload Adapter	-	-	-		
		06.16 Total					**-**	**-**	**-**		
06 Total							**2,580.58**	**475.24**	**3,055.82**		
Grand Total							**6,299.47**	**1,413.01**	**7,712.48**		

Notes:
1. Engineering Models (EM) for optics and science instruments + 10% spares assumed for costing
2. TRLs and example models noted where information is available and/or specific items included in DRM
3. For items with identified TRL and no example model, it is assumed parts are commonly available and no technology development is required
4. High TRL radiators available, but with mass impact

E. Work Breakdown Structure

Table E.1. *Lynx* work breakdown structure.

Lynx X-ray Observatory Work Breakdown Structure		
WBS Code	Level	WBS Elements
01	2	**Project Management**
01 01	3	Project Management
01 02	3	Project Planning and Control
01 03	3	Configuration Management
02	2	**Systems Engineering**
02 01	3	Systems Engineering Management
02 02	3	Requirements Development & Verification
02 03	3	System and Mission Analysis
03	2	**Safety and Mission Assurance**
03 01	3	Safety and Mission Assurance Management
03 02	3	Reliability Analysis
03 03	3	Quality Assurance
03 04	3	Mission Safety
04	2	**Science and Technology**
04 01	3	Science and Technology Management
04 02	3	Science Support (Phase A - D)
04 03	3	X-ray Mirror Assembly (XMA) Technology Development
04 04	3	Lynx X-Ray Microcalorimeter (LXM) Technology Development
04 05	3	High Definition X-ray Imager (HDXI) Technology Development
04 06	3	X-Ray Grating Spectrometer (XGS (Array (XGA) + Detector (XGD)) Technology Development
05	2	**X-ray Telescope (XRT)**
05 01	3	XRT Management
05 02	3	XRT Systems Engineering
05 03	3	XRT Product Assurance
05 04	3	XRT Integration and Test
05 05	3	XRT Calibration
05 06	3	Lynx Mirror Assembly (LMA)
05 06 01	4	LMA Management
05 06 02	4	LMA Systems Engineering
05 06 03	4	LMA Integration & Test (includes calibration)
05 06 04	4	Reserved
05 06 05	4	Reserved
05 06 06	4	LMA Ground Support Equipment (GSE)
05 06 07	4	X-ray Mirror Modules
05 06 07 01	5	XMA Management
05 06 07 02	5	XMA Systems Engineering
05 06 07 03	5	XMA Integration and Test (includes calibration)
05 06 07 04	5	XMA Optical Elements (segments, modules)
05 06 07 05	5	XMA Meta-Shell Forward / Aft Ring Structure
05 06 07 06	5	XMA Spider Structure
05 06 08	4	LMA Thermal Control
05 06 08 01	5	LMA MLI
05 06 08 02	5	LMA Collimators
05 06 08 02 01	6	LMA Pre-Collimator Assembly
05 06 08 02 02	6	LMA Post-Collimator Assembly
05 06 08 03	5	Spider Heaters
05 06 09	4	LMA Contamination Control Door Assemblies
05 06 09 01	5	Forward Contamination Door (FCD)
05 06 09 01 01	6	FCD Structure
05 06 09 01 02	6	FCD Motor
05 06 09 01 03	6	FCD Motor Mount
05 06 09 01 04	6	Forward Door Hold Down Mechanisms (Launch Locks)
05 06 09 02	5	Aft Contamination Door (ACD)
05 06 09 02 01	6	Aft Contamination Door (ACD) Structure
05 06 09 02 02	6	ACD Motor
05 06 09 02 03	6	ACD Motor Mount
05 06 09 02 04	6	Aft Door Hold Down Mechanisms (Launch Locks)

Table E.1. *Lynx* work breakdown structure. *Continued*

05	06	10					4	LMA Barrel Assembly
05	06	10	01				5	Barrel Structure
05	06	10	02				5	Subsystem Ring
05	06	10	03				5	LMA Flexures
05	07						3	X-ray Gratings Array (XGA)
05	07	01					4	XGA Management
05	07	02					4	XGA Systems Engineering
05	07	03					4	XGA Integration & Test (includes calibration)
05	07	04					4	XGA Controller
05	07	05					4	XGA Ground Support Equipment (GSE)
05	07	06					4	XGA Elements (gratings, facets)
05	07	07					4	XGA Grating Array Structure (GAS)
05	07	08					4	Grating Array Motor
05	07	09					4	Grating Array Motor Mount
05	07	10					4	Gratings Array Structure Hold Down Mechanisms (Launch Locks)
05	08						3	Optical Bench Assembly (OBA)
05	08	01					4	OBA Management
05	08	02					4	OBA Systems Engineering
05	08	03					4	OBA Integration & Test
05	08	04					4	OBA GSE
05	08	05					4	Magnetic Broom
05	08	06					4	OBA TCS
05	08	06	01				5	OBA Heaters
05	08	06	02				5	OBA MLI
05	08	06	03				5	OBA OSR Support Structure
05	08	06	04				5	Observatory Sunshade
05	08	07					4	OBA Structure
05	09						3	Integrated Science Instrument Module (ISIM)
05	09	01					4	ISIM Management
05	09	02					4	ISIM Systems Engineering
05	09	03					4	ISIM Integration & Test
05	09	04					4	ISIM Electronics System
05	09	05					4	ISIM GSE
05	09	06					4	ISIM TCS
05	09	06	01				5	TTA Heaters
05	09	06	02				5	ISIM Heaters
05	09	06	03				5	TTA MLI
05	09	06	04				5	ISIM MLI
05	09	06	05				5	Radiator, LXM Cryostat
05	09	06	06				5	Radiator, LXM Cryocooler
05	09	06	07				5	Radiator, LXM Electronics 1
05	09	06	08				5	Radiator, LXM Electronics 2
05	09	06	09				5	Radiator, HDXI Detector Assembly
05	09	06	10				5	Radiator, HDXI DEU
05	09	06	11				5	Radiator, XGD Assembly
05	09	06	12				5	Radiator, XGD DEU
05	09	06	13				5	Radiator, Mounting Plate XGD
05	09	06	14				5	Subsystem Cold Plates and Survival Heaters
05	09	07					4	ISIM Structural System
05	09	07	01				5	ISIM Box
05	09	07	02				5	Translation Table Assembly (TTA)
05	09	07	02	01			6	TTA Mounting Plate
05	09	07	02	02			6	LXM Struts
05	09	07	02	03			6	LXM Strut Fittings
05	09	07	02	04			6	Translation Table Hold Down Mechanisms (Launch Locks)
05	09	07	03				5	TTA Mechanisms
05	09	07	03	01			6	Horizontal TTA mechanisms
05	09	07	03	02			6	Vertical TTA Mechanisms
05	09	07	04				5	Mounting Plate XGD
05	09	07	05				5	XGD Fine Focus Motor w/ Tilt Offset

Table E.1. *Lynx* work breakdown structure. *Continued*

05	09	08			4	Lynx X-ray Microcalorimeter (LXM) Instrument
05	09	08	01		5	LXM Management
05	09	08	02		5	LXM Systems Engineering
05	09	08	03		5	LXM Integration & Test (includes calibration)
05	09	08	04		5	LXM Software
05	09	08	05		5	LXM Electronics System (includes avionics)
05	09	08	06		5	LXM Ground Support Equipment (GSE)
05	09	08	07		5	LXM Thermal Control System (heat pipes)
05	09	08	08		5	LXM Miscellaneous Hardware (includes GSE stays)
05	09	08	09		5	LXM Harnesses
05	09	08	10		5	LXM Instrument Deck Assembly
05	09	08	11		5	LXM Dewar Assembly
05	09	09			4	High Definition X-ray Imager (HDXI) Instrument
05	09	09	01		5	HDXI Management
05	09	09	02		5	HDXI Systems Engineering
05	09	09	03		5	HDXI Integration & Test (includes calibration)
05	09	09	04		5	HDXI Software
05	09	09	05		5	HDXI Avionics
05	09	09	06		5	HDXI Ground Support Equipment (GSE)
05	09	09	07		5	HDXI Thermal Interface Material
05	09	09	08		5	HDXI Miscellaneous Hardware
05	09	09	09		5	HDXI Harnesses
05	09	09	10		5	HDXI Detector Assembly (DA)
05	09	09	11		5	HDXI Detector Electronics Unit (DEU)
05	09	10			4	X-ray Gratings Detector (XGD) Instrument
05	09	10	01		5	XGD Management
05	09	10	02		5	XGD Systems Engineering
05	09	10	03		5	XGD Integration & Test (includes calibration)
05	09	10	04		5	XGD Software
05	09	10	05		5	XGD Ground Support Equipment (GSE)
05	09	10	06		5	XGD Miscellaneous Hardware
05	09	10	07		5	XGD Assembly
05	09	10	07	01	6	XGD Electronics
05	09	10	07	02	6	XGD Thermal
05	09	10	07	03	6	XGD Structures
05	09	10	07	04	6	XGD Mechanisms
05	09	10	08		5	XGD Detector Electronics Unit (DEU)
05	09	10	08	01	6	XGD DEU Avionics
05	09	10	08	02	6	XGD DEU Power
05	09	10	08	03	6	XGD DEU Thermal
05	09	10	08	04	6	XGD DEU Structures
05	10	12			3	Reserved
05	11	13			3	Reserved
05	12	14			3	Lynx Calibration Facility
06					**2**	**Spacecraft Element (SCE)**
06	01				3	SCE Management
06	02				3	SCE Systems Engineering
06	03				3	SCE Product Assurance
06	04				3	SCE Integration & Test
06	05				3	SCE Flight Software (FSW)
06	06				3	SCE Ground Support Equipment (GSE)
06	07				3	SCE Structural System
06	07	01			4	Spacecraft Bus
06	07	02			4	Interface Struts (OBA/Bus/LMA)
06	07	02	01		5	Struts
06	07	02	02		5	Strut Fittings
06	07	03			4	Secondary Structures
06	07	04			4	Sunshade Door Assembly (SDA)
06	07	04	01		5	Sunshade Door
06	07	04	02		5	SSD Motor
06	07	04	03		5	SSD Motor Mount

Table E.1. *Lynx* work breakdown structure. *Continued*

06 08	3	SCE Thermal Control System
06 08 01	4	Heaters, SCE Bus
06 08 02	4	Multilayer Insulation (MLI), SCE Bus
06 08 03	4	Radiator SCE Bus
06 08 04	4	SSD MLI
06 08 05	4	Heaters, Propulsion Tanks
06 08 06	4	MLI, Propulsion Tanks
06 09	3	SCE Electrical Power System (EPS)
06 09 01	4	Solar Array Wing (with Boom)
06 09 02	4	Solar Array Drive Actuator
06 09 03	4	Integrated Power Electronics
06 09 04	4	Secondary Distribution
06 09 05	4	Secondary Batteries
06 09 06	4	Cabling
06 09 07	4	Solar Array Deployment Mechanism
06 10	3	SCE Command and Data Handling (C&DH) System
06 10 01	4	Flight Computer
06 10 02	4	Safe Mode Electronics Unit
06 10 03	4	Solid State Recorder
06 10 04	4	Data Acquisition Unit
06 10 05	4	MPS Controller
06 10 06	4	RCS Controller
06 10 07	4	RW Controller
06 10 08	4	LMA Heater Controller
06 10 09	4	SC/OBA/ISIM Heater Controller
06 10 10	4	Avionics / Propulsion Heater Controller
06 10 11	4	Translation Table Controller
06 10 12	4	Doors/Gratings Controller
06 10 13	4	Instrumentation and Monitoring
06 10 14	4	Avionics Cabling
06 10 15	4	Heater and Temp Sensor Cabling
06 11	3	SCE Communications
06 11 01	4	Ka Phased Array Antenna
06 11 02	4	X Transponder
06 11 03	4	Ka Transceiver
06 11 04	4	Ka Diplexer
06 11 05	4	X-Band TWTA
06 11 06	4	X-TWT Amp
06 11 07	4	Ka-Band TWT
06 11 08	4	Ka-Band TWT Amp
06 11 09	4	Waveguides
06 11 10	4	RF Combiner
06 11 11	4	RF Switch 1-2
06 11 12	4	RF Switch 1-3
06 11 13	4	X-Band Conical Patch Antenna
06 11 14	4	X-Band MGA Array
06 11 15	4	Coax Cabling, Misc
06 12	3	SCE Guidance, Navigation and Control (GN&C) System
06 12 01	4	Coarse Sun Sensor
06 12 02	4	Ultra Fine Sun Sensor
06 12 03	4	Inertial Measurement Unit
06 12 04	4	Reaction Wheel System
06 12 04 01	5\	Reaction Wheels
06 12 04 02	5	Reaction Wheel Drive Electronics
06 12 04 03	5	Reaction Wheel Isolation System
06 12 05	4	Pointing Control and Aspect Determination (PCAD) System
06 12 05 01	5	Aspect Camera Assembly
06 12 05 02	5	Periscope
06 12 05 03	5	Fiducial Light Assembly
06 12 05 03 01	6	Fiducial Light
06 12 05 03 02	6	Fiducial Light Controller Assembly

Table E.1. *Lynx* work breakdown structure. *Continued*

06	12	06		4		Star Tracker System
06	12	06	01	5		Star Tracker Camera Head (DTU micro ASC)
06	12	06	02			Star Tracker Double Data Processing Unit (DPU) (Internally Redundant)
06	13			3		SCE Propulsion System
06	13	01		4		Main Propulsion System (MPS) Engine
06	13	02		4		Reaction Control System (RCS)/Attitude Control System (ACS) Engine
06	13	03		4		Propellant Tanks
06	13	04		4		Feed System Components
06	13	04	01	5		Service Valve
06	13	04	02	5		Latch Valve
06	13	04	03	5		Flow Control Orifice
06	13	04	04	5		Filter
06	13	04	05	5		Pressure Transducer
06	13	05		4		Miscellaneous Hardware
06	14			3		SCE Propellant
06	14	01		4		Propellant (N2H4)
06	15			3		SCE Non Propellant Fluids
06	15	01		4		Residual Propellant (N2H4)
06	15	02		4		Monoprop Pressurant (GN2)
06	16			3		Payload Adapter
07				**2**		**Mission Operations**
07	01			**3**		Management
07	02			**3**		Systems Engineering
07	03			**3**		Science Operations (Phase E - F)
07	04			**3**		Science Data Systems
07	05			**3**		Science Instrument Teams (Phase E - F)
07	06			**3**		Operations
07	07			**3**		Grants Program
08				**2**		**Launch Vehicle Services**
08	01			3		Launch Vehicle Liaison
08	02			3		Launch Vehicle Integration and Test
09				**2**		**Ground Systems**
09	01			**3**		Management
09	02			**3**		Systems Engineering
09	03			**3**		Science Operations (Phase A - D)
09	04			**3**		Science Data System
09	05			**3**		Science Instrument Teams (Phase A - D)
09	06			**3**		Operations
09	07			**3**		Grants Program
10				**2**		**Systems Integration and Test**
10	01			3		I&T Management
10	02			3		I&T Systems Engineering
10	03			3		Lynx Observatory [XRT+SCE] Assembly, Integration & Test
10	04			3		Observatory I&T GSE
10	05			3		Observatory I&T Facilities
10	06			3		Observatory Test and Checkout
11				**2**		**Public Outreach**

Acronyms

$FY	Fiscal Year Dollars
$RY	Real Year Dollars
AA	Associate Administrator
ACH	Atomic Cooling Halos
ACIS	Application Specific Integrated Circuit
ACO	Advanced Concepts Office
ACS	Attitude Control System
ACT	Atacama Cosmology Telescope
ACTDP	Advanced Cryocooler Development Program
AD2	Advancement Degree of Difficulty
ADA	Aft Door Assembly
ADR	Adiabatic Demagnetization Refrigerator
AGN	Active Galactic Nuclei
AI&T	Assembly Integration and Test
AIAA	American Institute of Aeronautics and Astronautics
Al	Aluminum
ALD	Atomic Layer Deposition
ALMA	Atacama Large Millimeter/submillimeter Array
AO	Announcement of Opportunity
APD	Astrophysics Projects Division
APRA	Astrophysics Research and Analysis
APS	Active Pixel Sensor
ASCA	Advanced Satellite for Cosmology and Astrophysics
ASI	Italian Space Agency
ASIC	Application-Specific Integrated Circuit
ASM	Acquisition Strategy Meeting
BBXRT	Broadband X-ray Telescope
BDD	Block Definition Diagrams
BH	Black Hole
BHMF	Black Hole Mass Function
BOE	Basis of Estimate
C&DH	Command and Data Handling
CADR	Continuous Adiabatic Demagnetization Refrigerator
CADRe	Cost Analysis and Data Requirements
CAN	Cooperative Agreement Notice
CAP	Command Action Procedure
CAT	Critical Angle Transmission
CAT-XGS	Critical Angle Transmission Gratings
CATE	Cost and Technical Evaluation
CC	Core Collapse
CCD	Charge-Coupled Device
CCO	Central Compact Object
CCSDS	Consultative Committee for Space Data Systems
CDR	Critical Design Review
CE	Chief Engineer
CER	Cost-Estimating Relationship
CGM	Circumgalactic Medium
CIL	Critical Items List
CL	Confidence Level
CLA	Coupled Loads
CME	Coronal Mass Ejection
CMOS	Complementary Metal-Oxide Semiconductor
COBE	Cosmic Background Explorer
CoCoMo	Constructive Cost Model
COS	Cosmic Origins Spectrograph
COTS	Commercial Off-The-Shelf
CPR	Critical Path Reserve
CTE	Coefficient of Thermal Expansion
CTO	Chandra-type Orbit
CV	Coefficient of Variation
CXB	Cosmic X-Ray Background
DD	Double-Degenerate
DDT&E	Design, Development, Test, and Evaluation
DEEP	Digital Electronics and Event Processor
DEM	Differential Emission Measure
DEU	Detector Electronics Unit
DM	Dark Matter
DOF	Degrees of Freedom
DRIE	Deep Reactive-Ion Etching
DRM	Design Reference Mission
DSN	Deep Space Network
EAGLE	Evolution and Assembly of GaLaxies and their Environments
EDU	Engineering Development Unit
EEE	Electrical, Electronic, and Electromechanical
EGSE	Electrical Ground Support Equipment
ELT	Extremely Large Telescopes
EM	Electromagnetic (radiation, probe)
EM	Engineering Model
EMA	Enhanced Main Array

EMC	Electromagnetic Compatibility
EMI	Electromagnetic Interference
EOB	Extendable Optical Bench
EOL	End-of-Life
EOR	Epoch of Reionization
EPB	Event Processing Board
EPS	Electrical Power System
ERP	Event Recognition Processor
ESA	European Space Agency
ESLOC	Equivalent Source Lines of Code
ESO	European Southern Observatory
ETU	Engineering Test Unit
EUV	Extreme Ultraviolet
EW	Equivalent Width
FDA	Forward Door Assembly
FEM	Finite Element Model
FEMB	Front-End Motherboard
FIRE	Feedback In Realistic Environments
FMEA	Failure Mode and Effects Analysis
FOM	Figure of Merit
FOT	Flight Operations Team
FOV	Field of View
FPA	Focal Plane Assembly
FPGA	Field Programmable Gate Array
FSW	Flight Software
FTE	Full-Time Equivalent
FTS	Fiducial Transfer System
FU	Flight Unit
FWHM	Full Width at Half Maximum
FY	Fiscal Year
GA	Grating Array
GAO	Government Accountability Office
GAS	Grating Array Structure
GDS	Ground Data Systems
GMC	Giant Molecular Cloud
GN&C	Guidance, Navigation, and Control
GO	General Observer
GOES	Geostationary Operational Environmental Satellite
GOT	Ground Operations Team
GPI	Gemini Planet Imager
GPR	Goddard Procedural Requirements
GPU	Graphics Processing Unit
GR&A	Ground Rules and Assumptions
GSE	Ground Support Equipment
GSFC	Goddard Space Flight Center
GW	Gravitational Wave
HAST	High Accuracy Star Tracker
HDXI	High Definition X-ray Imager
HEMT	High-Electron Mobility Transistor
HEO	High-Earth Orbit
HERA	Hydrogen Epoch of Reionization Array
HETG	High-Energy Transmission Grating
HETGS	High-Energy Transmission Grating Spectrometer
HiCIAO	High-Contrast Coronographic Imager for Adaptive Optics
HNA	HF/Nitric/Acetic Acid
HOD	Halo Occupation Distribution
HPD	Half-Power Diameter
HQ	Headquarters
HRMA	High-Resolution Mirror Assembly
HST	Hubble Space Telescope
I&T	Integration and Test
IBD	Internal Block Diagram
ICD	Interface Control Document
ICE	Independent Cost Estimate
IDL	Instrument Design Lab
IFU	Integral Field Unit
IGM	Intergalactic Medium
IMAGE	Imager for Magnetopause-to-Aurora Global Exploration
IMF	Initial Mass Function
INAF	Instituto Nazionale Di Astrofisica
INTEGRAL	INTErnational Gamma-Ray Astrophysics Laboratory
IR	Infrared
IRAS	Infrared Astronomical Satellite
IRD	Interface Requirements Document
IRU	Inertial Reference Unit
ISFM	Internal Scientist Funding Mode
ISIM	Integrated Science Instrument Module
ISM	Interstellar Medium
ISO	Infrared Space Observatory
ITA	Independent Technical Authority
IXO	International X-ray Observatory

JATIS	Journal of Astronomical Telescopes, Instruments, and Systems
JPL	Jet Propulsion Laboratory
JWST	James Webb Space Telescope
KDP	Key Decision Point
KSC	Kennedy Space Center
KSLOC	Kilo Source Lines of Code
L1	Level 1 (requirements)
L2	Level 2 (requirements)
L2	Sun-Earth Lagrangian L_2 point
LADEE	Lunar Atmosphere and Dust Environment Explorer
LCR	Lifecycle Review
LDRO	Lunar Distant Retrograde Orbit
LEO	Low-Earth Orbit
LETG	Low-Energy Transmission Grating
LIGO	Laser Interferometer Gravitational-Wave Observatory
LISA	Laser Interferometer Space Antenna
LL	Lincoln Laboratory
LLCD	Lunar Laser Communication Demonstration
LMA	Lynx Mirror Assembly
LMAT	Lynx Mirror Architecture Trade
LMC	Large Magellanic Cloud
LRD	Launch Readiness Date
LSC	Lynx Science Center
LSE	Lead Systems Engineer
LSF	Line Spread Function
LSP	Launch Services Program
LSS	Large Scale Structure
LSST	Large Synoptic Survey Telescope
LV	Launch Vehicle
LXM	Lynx X-ray Microcalorimeter
LXO	Lynx X-ray Observatory
MA	Main Array
MAC	Mass Acceleration Curve; Molecular Absorber Coating
MBSE	Model-Based Systems Engineering
MCR	Mission Concept Review
MCR	MCR Technologies, LLC
MDL	Mission Design Lab
MDR	Mission Definition Review
MEB	Main Electronic Box
MEL	Master Equipment List
MEM	Meteoroid Engineering Model
MEMS	Micro-Electrical Mechanical Systems
MGA	Mass Growth Allowance
MGSE	Mechanical Ground Support Equipment
MIMU	Miniature Inertial Measurement Unit
MIRI	Mid-Infrared Instrument
MIT	Massachusetts Institute of Technology
MLI	Multilayer Insulation
MOE	Measure of Effectiveness
MOP	Measure of Performance
MOS	Mission Operations Systems
MPE	Max Planck Institute for Extraterrestrial Physics
MPS	Main Propulsion System
MSE	Mission Systems Engineer
MSFC	Marshall Space Flight Center
MUSE	Multi Unit Spectroscopic Explorer
MW	Milky Way
MXS	Modulated X-ray Source
ngVLA	Next Generation Very Large Array
NICER	Neutron star Interior Composition Explorer
NICM	NASA Instrument Cost Model
NIR	Near-Infrared
NPR	NASA Procedural Requirements
NS	Neutron Star
NSL	NASA Launch Services
OAB	Astronomical Observatory of Brera
OBA	Optical Bench Assembly
OBC	Onboard Computer
OBF	Optical Blocking Filter
OCC	Operations Control Center
ODC	Other Direct Costs
OGRE	Off-plane Grating Rocket Experiment
OIR	Optical Infrared
OP	Off-Plane
OP-XGS	Off-Plane X-ray Grating Spectrometer
OPG	Off-Plane Gratings
ORR	Operational Readiness Review
OSR	Optical Solar Reflector
OWG	Optics Working Group
PBS	Product Breakdown Structure
PCAD	Pointing Control and Aspect Determination

PCEC	Project Cost Estimating Capability
PCOS	Physics of the Cosmos
PDR	Preliminary Design Review
PEL	Power Equipment List
PLATO	PLAnetary Transits and Oscillations of stars
PM	Project Management
POP	III Population III
PRICE	Programmed Review of Information for Costing and Evaluation
PS	Project Scientist
PSF	Point Spread Function
PSU	Pennsylvania State University
PZT	Lead Zirconate Titanate
QE	Quantum Efficiency
RB	Reverse Brayton
RCS	Reaction Control System
REDSTAR	Resource Data Analysis and Retrieval
RFP	Request for Proposal
RGS	Reflection Grating Spectrometer
RM	Relative Motion
RMS	Root Mean Square
ROIC	Readout Integrated Circuit
ROSAT	Roentgen Satellite
ROSES	Research Opportunities in Space and Earth Sciences
RRM	Risk Reduction Margin
RTF	Roman Technology Fellowship
RWA	Reaction Wheel Assembly
RXTE	Rossi X-ray Timing Explorer
S&MA	Safety and Mission Assurance
SAO	Smithsonian Astrophysical Observatory
SAT	Strategic Astrophysics Technology
SCaN	Space Communications and Navigation
SCE	Spacecraft Element
SD	Single-Degenerate
SDO	Solar Dynamics Observatory
SDSS	Sloan Digital Sky Surveys
SE	Systems Engineering
SE-L2	Sun-Earth L2
SE&I	Systems Engineering and Integration
SEMP	Systems Engineering Management Plan
SFR	Star Formation Rate
SI	Science Instrument
SiGe HBT	Silicon-Germanium Heterojunction Bipolar Transistor
SiO2	Silica
SIR	System Integration Review
SKA	Square Kilometer Array
SLOC	Software Lines of Code
SLS	Space Launch System
SLTF	Stray Light Test Facility
SMBH	Supermassive Black Hole
SMC	Small Magellanic Cloud
SMD	Science Mission Directorate
SME	Subject Matter Expert
SMEU	Safe Mode Electronics Unit
SMO	Silicon Meta-shell Optics
SN	Supernova
SNe	Supernovae
SNR	Supernova Remnant
SOA	State of the Art
SOCM	Space Operations Cost Model
SOHO	Solar and Heliospheric Observatory
SOI	Silicon-On-Insulator
SOT	Science Operations Team
SPHERE	Spectro-Polarimetric High-contrast Exoplanet REsearch
SQUID	Superconducting Quantum Interference Device
SRB	Standing Review Board
SRI	Sarnoff Research Institute
SRR	Systems Requirement Review
SSDIF	Systems Development and Integration Facility
SSS	Shell Supporting Structure
Pan-STARRS	Panoramic Survey Telescope and Rapid Response System
STDT	Science and Technology Definition Team
STM	Science Traceability Matrix
SWG	Science Working Group
Swift/BAT	Swift/Burst Alert Telescope
SXS	Soft X-ray Spectrometer
SysML	Systems Modeling Language
SZ	Sunyaev-Zeldovich
TBD	To Be Determined
TBR	To Be Resolved
TCS	Thermal Control System

TDE	Tidal Disruption Events
TDM	Time-Division Multiplexing
TES	Transition-Edge Sensor
TESS	Transiting Exoplanet Survey Satellite
TGCAT	Transmission Grating Data Archive and Catalog
ToO	Target of Opportunity
TPM	Technical Performance Measure
TRL	Technology Readiness Level
TT&C	Telemetry, Tracking, and Command
TTA	Translation Table Assembly
TTI	Transfer Trajectory Insertion
TWINS	Two Wide-Angle Imaging Neutral-Atom Spectrometers
UAH	University of Alabama in Huntsville
UFO	Ultra-Fast Outflow
UHR	Ultra-High-Resolution
UHRA	Ultra-High-Resolution Array
ULX	Ultraluminous X-ray
USAF	United States Air Force
UV	Ultraviolet
VLT	Very Large Telescope
V&V	Verification and Validation
W-I	Wolter Type I
W-S	Wolter-Schwarzchild
WBS	Work Breakdown Structure
WFIRST	Wide-Field Infrared Survey Telescope
WFXT	Wide Field X-ray Telescope
WHIM	Warm Hot Intergalactic Medium
WRXR	Water Recovery X-ray Rocket
WSS	Wolter-Schwarzchild-Saha
WYE	Work Year Equivalent
X-IFU	X-ray Integral Field Unit
XARM	X-ray Astronomy Recovery Mission
XEUV	X-ray-Extreme Ultraviolet
XGA	X-ray Grating Array
XGD	X-ray Grating Detector
XGS	X-ray Grating Spectrometer
XIS	X-ray Imaging Spectrometer
XLF	X-ray Luminosity Function
XMA	X-ray Mirror Assembly
XMM	X-ray Multi-Mirror
XRB	X-ray Binaries
XRCF	X-ray and Cryogenic Facility
XRISM	X-Ray Imaging and Spectroscopy Mission
XRT	X-ray Telescope
XUV	X-ray and Extreme Ultraviolet
YSO	Young Stellar Objects
ZnO	Zinc Oxide
μMUX	Microwave SQUID Multiplexer

References

[1] in *Special Section on the* Lynx *X-Ray Observatory, J. Astron. Telesc. Instrum. Syst., 2019, 5(2)*, all of the papers are open source and online at: `https://tinyurl.com/yxrd6w38`

[2] Natarajan, P. et al., 2019, in *"Disentangling nature from nurture: tracing the origin of seed black holes"; Astro2020 science white paper*, `http://tinyurl.com/y3ytdq3e`

[3] Greene, J. E., 2012, Nature Communications, 3, 1304

[4] Gallo, E. et al., 2019, in *"Towards a high accuracy measurement of the local black hole occupation fraction in low mass galaxies"; Astro2020 science white paper*, `http://tinyurl.com/y44u9j4j`

[5] Greene, J. et al., 2019, in *"The Local Relics of of Supermassive Black Hole Seeds"; Astro2020 science white paper*, `http://tinyurl.com/y699fg7r`

[6] Wrobel, J. et al., 2019, in *"Intermediate-Mass Black Holes in Extragalactic Globular Clusters"; Astro2020 science white paper*, `http://tinyurl.com/y68q88dk`

[7] Kormendy, J. & Ho, L. C., 2013, ARA&A, 51, 511

[8] Soltan, A., 1982, MNRAS, 200, 115

[9] Yu, Q. & Tremaine, S., 2002, MNRAS, 335, 965

[10] Martini, P., 2004, Coevolution of Black Holes and Galaxies, 169

[11] Rees, M. J., 1984, ARA&A, 22, 471

[12] Woods, T. E. et al., 2018, arXiv e-prints, arXiv:1810.12310

[13] Fan, X. et al., 2001, AJ, 122, 2833

[14] Willott, C. J. et al., 2010, AJ, 139, 906

[15] Venemans, B. P. et al., 2013, ApJ, 779, 24

[16] Mortlock, D. J. et al., 2011, Nature, 474, 616

[17] Wu, X.-B. et al., 2015, Nature, 518, 512

[18] Bañados, E. et al., 2018, Nature, 553, 473

[19] Smith, A., Bromm, V. & Loeb, A., 2017, Astronomy and Geophysics, 58, no. 3, 3.22

[20] Madau, P., Haardt, F. & Dotti, M., 2014, ApJ, 784, L38

[21] Volonteri, M., 2012, Science, 337, 544

[22] Volonteri, M. & Bellovary, J., 2012, Reports on Progress in Physics, 75, no. 12, 124901

[23] Haiman, Z., 2013, in T. Wiklind, B. Mobasher & V. Bromm, eds., *The First Galaxies*, *Astrophysics and Space Science Library*, vol. 396, 293

[24] Natarajan, P., 2014, General Relativity and Gravitation, 46, 1702

[25] Schleicher, D. R. G., 2018, arXiv e-prints, arXiv:1807.06055

[26] Wise, J. H., 2018, arXiv e-prints, arXiv:1807.06080

[27] Barkana, R. & Loeb, A., 2001, Phys. Rep., 349, 125

[28] Haiman, Z. & Loeb, A., 2001, ApJ, 552, 459

[29] Whalen, D., Abel, T. & Norman, M. L., 2004, ApJ, 610, 14

[30] O'Shea, B. W. et al., 2005, ApJ, 628, L5

[31] Johnson, J. L. & Bromm, V., 2007, MNRAS, 374, 1557

[32] Milosavljević, M. et al., 2009, ApJ, 698, 766

[33] Haiman, Z., 2004, ApJ, 613, 36

[34] Oh, S. P. & Haiman, Z., 2002, ApJ, 569, 558

[35] Lodato, G. & Natarajan, P., 2006, MNRAS, 371, 1813

[36] Lodato, G. & Natarajan, P., 2007, MNRAS, 377, L64

[37] Omukai, K., 2001, ApJ, 546, 635

[38] Shang, C., Bryan, G. L. & Haiman, Z., 2010, MNRAS, 402, 1249

[39] Wolcott-Green, J. & Haiman, Z., 2011, MNRAS, 412, 2603

[40] Wolcott-Green, J., Haiman, Z. & Bryan, G. L., 2017, MNRAS, 469, 3329

[41] Dijkstra, M. et al., 2008, MNRAS, 391, 1961

[42] Visbal, E., Haiman, Z. & Bryan, G. L., 2014, MNRAS, 445, 1056

[43] Regan, J. A. et al., 2017, Nature Astronomy, 1, 0075

[44] Fernandez, R. et al., 2014, MNRAS, 439, 3798

[45] Tanaka, T. L., 2014, Classical and Quantum Gravity, 31, no. 24, 244005

[46] Wise, J. H. et al., 2019, Nature, in press; e-print arXiv:1901.07563

[47] Hirano, S. et al., 2017, Science, 357, 1375

[48] Schauer, A. T. P. et al., 2017, MNRAS, 471, 4878

[49] Inayoshi, K., Li, M. & Haiman, Z., 2018, MNRAS, 479, 4017

[50] Bromm, V. & Loeb, A., 2003, ApJ, 596, 34

[51] Hosokawa, T., Omukai, K. & Yorke, H. W., 2012, ApJ, 756, 93

[52] Hosokawa, T. et al., 2015, ArXiv e-prints, arXiv:1510.01407

[53] Sakurai, Y. et al., 2016, MNRAS, 459, 1137

[54] Haemmerlé, L. et al., 2018, MNRAS, 474, 2757

[55] Alexander, T. & Natarajan, P., 2014, Science, 345, 1330

[56] Inayoshi, K., Haiman, Z. & Ostriker, J. P., 2016, MNRAS, 459, 3738

[57] Sakurai, Y., Inayoshi, K. & Haiman, Z., 2016, MNRAS, 461, 4496

[58] Omukai, K., Schneider, R. & Haiman, Z., 2008, ApJ, 686, 801

[59] Devecchi, B. & Volonteri, M., 2009, ApJ, 694, 302

[60] Ricarte, A. & Natarajan, P., 2018, MNRAS, 481, 3278

[61] Vito, F. et al., 2016, MNRAS, 463, 348

[62] Vito, F. et al., 2018, MNRAS, 473, 2378

[63] Pacucci, F. et al., 2015, MNRAS, 454, 3771

[64] Natarajan, P. et al., 2017, ApJ, 838, 117

[65] Haehnelt, M. G., 1994, MNRAS, 269, 199

[66] Sesana, A., Volonteri, M. & Haardt, F., 2007, MNRAS, 377, 1711

[67] Berti, E. & Volonteri, M., 2008, ApJ, 684, 822

[68] Sesana, A. et al., 2011, Phys. Rev. D, 83, 044036

[69] Klein, A. et al., 2016, Phys. Rev. D, 93, no. 2, 024003

[70] Tanaka, T. & Haiman, Z., 2009, ApJ, 696, 1798

[71] Habouzit, M., Volonteri, M. & Dubois, Y., 2017, MNRAS, 468, 3935

[72] Alvarez, M. et al., 2019, in *"Unique Probes of Reionization with the CMB:From the First Stars to Fundamental Physics"; Astro2020 science white paper*, `http://tinyurl.com/y34ukydz`

[73] Pacucci, F. et al., 2019, in *"Detecting the Birth of Supermassive Black Holes Formed from Heavy Seeds"; Astro2020 science white paper*, `http://tinyurl.com/y4m4bl8j`

[74] Dijkstra, M., Sethi, S. & Loeb, A., 2016, ApJ, 820, 10

[75] Dijkstra, M., Gronke, M. & Sobral, D., 2016, ApJ, 823, 74

[76] Visbal, E. & Haiman, Z., 2018, ApJ, 865, L9

[77] Bellovary, J. et al., 2011, ApJ, 742, 13

[78] Volonteri, M. et al., 2017, ApJ, 849, 155

[79] Ricarte, A. & Natarajan, P., 2018, MNRAS, 474, 1995

[80] Snyder, G. F. et al., 2017, MNRAS, 468, 207, `https://archive.stsci.edu/prepds/illustris/`

[81] Lehmer, B. D. et al., 2016, ApJ, 825, 7

[82] Visbal, E., Haiman, Z. & Bryan, G. L., 2015, MNRAS, 453, 4456

[83] Agarwal, B. et al., 2012, MNRAS, 425, 2854

[84] Driver, S. P. & Robotham, A. S. G., 2010, MNRAS, 407, 2131

[85] Moster, B. P. et al., 2011, ApJ, 731, 113

[86] Mason, C. A., Trenti, M. & Treu, T., 2015, ApJ, 813, 21

[87] Hickox, R. C. et al., 2014, ApJ, 782, no. 1, 9

[88] Chen, C.-T. J. et al., 2013, ApJ, 773, no. 1, 3

[89] Yang, G. et al., 2017, ApJ, 842, no. 2, 72

[90] Powell, M. C. et al., 2018, ApJ, 858, no. 2, 110

[91] Brusa, M. et al., 2010, ApJ, 716, no. 1, 348

[92] Nandra, K. et al., 2015, ApJS, 220, no. 1, 10

[93] LaMassa, S. M. et al., 2016, ApJ, 817, no. 2, 172

[94] Civano, F. et al., 2016, ApJ, 819, no. 1, 62

[95] Luo, B. et al., 2017, ApJS, 228, no. 1, 2

[96] Chen, C. T. J. et al., 2018, MNRAS, 478, no. 2, 2132

[97] Merloni, A. et al., 2012, arXiv e-prints, arXiv:1209.3114

[98] Mereminskiy, I. A. et al., 2018, Astronomy Letters, 44, no. 2, 67

[99] Marchesi, S. et al., 2016, ApJ, 827, no. 2, 150

[100] Merloni, A., Heinz, S. & di Matteo, T., 2003, MNRAS, 345, no. 4, 1057

[101] Gültekin, K. et al., 2019, ApJ, 871, no. 1, 80

[102] Starikova, S. et al., 2011, ApJ, 741, no. 1, 15

[103] Mendez, A. J. et al., 2016, ApJ, 821, no. 1, 55

[104] Allevato, V. et al., 2016, ApJ, 832, no. 1, 70

[105] Plionis, M. et al., 2018, A&A, 620, A17

[106] Yang, G. et al., 2018, MNRAS, 480, no. 1, 1022

[107] Fornasini, F. M. et al., 2018, ApJ, 865, no. 1, 43

[108] Hopkins, P. F. et al., 2005, ApJ, 625, no. 2, L71

[109] Blecha, L. et al., 2018, MNRAS, 478, no. 3, 3056

[110] Risaliti, G., Maiolino, R. & Salvati, M., 1999, ApJ, 522, no. 1, 157

[111] Liu, T. et al., 2017, ApJS, 232, no. 1, 8

[112] Zappacosta, L. et al., 2018, A&A, 618, A28

[113] Stern, D. et al., 2005, ApJ, 631, no. 1, 163

[114] Alexander, D. M. et al., 2008, ApJ, 687, no. 2, 835

[115] Gandhi, P. et al., 2009, A&A, 502, no. 2, 457

[116] Goulding, A. D. et al., 2011, MNRAS, 411, no. 2, 1231

[117] Civano, F. et al., 2015, ApJ, 808, no. 2, 185

[118] Lansbury, G. B. et al., 2017, ApJ, 846, no. 1, 20

[119] Masini, A. et al., 2018, ApJ, 867, no. 2, 162

[120] Lemons, S. M. et al., 2015, ApJ, 805, 12

[121] Foord, A. et al., 2017, ApJ, 841, no. 1, 51

[122] Lee, N. et al., 2019, ApJ, 874, no. 1, 77

[123] Volonteri, M. & Natarajan, P., 2009, MNRAS, 400, 1911

[124] Volonteri, M., 2010, A&A Rev., 18, no. 3, 279

[125] Agarwal, B. et al., 2016, MNRAS, 459, no. 4, 4209

[126] Valiante, R. et al., 2018, MNRAS, 476, 407

[127] Sijacki, D. et al., 2015, MNRAS, 452, no. 1, 575

[128] Pacucci, F., Natarajan, P. & Ferrara, A., 2017, ApJ, 835, no. 2, L36

[129] Dashyan, G. et al., 2018, MNRAS, 473, no. 4, 5698

[130] Dickey, C. et al., 2019, arXiv e-prints, arXiv:1902.01401

[131] Stone, N. C. & Metzger, B. D., 2016, MNRAS, 455, no. 1, 859

[132] Werner, N. et al., 2013, Nature, 502, no. 7473, 656

[133] Urban, O. et al., 2017, MNRAS, 470, no. 4, 4583

[134] De Grandi, S. & Molendi, S., 2001, ApJ, 551, no. 1, 153

[135] Leccardi, A. & Molendi, S., 2008, A&A, 487, no. 2, 461

[136] Madau, P. & Dickinson, M., 2014, ARA&A, 52, 415

[137] Ettori, S. et al., 2015, A&A, 578, A46

[138] Mantz, A. B. et al., 2017, MNRAS, 472, no. 3, 2877

[139] McDonald, M. et al., 2016, ApJ, 826, no. 2, 124

[140] Greene, J. E. et al., 2014, ApJ, 788, no. 1, 54

[141] Powell, M. C. et al., 2018, A&A, 618, A27

[142] Ruszkowski, M. et al., 2019, in *"Supermassive Black Hole Feedback"; Astro2020 science white paper*, `http://tinyurl.com/y6affway`

[143] Churazov, E. et al., 2016, MNRAS, 463, no. 1, 1057

[144] McNamara, B. R. & Nulsen, P. E. J., 2007, ARA&A, 45, 117

[145] Fabian, A. C., 2012, ARA&A, 50, 455

[146] Zhuravleva, I. et al., 2014, Nature, 515, 85

[147] Hitomi Collaboration et al., 2016, Nature, 535, no. 7610, 117

[148] Tombesi, F. et al., 2010, A&A, 521, A57

[149] Allen, S. W. et al., 2006, MNRAS, 372, no. 1, 21

[150] Springel, V., 2005, MNRAS, 364, no. 4, 1105

[151] Henriques, B. M. B. et al., 2015, MNRAS, 451, 2663

[152] Behroozi, P. S., Wechsler, R. H. & Conroy, C., 2013, ApJ, 770, 57

[153] Werk, J. K. et al., 2014, ApJ, 792, 8

[154] Tumlinson, J. et al., 2011, Science, 334, 948

[155] Hummels, C. B. et al., 2013, MNRAS, 430, 1548

[156] Oppenheimer, B. D. et al., 2016, MNRAS, 460, 2157

[157] Nelson, D. et al., 2018, MNRAS, 477, 450

[158] Tumlinson, J., Peeples, M. S. & Werk, J. K., 2017, ARA&A, 55, 389

[159] Rees, M. J. & Ostriker, J. P., 1977, MNRAS, 179, 541

[160] White, S. D. M. & Rees, M. J., 1978, MNRAS, 183, 341

[161] White, S. D. M. & Frenk, C. S., 1991, ApJ, 379, 52

[162] Kereš, D. et al., 2005, MNRAS, 363, 2

[163] Dekel, A. & Birnboim, Y., 2006, MNRAS, 368, 2

[164] Balogh, M. L. et al., 2001, MNRAS, 326, 1228

[165] Martin, C. L., 2005, ApJ, 621, 227

[166] Rupke, D. S., Veilleux, S. & Sanders, D. B., 2005, ApJS, 160, 115

[167] Strickland, D. K. & Heckman, T. M., 2009, ApJ, 697, 2030

[168] Cicone, C. et al., 2014, A&A, 562, A21

[169] Heckman, T. M. & Best, P. N., 2014, ARA&A, 52, 589

[170] Springel, V. & Hernquist, L., 2003, MNRAS, 339, 312

[171] Oppenheimer, B. D. & Davé, R., 2006, MNRAS, 373, 1265

[172] Schaye, J. et al., 2010, MNRAS, 402, 1536

[173] Schaye, J. et al., 2015, MNRAS, 446, 521

[174] Nelson, D. et al., 2018, MNRAS, 475, 624

[175] Hopkins, P. F. et al., 2018, MNRAS, 480, 800

[176] Oppenheimer, B. D. et al., 2018, MNRAS, 481, 835

[177] Anglés-Alcázar, D. et al., 2017, MNRAS, 472, L109

[178] Bower, R. G. et al., 2017, MNRAS, 465, 32

[179] Weinberger, R. et al., 2017, MNRAS, 465, 3291

[180] Davies, J. J. et al., 2018, ArXiv e-prints, arXiv:1810.07696

[181] Schawinski, K. et al., 2014, MNRAS, 440, 889

[182] Bregman, J. N. et al., 2018, ApJ, 862, 3

[183] Keeney, B. A. et al., 2017, ApJS, 230, 6

[184] Peeples, M. S. et al., 2014, ApJ, 786, 54

[185] Shull, J. M., Danforth, C. W. & Tilton, E. M., 2014, ApJ, 796, 49

[186] Sutherland, R. S. & Dopita, M. A., 1993, ApJS, 88, 253

[187] Gupta, A. et al., 2012, ApJ, 756, L8

[188] Fielding, D. et al., 2017, MNRAS, 466, 3810

[189] Hodges-Kluck, E. J., Miller, M. J. & Bregman, J. N., 2016, ApJ, 822, 21

[190] Ji, S., Oh, S. P. & Masterson, P., 2018, arXiv e-prints, arXiv:1809.09101

[191] Butsky, I. S. & Quinn, T. R., 2018, ApJ, 868, 108

[192] Planck Collaboration et al., 2013, A&A, 557, A52

[193] Schaan, E. et al., 2016, Phys. Rev. D, 93, no. 8, 082002

[194] Battaglia, N. et al., 2017, JCAP, 11, 040

[195] Bregman, J. et al., 2019, in *"A Survey of Hot Gas in the Universe"; Astro2020 science white paper*, `http://tinyurl.com/y2d22nye`

[196] Tremblay, G. et al., 2019, in *"Galaxy Winds in the Age of Hyperdimensional Astrophysics"; Astro2020 science white paper*, `http://tinyurl.com/y6sygscu`

[197] Barcons, X. et al., 2017, Astronomische Nachrichten, 338, 153

[198] Nicastro, F. et al., 2018, Nature, 558, 406

[199] Kovács, O. E. et al., 2019, ApJ, 872, 83

[200] Bregman, J. N. et al., 2015, Journal of Astronomical Telescopes, Instruments, and Systems, 1, no. 4, 045003

[201] Qu, Z. & Bregman, J. N., 2018, ApJ, 862, 23

[202] Somerville, R. S. & Davé, R., 2015, ARA&A, 53, 51

[203] Veilleux, S., Cecil, G. & Bland-Hawthorn, J., 2005, ARA&A, 43, no. 1, 769

[204] Schneider, E. E. & Robertson, B. E., 2015, ApJS, 217, no. 2, 24

[205] Schneider, E. E. & Robertson, B. E., 2018, ApJ, 860, no. 2, 135

[206] Schneider, E. E., Robertson, B. E. & Thompson, T. A., 2018, ApJ, 862, no. 1, 56

[207] Tremblay, G. R. et al., 2016, Nature, 534, no. 7606, 218

[208] Tremblay, G. R. et al., 2018, ApJ, 865, no. 1, 13

[209] Behroozi, P. S., Conroy, C. & Wechsler, R. H., 2010, ApJ, 717, 379

[210] Zhang, D., 2018, Galaxies, 6, no. 4, 114

[211] Mac Low, M.-M. & Ferrara, A., 1999, ApJ, 513, no. 1, 142

[212] Martin, C. L., Kobulnicky, H. A. & Heckman, T. M., 2002, ApJ, 574, 663

[213] Thuan, T. X. et al., 2004, ApJ, 606, no. 1, 213

[214] Sormani, M. C. et al., 2018, MNRAS, 481, 3370

[215] Sormani, M. C. & Sobacchi, E., 2019, MNRAS, 486, 215

[216] Oppenheimer, B. D., 2018, MNRAS, 480, 2963

[217] Stevens, A. R. H. et al., 2017, MNRAS, 467, 2066

[218] Miller, M. J., Hodges-Kluck, E. J. & Bregman, J. N., 2016, ApJ, 818, 112

[219] Lehner, N. & Howk, J. C., 2011, Science, 334, 955

[220] Richter, P. et al., 2017, A&A, 607, A48

[221] Kataoka, J. et al., 2018, Galaxies, 6, no. 1, 27

[222] Ponti, G. et al., 2019, Nature, 567, no. 7748, 347

[223] Dobler, G. et al., 2010, ApJ, 717, no. 2, 825

[224] Su, M., Slatyer, T. R. & Finkbeiner, D. P., 2010, ApJ, 724, no. 2, 1044

[225] Crocker, R. M. & Aharonian, F., 2011, Phys. Rev. Lett., 106, no. 10, 101102

[226] Lacki, B. C., 2014, MNRAS, 444, L39

[227] Guo, F. & Mathews, W. G., 2012, ApJ, 756, no. 2, 181

[228] Inoue, Y. et al., 2015, PASJ, 67, no. 3, 56

[229] Revnivtsev, M. et al., 2009, Nature, 458, no. 7242, 1142

[230] Nazé, Y., Rauw, G. & Manfroid, J., 2008, A&A, 483, no. 1, 171

[231] Yadav, R. K. et al., 2016, ApJ, 833, L28

[232] Favata, F. & Micela, G., 2003, Space Sci. Rev., 108, 577

[233] Wright, N. J. et al., 2013, Astronomische Nachrichten, 334, 151

[234] Kuhn, M. A. et al., 2014, ApJ, 787, 107

[235] Kuhn, M. A., Getman, K. V. & Feigelson, E. D., 2015, ApJ, 802, 60

[236] Brickhouse, N. S. et al., 2010, ApJ, 710, 1835

[237] Cleeves, L. I. et al., 2015, ApJ, 799, 204

[238] Owen, J. E., Ercolano, B. & Clarke, C. J., 2011, MNRAS, 412, 13

[239] Mac Low, M.-M. & Klessen, R. S., 2004, Reviews of Modern Physics, 76, 125

[240] Alves, J. & Bouy, H., 2012, A&A, 547, A97

[241] Megeath, S. T. et al., 2012, AJ, 144, no. 6, 192

[242] Megeath, S. T. et al., 2016, AJ, 151, no. 1, 5

[243] Getman, K. V. et al., 2005, ApJS, 160, no. 2, 353

[244] Pravdo, S. H. et al., 2001, Nature, 413, no. 6857, 708

[245] Tsujimoto, M. et al., 2005, ApJS, 160, no. 2, 503

[246] Mamajek, E. E., 2009, in T. Usuda, M. Tamura & M. Ishii, eds., *American Institute of Physics Conference Series*, *American Institute of Physics Conference Series*, vol. 1158, 3–10

[247] Wolk, S. J. & Walter, F. M., 1996, AJ, 111, 2066

[248] Allen, L. E. et al., 2004, ApJS, 154, no. 1, 363

[249] Winston, E. et al., 2010, AJ, 140, no. 1, 266

[250] Townsley, L. K. et al., 2003, ApJ, 593, no. 2, 874

[251] Wolk, S. J. et al., 2002, ApJ, 580, no. 2, L161

[252] Feigelson, E. D. et al., 2005, ApJS, 160, no. 2, 379

[253] Johnstone, C. P. et al., 2015, ApJ, 815, L12

[254] Kochukhov, O. & Lavail, A., 2017, ApJ, 835, L4

[255] Kastner, J. H. et al., 2002, ApJ, 567, no. 1, 434

[256] Brickhouse, N. S. et al., 2010, ApJ, 710, no. 2, 1835

[257] Telleschi, A. et al., 2007, A&A, 468, no. 2, 541

[258] Güdel, M. et al., 2007, A&A, 468, no. 2, 529

[259] Güdel, M. & Telleschi, A., 2007, A&A, 474, no. 2, L25

[260] Curran, R. L. et al., 2011, A&A, 526, A104

[261] Brickhouse, N. S. et al., 2012, ApJ, 760, no. 2, L21

[262] Argiroffi, C. et al., 2009, A&A, 507, no. 2, 939

[263] Sacco, G. G. et al., 2008, A&A, 491, no. 2, L17

[264] Adams, F. C. & Gregory, S. G., 2012, ApJ, 744, no. 1, 55

[265] Donati, J. F. et al., 2007, MNRAS, 380, no. 4, 1297

[266] Günther, H. M. et al., 2007, A&A, 466, no. 3, 1111

[267] Günther, H. M., Huenemoerder, D. P. & Schulz, N. S. S., 2015, Resolving kinematics in young stars

[268] Preibisch, T. et al., 2005, ApJS, 160, 401

[269] Rutledge, R. E. et al., 2000, ApJ, 538, no. 2, L141

[270] Wright, N. J. et al., 2018, MNRAS, 479, no. 2, 2351

[271] Cook, B. A., Williams, P. K. G. & Berger, E., 2014, ApJ, 785, no. 1, 10

[272] Williams, P. K. G., Cook, B. A. & Berger, E., 2014, ApJ, 785, no. 1, 9

[273] Hussain, G. A. J. et al., 2012, MNRAS, 423, 493

[274] Wright, N. J. et al., 2011, ApJ, 743, 48

[275] Lingam, M. & Loeb, A., 2018, JCAP, 5, 020

[276] Johnstone, C. P. et al., 2015, A&A, 577, A28

[277] Garraffo, C., Drake, J. J. & Cohen, O., 2016, ApJ, 833, L4

[278] See, V. et al., 2016, MNRAS, 462, 4442

[279] Cohen, O. et al., 2017, ApJ, 834, 14

[280] Chung, S. M. et al., 2004, ApJ, 606, 1184

[281] Aschwanden, M. J. et al., 2016, Space Sci. Rev., 198, 47

[282] Antonucci, E., Dodero, M. A. & Martin, R., 1990, ApJS, 73, 147

[283] Antonucci, E. et al., 1982, Sol. Phys., 78, 107

[284] Poppenhaeger, K., Schmitt, J. H. M. M. & Wolk, S. J., 2013, ApJ, 773, no. 1, 62

[285] Wolk, S. et al., 2019, in *"X-ray Studies of Exoplanets"; Astro2020 science white paper*, `http://tinyurl.com/y6kqc2h6`

[286] Vidal-Madjar, A. et al., 2003, Nature, 422, no. 6928, 143

[287] Linsky, J. L. et al., 2010, ApJ, 717, no. 2, 1291

[288] Lecavelier des Etangs, A. et al., 2012, A&A, 543, L4

[289] Lavie, B. et al., 2017, A&A, 605, L7

[290] McCray, R. & Fransson, C., 2016, ARA&A, 54, 19

[291] Badenes, C., Maoz, D. & Draine, B. T., 2010, MNRAS, 407, no. 2, 1301

[292] Ferrand, G. & Safi-Harb, S., 2012, Advances in Space Research, 49, no. 9, 1313

[293] Sasaki, M. et al., 2012, A&A, 544, A144

[294] Maggi, P. et al., 2016, A&A, 585, A162

[295] Garofali, K. et al., 2017, MNRAS, 472, no. 1, 308

[296] Dewey, D. et al., 2008, ApJ, 676, no. 2, L131

[297] Bhalerao, J. et al., 2015, ApJ, 800, no. 1, 65

[298] Hitomi Collaboration et al., 2018, PASJ, 70, no. 2, 16

[299] Long, K. S. et al., 2010, ApJS, 187, no. 2, 495

[300] Xi, L. et al., 2019, ApJ, 874, no. 1, 14

[301] Yamaguchi, H. et al., 2016, ApJ, 820, no. 1, L3

[302] Orlando, S. et al., 2015, ApJ, 810, no. 2, 168

[303] Lopez, L. A. et al., 2011, ApJ, 732, no. 2, 114

[304] Vink, J., 2012, A&A Rev., 20, 49

[305] Yamaguchi, H. et al., 2014, ApJ, 785, no. 2, L27

[306] Maoz, D., Mannucci, F. & Nelemans, G., 2014, ARA&A, 52, 107

[307] Nomoto, K. & Leung, S.-C., 2017, *Thermonuclear Explosions of Chandrasekhar Mass White Dwarfs*, 1275

[308] Seitenzahl, I. R. & Townsley, D. M., 2017, *Nucleosynthesis in Thermonuclear Supernovae*, 1955

[309] Yamaguchi, H. et al., 2015, ApJ, 801, no. 2, L31

[310] Martínez-Rodríguez, H. et al., 2017, ApJ, 843, no. 1, 35

[311] Radice, D. et al., 2018, Journal of Physics G Nuclear Physics, 45, no. 5, 053003

[312] Hughes, J. P. et al., 2000, ApJ, 528, no. 2, L109

[313] DeLaney, T. et al., 2010, ApJ, 725, no. 2, 2038

[314] Safi-Harb, S. et al., 2019, in *"High-Resolution X-ray Imaging Studies of Neutron Stars, Pulsar Wind Nebulae and Supernova Remnants""; Astro2020 science white paper*, `http://tinyurl.com/y2sz4mgv`

[315] Faucher-Giguère, C.-A. & Kaspi, V. M., 2006, ApJ, 643, no. 1, 332

[316] Holland-Ashford, T. et al., 2017, ApJ, 844, no. 1, 84

[317] Katsuda, S. et al., 2018, ApJ, 856, no. 1, 18

[318] Marchant, P. et al., 2016, A&A, 588, A50

[319] Zezas, A. et al., 2019, in *"X-ray binaries: laboratories for understanding the evolution of compact objects from their birth to their mergers"; Astro2020 science white paper*, `http://tinyurl.com/y6sqg4oh`

[320] Fragos, T. & McClintock, J. E., 2015, ApJ, 800, no. 1, 17

[321] Qin, Y. et al., 2018, A&A, 616, A28

[322] Qin, Y. et al., 2019, ApJ, 870, no. 2, L18

[323] Bhattacharya, D. & van den Heuvel, E. P. J., 1991, Phys. Rep., 203, no. 1-2, 1

[324] Tauris, T. M. & van den Heuvel, E. P. J., 2006, *Formation and evolution of compact stellar X-ray sources*, vol. 39, 623–665

[325] Farris, B. D. et al., 2014, ApJ, 783, 134

[326] Haiman, Z., 2017, Phys. Rev. D, 96, no. 2, 023004

[327] The LIGO Scientific Collaboration et al., 2018, arXiv e-prints, arXiv:1811.12907

[328] Shoemaker, D. & LIGO Scientific Collaboration, 2019, in *Bulletin of the American Astronomical Society*, *BAAS*, vol. 51, 452

[329] Pooley, D. et al., 2018, ApJ, 859, no. 2, L23

[330] Barnes, J. E. & Hernquist, L., 1996, ApJ, 471, 115

[331] Artymowicz, P. & Lubow, S. H., 1994, ApJ, 421, 651

[332] Artymowicz, P. & Lubow, S. H., 1996, ApJ, 467, L77

[333] MacFadyen, A. I. & Milosavljević, M., 2008, ApJ, 672, 83

[334] Cuadra, J. et al., 2009, MNRAS, 393, 1423

[335] Roedig, C. et al., 2011, MNRAS, 415, 3033

[336] Nixon, C. J., King, A. R. & Pringle, J. E., 2011, MNRAS, 417, L66

[337] Shi, J.-M. et al., 2012, ApJ, 749, 118

[338] D'Orazio, D. J., Haiman, Z. & MacFadyen, A., 2013, MNRAS, 436, 2997

[339] Gold, R. et al., 2014, Phys. Rev. D, 90, no. 10, 104030

[340] Farris, B. D. et al., 2015, MNRAS, 447, L80

[341] Tang, Y., Haiman, Z. & MacFadyen, A., 2018, MNRAS, 476, 2249

[342] Paczynski, B., 1977, ApJ, 216, 822

[343] Roedig, C., Krolik, J. H. & Miller, M. C., 2014, ApJ, 785, no. 2, 115

[344] Reynolds, C. S. & Nowak, M. A., 2003, Phys. Rep., 377, no. 6, 389

[345] Miniutti, G. & Fabian, A. C., 2004, MNRAS, 349, 1435

[346] Dai, X. et al., 2010, ApJ, 709, no. 1, 278

[347] Jiménez-Vicente, J. et al., 2015, ApJ, 806, no. 2, 251

[348] Guerras, E. et al., 2017, ApJ, 836, no. 2, 206

[349] Kocsis, B., Haiman, Z. & Menou, K., 2008, ApJ, 684, 870

[350] Lang, R. N. & Hughes, S. A., 2008, ApJ, 677, 1184

[351] McWilliams, S. T. et al., 2011, Phys. Rev. D, 84, no. 6, 064003

[352] Phinney, E. S., 2009, in *Astro2010 White Paper*, arXiv:0903.0098

[353] Abbott, B. P. et al., 2017, Phys. Rev. Lett., 119, no. 16, 161101

[354] Metzger, B. D., 2017, arXiv e-prints, arXiv:1710.05931

[355] Haggard, D. et al., 2017, ApJ, 848, no. 2, L25

[356] Margutti, R. et al., 2017, ApJ, 848, no. 2, L20

[357] Mooley, K. P. et al., 2018, Nature, 554, no. 7691, 207

[358] Ruan, J. J. et al., 2018, ApJ, 853, no. 1, L4

[359] Margutti, R. et al., 2018, ApJ, 856, no. 1, L18

[360] Piro, L. et al., 2019, MNRAS, 483, no. 2, 1912

[361] Remillard, R. A. & McClintock, J. E., 2006, ARA&A, 44, no. 1, 49

[362] Bright, J. S. et al., 2018, MNRAS, 475, no. 3, 4011

[363] Pooley, D. et al., 2007, ApJ, 661, no. 1, 19

[364] Blaes, O., 2007, in L. C. Ho & J. W. Wang, eds., *The Central Engine of Active Galactic Nuclei*, *Astronomical Society of the Pacific Conference Series*, vol. 373, 75

[365] Event Horizon Telescope Collaboration et al., 2019, ApJ, 875, no. 1, L1

[366] Kara, E. et al., 2019, Nature, 565, no. 7738, 198

[367] Uttley, P. et al., 2014, A&A Rev., 22, 72

[368] Moustakas, L. et al., 2019, in *"Quasar microlensing: Revolutionizing our understanding of quasar structure and dynamics"; Astro2020 science white paper*, `http://tinyurl.com/y5eokw8z`

[369] Krawczynski, H., Chartas, G. & Kislat, F., 2019, ApJ, 870, no. 2, 125

[370] Chartas, G. et al., 2017, ApJ, 837, no. 1, 26

[371] Chartas, G. et al., 2019, in *"A New Era for X-ray Lensing Studies of Quasars and Galaxies"; Astro2020 science white paper*, `http://tinyurl.com/yxwba5la`

[372] Frank, J. & Rees, M. J., 1976, MNRAS, 176, 633

[373] Hills, J. G., 1975, Nature, 254, no. 5498, 295

[374] Rees, M. J., 1988, Nature, 333, no. 6173, 523

[375] Jonker, P. G. et al., 2019, arXiv e-prints, arXiv:1906.12236

[376] Fender, R. & Belloni, T., 2004, ARA&A, 42, no. 1, 317

[377] Auchettl, K., Guillochon, J. & Ramirez-Ruiz, E., 2017, ApJ, 838, no. 2, 149

[378] Komossa, S. & Bade, N., 1999, A&A, 343, 775

[379] Khabibullin, I., Sazonov, S. & Sunyaev, R., 2014, MNRAS, 437, no. 1, 327

[380] Shiokawa, H. et al., 2015, ApJ, 804, no. 2, 85

[381] Guillochon, J. & Ramirez-Ruiz, E., 2015, ApJ, 809, no. 2, 166

[382] Hayasaki, K., Stone, N. & Loeb, A., 2016, MNRAS, 461, no. 4, 3760

[383] Kaspi, S. et al., 2002, ApJ, 574, no. 2, 643

[384] Danehkar, A. et al., 2018, ApJ, 853, no. 2, 165

[385] Miller, J. M. et al., 2006, Nature, 441, no. 7096, 953

[386] Neilsen, J., Remillard, R. A. & Lee, J. C., 2011, ApJ, 737, no. 2, 69

[387] Basu-Zych, A. et al., 2019, in *Bulletin of the American Astronomical Society*, *BAAS*, vol. 51, 70

[388] Mesinger, A., Ferrara, A. & Spiegel, D. S., 2013, MNRAS, 431, 621

[389] NWNH, 2010, *New Worlds, New Horizons in Astronomy and Astrophysics*

[390] Fragos, T. et al., 2013, ApJ, 776, no. 2, L31

[391] Fragos, T. et al., 2013, ApJ, 764, no. 1, 41

[392] Madau, P. & Fragos, T., 2017, ApJ, 840, 39

[393] Mirabel, I. F. et al., 2011, A&A, 528, A149

[394] Kaaret, P., 2014, MNRAS, 440, L26

[395] Pacucci, F. et al., 2014, MNRAS, 443, 678

[396] Das, A. et al., 2017, MNRAS, 469, 1166

[397] McQuinn, M., 2012, MNRAS, 426, 1349

[398] Fialkov, A. et al., 2017, MNRAS, 464, 3498

[399] Ma, Q. et al., 2018, MNRAS, 480, 26

[400] Bahé, Y. M. et al., 2017, MNRAS, 470, 4186

[401] Dolag, K. et al., 2006, MNRAS, 370, no. 2, 656

[402] Cen, R. & Ostriker, J. P., 1999, ApJ, 514, 1

[403] Davé, R. et al., 2001, ApJ, 552, 473

[404] Davé, R. et al., 2010, MNRAS, 408, 2051

[405] Savage, B. D. et al., 2011, ApJ, 731, 14

[406] Danforth, C. W. et al., 2016, ApJ, 817, 111

[407] Fabian, A. C. et al., 2003, MNRAS, 344, L43

[408] Willis, J. P. et al., 2013, MNRAS, 430, no. 1, 134

[409] Mantz, A. et al., 2019, BAAS, 51, no. 3, 279

[410] LSST Dark Energy Science Collaboration, 2012, arXiv e-prints, arXiv:1211.0310

[411] Benson, B. A. et al., 2014, in *Proc. SPIE, Society of Photo-Optical Instrumentation Engineers (SPIE) Conference Series*, vol. 9153, 91531P

[412] De Bernardis, F. et al., 2016, in *Proc. SPIE, Society of Photo-Optical Instrumentation Engineers (SPIE) Conference Series*, vol. 9910, 991014

[413] Ade, P. et al., 2019, JCAP, 2019, no. 2, 056

[414] Stacey, G. J. et al., 2018, in *Proc. SPIE, Society of Photo-Optical Instrumentation Engineers (SPIE) Conference Series*, vol. 10700, 107001M

[415] Abazajian, K. N. et al., 2016, in *CMB-S4 Science Book, First Edition*, arXiv:1610.02743

[416] Mantz, A. et al., 2019, in *"The Future Landscape of High-Redshift Galaxy Cluster Science"; Astro2020 science white paper*, `http://tinyurl.com/yxlj5zwq`

[417] Ettori, S. et al., 2013, arXiv e-prints, arXiv:1306.2322

[418] Pointecouteau, E. et al., 2013, arXiv e-prints, arXiv:1306.2319

[419] Gaspari, M., Ruszkowski, M. & Sharma, P., 2012, ApJ, 746, 94

[420] McDonald, M. et al., 2018, ApJ, 858, 45

[421] Aird, J. et al., 2015, MNRAS, 451, no. 2, 1892

[422] Ehlert, S. et al., 2015, MNRAS, 446, no. 3, 2709

[423] Miller, T. B. et al., 2018, Nature, 556, no. 7702, 469

[424] Jiang, L. et al., 2018, Nature Astronomy, 2, 962

[425] Riess, A. G. et al., 2019, ApJ, 876, no. 1, 85

[426] Abbott, T. M. C. et al., 2018, Phys. Rev. D, 98, no. 4, 043526

[427] Allen, S. W., Evrard, A. E. & Mantz, A. B., 2011, ARA&A, 49, no. 1, 409

[428] Timmes, F. et al., 2019, in *"Catching Element Formation In The Act ; The Case for a New MeV Gamma-Ray Mission: Radionuclide Astronomy in the 2020s"; Astro2020 science white paper*, `http://tinyurl.com/y694lrj3`

[429] Fukugita, M. & Peebles, P. J. E., 2004, ApJ, 616, 643

[430] Gallazzi, A. et al., 2005, MNRAS, 362, 41

[431] Rafelski, M. et al., 2012, ApJ, 755, 89

[432] Lehner, N. et al., 2019, arXiv e-prints, arXiv:1902.10147

[433] Rahmati, A. & Oppenheimer, B. D., 2018, MNRAS, 476, 4865

[434] Cen, R. & Ostriker, J. P., 2006, ApJ, 650, 560

[435] Cen, R., 2012, ApJ, 753, 17

[436] Churazov, E. et al., 2019, BAAS, 51, no. 3, 325

[437] Corrales, L. et al., 2019, in *"Astromineralogy of interstellar dust with X-ray spectroscopy"; Astro2020 science white paper*, `http://tinyurl.com/y4ypjhda`

[438] Jenkins, E. B., 2009, ApJ, 700, no. 2, 1299

[439] Valencic, L. et al., 2019, in *"Probing the Structure of Interstellar Dust from Micron to Kpc Scales with X-ray Imaging"; Astro2020 science white paper*, `http://tinyurl.com/y5cxy45u`

[440] McKee, C. F. & Ostriker, E. C., 2007, ARA&A, 45, no. 1, 565

[441] Heyer, M. & Dame, T. M., 2015, ARA&A, 53, 583

[442] Onus, A., Krumholz, M. R. & Federrath, C., 2018, MNRAS, 479, 1702

[443] Khullar, S. et al., 2019, arXiv e-prints, arXiv:1902.00934

[444] Goodman, A. A. et al., 1998, ApJ, 504, no. 1, 223

[445] Rathborne, J. M. et al., 2015, ApJ, 802, no. 2, 125

[446] Uehara, K. et al., 2017, in R. M. Crocker, S. N. Longmore & G. V. Bicknell, eds., *The Multi-Messenger Astrophysics of the Galactic Centre*, *IAU Symposium*, vol. 322, 162–163

[447] Federrath, C. et al., 2016, ApJ, 832, no. 2, 143

[448] Churazov, E. et al., 2017, MNRAS, 465, 45

[449] Churazov, E. et al., 2019, in *"Probing 3D Density and Velocity Fields of ISM in Centers of Galaxies with Future X-Ray Observations"; Astro2020 science white paper*, `http://tinyurl.com/y6bg3lr5`

[450] Lee, J. C. & Ravel, B., 2005, ApJ, 622, 970

[451] Lee, J. C. et al., 2009, ApJ, 702, 970

[452] Corrales, L. R. et al., 2016, MNRAS, 458, 1345

[453] Hoffman, J. & Draine, B. T., 2016, ApJ, 817, 139

[454] Zeegers, S. T. et al., 2017, A&A, 599, A117

[455] Overbeck, J. W., 1965, ApJ, 141, 864

[456] Mathis, J. S. & Lee, C.-W., 1991, ApJ, 376, 490

[457] Draine, B. T., 2003, ApJ, 598, 1026

[458] Pooley, D. et al., 2019, in *"The Most Powerful Lenses in the Universe: Quasar Microlensing as a Probe of the Lensing Galaxy"; Astro2020 science white paper*, `http://tinyurl.com/yyvfejdk`

[459] Calzetti, D. et al., 2019, in *"How Do Stars Form? Open Questions on the Stellar Initial Mass Function"; Astro2020 science white paper*, `http://tinyurl.com/y58hcwql`

[460] Schechter, P. L. et al., 2014, ApJ, 793, no. 2, 96

[461] National Academies of Sciences, E. & Medicine, 2018, *Exoplanet Science Strategy* (Washington, DC: The National Academies Press)

[462] Drake, J. et al., 2019, in *"High-Energy Photon and Particle Effects on Exoplanet Atmospheres and Habitability"; Astro2020 science white paper*, `http://tinyurl.com/yygedrtl`

[463] Owen, J. E. & Jackson, A. P., 2012, MNRAS, 425, no. 4, 2931

[464] Drake, J. et al., 2019, BAAS, 51, no. 3, 113

[465] Brain, D. A. et al., 2016, Journal of Geophysical Research (Planets), 121, no. 12, 2364

[466] Wood, B. E. et al., 2014, ApJ, 781, no. 2, L33

[467] Wood, B. E. et al., 2005, ApJ, 628, L143

[468] Wargelin, B. J. & Drake, J. J., 2002, ApJ, 578, no. 1, 503

[469] Drake, J. J. et al., 2013, ApJ, 764, 170

[470] Segura, A. et al., 2010, Astrobiology, 10, no. 7, 751

[471] Airapetian, V. S. et al., 2016, Nature Geoscience, 9, no. 6, 452

[472] Crosley, M. K. & Osten, R. A., 2018, ApJ, 856, 39

[473] Crosley, M. K. & Osten, R. A., 2018, ApJ, 862, 113

[474] Alvarado-Gómez, J. D. et al., 2019, (Submitted to ApJ Letters)

[475] Argiroffi, C. et al., 2019, Nature Astronomy, 328

[476] Haisch, B. M. et al., 1983, ApJ, 267, 280

[477] Moschou, S.-P. et al., 2017, ApJ, 850, no. 2, 191

[478] Bhardwaj, A., Lisse, C. M. & Dennerl, K., 2014, in T. Spohn, D. Breuer & T. V. Johnson, eds., *Encyclopedia of the Solar System* (Boston: Elsevier), 1019, third ed.

[479] Wargelin, B. J. et al., 2004, ApJ, 607, no. 1, 596

[480] Dennerl, K., 2008, Planet. Space Sci, 56, no. 10, 1414

[481] Elsner, R. F. et al., 2005, JGR: Space Physics, 110, no. A1, A01207

[482] Bhardwaj, A. et al., 2007, JASTP, 69, no. 1, 179

[483] Branduardi-Raymont, G. et al., 2008, JGRA, 113, no. A2, A02202

[484] Dunn, W. R. et al., 2017, Nature Astronomy, 1, no. 11, 758

[485] Gladstone, G. R. et al., 2002, Nature, 415, 1000

[486] Bodewits, D. et al., 2007, A&A, 469, 1183

[487] Bhardwaj, A. et al., 2007, Planet. Space Sci., 55, 1135

[488] Snios, B. et al., 2016, ApJ, 818, no. 2, 199

[489] Jackman, C. M. et al., 2018, JGR: Space Physics, 123, no. 11, 9204

[490] Ness, J.-U., Schmitt, J. H. M. M. & Robrade, J., 2004, A&A, 414, no. 3, L49

[491] Bhardwaj, A. et al., 2005, ApJ, 624, no. 2, L121

[492] Branduardi-Raymont, G. et al., 2010, A&A, 510, A73

[493] Tremblay, G. R. et al., 2018, LPI Contributions, 2100, 3024

[494] Lisse, C. M. et al., 1996, Science, 274, no. 5285, 205

[495] Kharchenko, V. et al., 2003, ApJ, 585, L73

[496] Bodewits, D. et al., 2004, Physica Scripta, 70, no. 6, C17

[497] Snios, B., Lichtman, J. & Kharchenko, V., 2018, ApJ, 852, no. 2, 138

[498] Markevitch, M. et al., 2019, in *"Physics of cosmic plasmas from high angular resolution X-ray imaging of galaxy clusters"; Astro2020 science white paper*, `https://tinyurl.com/y4b44cac`

[499] Caprioli, D. et al., 2019, arXiv e-prints, arXiv:1903.08751

[500] Sanders, J. et al., 2018, Chandra News, 25, 1

[501] Loeb, A., 2002, New Astronomy, 7, no. 6, 279

[502] Sijacki, D. & Springel, V., 2006, MNRAS, 371, 1025

[503] Su, K.-Y. et al., 2017, MNRAS, 471, no. 1, 144

[504] Su, K.-Y. et al., 2019, MNRAS, 487, no. 3, 4393

[505] Hopkins, P. F. et al., 2019, arXiv e-prints, arXiv:1905.04321

[506] Schekochihin, A. A. et al., 2008, Phys. Rev. Lett., 100, no. 8, 081301

[507] Kunz, M. W., Schekochihin, A. A. & Stone, J. M., 2014, Phys. Rev. Lett., 112, no. 20, 205003

[508] Komarov, S. V. et al., 2016, MNRAS, 460, no. 1, 467

[509] Roberg-Clark, G. T. et al., 2018, ApJ, 867, no. 2, 154

[510] ZuHone, J. A., Markevitch, M. & Lee, D., 2011, ApJ, 743, no. 1, 16

[511] ZuHone, J. A. et al., 2013, Astrophys. J., 762, 69

[512] Ichinohe, Y. et al., 2017, MNRAS, 467, no. 3, 3662

[513] Wang, Q. H. S. & Markevitch, M., 2018, ApJ, 868, no. 1, 45

[514] Kraft, R. P. et al., 2017, ApJ, 848, no. 1, 27

[515] Su, Y. et al., 2017, ApJ, 834, no. 1, 74

[516] Schuecker, P. et al., 2004, A&A, 426, 387

[517] Zhuravleva, I. et al., 2015, MNRAS, 450, no. 4, 4184

[518] Wang, Q. H. S., Markevitch, M. & Giacintucci, S., 2016, ApJ, 833, no. 1, 99

[519] Werner, N. et al., 2016, MNRAS, 455, no. 1, 846

[520] Ichinohe, Y. et al., 2019, MNRAS, 483, no. 2, 1744

[521] Fox, D. C. & Loeb, A., 1997, ApJ, 491, no. 2, 459

[522] Markevitch, M. et al., 1996, ApJ, 456, 437

[523] Markevitch, M. & Vikhlinin, A., 2007, Phys. Rep., 443, no. 1, 1

[524] Russell, H. R. et al., 2012, MNRAS, 423, no. 1, 236

[525] Wang, Q. H. S., Giacintucci, S. & Markevitch, M., 2018, ApJ, 856, no. 2, 162

[526] Vink, J. & Laming, J. M., 2003, ApJ, 584, 758

[527] Eriksen, K. A. et al., 2011, ApJ, 728, L28

[528] Laming, J. M., 2015, ApJ, 805, 102

[529] van Weeren, R. J. et al., 2019, Space Sci. Rev., 215, 16

[530] Kaastra, J. S., Bykov, A. M. & Werner, N., 2009, A&A, 503, 373

[531] Brunetti, G. & Lazarian, A., 2007, MNRAS, 378, 245

[532] Brunetti, G. & Lazarian, A., 2011, MNRAS, 410, 127

[533] in *Special Section on the* Lynx *X-Ray Observatory, J. Astron. Telesc. Instrum. Syst., 2019, 5(2)*, all of the papers are open source and online at: `https://tinyurl.com/yxrd6w38`

[534] Weisskopf, M. C. et al., 2000, in J. E. Truemper & B. Aschenbach, eds., *Proc. SPIE*, *Society of Photo-Optical Instrumentation Engineers (SPIE) Conference Series*, vol. 4012, 2–16

[535] Chase, R. C. & van Speybroeck, L. P., 1973, Appl. Opt., 12, 1042

[536] Chandra X-ray Center, Chandra Project Science, MSFC & Chandra IPI Teams, 2018, The Chandra Proposers' Observatory Guide, Version 21.0

[537] Zhang, W. W. et al., 2019, Journal of Astronomical Telescopes, Instruments, and Systems, 5, 021012

[538] Civitani, M. M. et al., 2019, Journal of Astronomical Telescopes, Instruments, and Systems, 5, 021014

[539] Kilaru, K. et al., 2019, Journal of Astronomical Telescopes, Instruments, and Systems, 5, 021010

[540] Bishop, N. et al., 2019, Journal of Astronomical Telescopes, Instruments, and Systems, 5, 021005

[541] DeRoo, C. T. et al., 2018, Journal of Astronomical Telescopes, Instruments, and Systems, 4, 019004

[542] Arenberg, J. W., 2019, Journal of Astronomical Telescopes, Instruments, and Systems, 5, 021016

[543] 2016, Structural Design and Test Factors of Safety for Spaceflight Hardware, https://standards.nasa.gov/standard/nasa/nasa-std-5001

[544] Garmire, G. P. et al., 2003, in J. E. Truemper & H. D. Tananbaum, eds., *Proc. SPIE*, *Society of Photo-Optical Instrumentation Engineers (SPIE) Conference Series*, vol. 4851, 28–44

[545] Turner, M. J. L. et al., 2001, A&A, 365, L27

[546] Strüder, L. et al., 2001, A&A, 365, L18

[547] Koyama, K. et al., 2007, PASJ, 59, 23

[548] Falcone, A. D. et al., 2019, Journal of Astronomical Telescopes, Instruments, and Systems, 5, 021019

[549] Hull, S. V. et al., 2019, Journal of Astronomical Telescopes, Instruments, and Systems, 5, 021018

[550] Bautz, M. W. et al., 2019, Journal of Astronomical Telescopes, Instruments, and Systems, 5, 021015

[551] Kenter, A. et al., 2017, in *Proc. SPIE*, *Society of Photo-Optical Instrumentation Engineers (SPIE) Conference Series*, vol. 10397, 1039703

[552] https://wwwastro.msfc.nasa.gov/spectops/magbroom/

[553] Ferreira, I. et al., 2018, in *Proc. SPIE*, *Society of Photo-Optical Instrumentation Engineers (SPIE) Conference Series*, vol. 10699, 106994A

[554] 2019, Users Guide to the XMM-Newton Science Analysis System, https://tinyurl.com/y2rmag57

[555] Günther, H. M. & Heilmann, R. K., 2019, Journal of Astronomical Telescopes, Instruments, and Systems, 5, 021003

[556] McEntaffer, R. L., 2019, Journal of Astronomical Telescopes, Instruments, and Systems, 5, 021002

[557] Canizares, C. R. et al., 2005, PASP, 117, no. 836, 1144

[558] Paerels, F., 2010, Space Sci. Rev., 157, no. 1-4, 15

[559] Beuermann, K. P., Braeuninger, H. & Truemper, J., 1978, Appl. Opt., 17, no. 15, 2304

[560] Bandler, S. R. et al., 2019, Journal of Astronomical Telescopes, Instruments, and Systems, 5, 021017

[561] Risaliti, G. et al., 2013, Nature, 494, no. 7438, 449

[562] Fabian, A. C. et al., 2017, MNRAS, 467, no. 3, 2566

[563] Nardini, E. et al., 2015, Science, 347, no. 6224, 860

[564] Lansbury, G. B. et al., 2014, ApJ, 785, no. 1, 17

[565] Bauer, F. E. et al., 2015, ApJ, 812, no. 2, 116

[566] Kara, E. et al., 2015, MNRAS, 446, no. 1, 737

[567] Walton, D. J. et al., 2018, ApJ, 856, no. 2, 128

[568] Hitomi Collaboration et al., 2016, Nature, 535, no. 7610, 117

[569] Barret, D. et al., 2016, in *Proc. SPIE*, *Society of Photo-Optical Instrumentation Engineers (SPIE) Conference Series*, vol. 9905, 99052F

[570] Smith, S. J. et al., 2019, Journal of Astronomical Telescopes, Instruments, and Systems, 5, 021008

[571] Irwin, K. D. & Hilton, G. C., 2005, in C. Enss, ed., *Cryogenic Particle Detection*, *Topics in Applied Physics*, vol. 99, 63–150

[572] Mates, J. A. B. et al., 2017, Applied Physics Letters, 111, no. 6, 062601

[573] Bennett, D. A. et al., 2019, Journal of Astronomical Telescopes, Instruments, and Systems, 5, 021007

[574] DiPirro, M. et al., 2019, Journal of Astronomical Telescopes, Instruments, and Systems, 5, 021006

[575] Eckart, M. E. et al., 2019, Journal of Astronomical Telescopes, Instruments, and Systems, 5, 021020

[576] de Vries, C. P. et al., 2018, Journal of Astronomical Telescopes, Instruments, and Systems, 4, 011204

[577] Macculi, C. et al., 2016, in *Proc. SPIE*, *Society of Photo-Optical Instrumentation Engineers (SPIE) Conference Series*, vol. 9905, 99052K

[578] Muhlfelder, B. et al., 2001, Verification of payload on-orbit radiation environment, S0610, https://tinyurl.com/yxqsulmq

[579] Delorme, Y. et al., 2005, in *Sixteenth International Symposium on Space Terahertz Technology*, 444–448

[580] Frunzio, L., Cristiano, R. & Pagano, S., 1998, Japanese Journal of Applied Physics Supplement, 37, no. S2, 40

[581] Barth, J. L., Isaacs, J. C. & Poivey, C., 2000, The Radiation Environment for the Next Generation Space Telescope, https://tinyurl.com/y3wpvq5v

[582] Sakai, K. et al., 2019, Journal of Astronomical Telescopes, Instruments, and Systems, 5, 021013

[583] Farquhar, R. W., 1970, Libration point satellite stationkeeping control, https://tinyurl.com/yybpldjv

[584] Yoon, S., Rosales, J. & Richon, K., 2014, no. 20140008973 in 24th International Symposium on Space Flight Dynamics, https://tinyurl.com/yx947s54

[585] Eckart, M. E. et al., 2018, Journal of Astronomical Telescopes, Instruments, and Systems, 4, 021406

[586] Foster, A. R. et al., 2012, ApJ, 756, no. 2, 128

[587] On-Orbit Satellite Servicing Study Project Report, 2010, https://tinyurl.com/y23o8tym

[588] Cooperative Service Valve Fact Sheet, 2017, https://tinyurl.com/yyynvvbn

[589] Zhang, W. W. et al., 2019, Journal of Astronomical Telescopes, Instruments, and Systems, 5, 021012

[590] Yao, Y. et al., 2019, Journal of Astronomical Telescopes, Instruments, and Systems, 5, 021011

[591] Civitani, M. M. et al., 2019, Journal of Astronomical Telescopes, Instruments, and Systems, 5, 021014

[592] Kilaru, K. et al., 2019, Journal of Astronomical Telescopes, Instruments, and Systems, 5, 021010

[593] Civitani, M. et al., 2018, in *Proc. SPIE*, *Society of Photo-Optical Instrumentation Engineers (SPIE) Conference Series*, vol. 10699, 106990T

[594] Kilaru, K., Kolodziejczak, J. & Atkins, C., 2017, in *Proc. SPIE*, *Society of Photo-Optical Instrumentation Engineers (SPIE) Conference Series*, vol. 10399, 103991F

[595] Civitani, M. M. et al., 2012, in *Proc. SPIE*, *Society of Photo-Optical Instrumentation Engineers (SPIE) Conference Series*, vol. 8443, 84430Q

[596] Murray, S. S. et al., 2008, in *Proc. SPIE*, *Society of Photo-Optical Instrumentation Engineers (SPIE) Conference Series*, vol. 7011, 70111J

[597] Gubarev, M. et al., 2016, in *Proc. SPIE*, *Society of Photo-Optical Instrumentation Engineers (SPIE) Conference Series*, vol. 9905, 99051V

[598] Civitani, M. M. et al., 2017, in *Proc. SPIE*, *Society of Photo-Optical Instrumentation Engineers (SPIE) Conference Series*, vol. 10399, 103990W

[599] Hull, S. V. et al., 2019, Journal of Astronomical Telescopes, Instruments, and Systems, 5, 021018

[600] Kenter, A., Kraft, R. & Gauron, T., 2018, in *Proc. SPIE*, *Society of Photo-Optical Instrumentation Engineers (SPIE) Conference Series*, vol. 10762, 1076209

[601] Bautz, M. W. et al., 2019, Journal of Astronomical Telescopes, Instruments, and Systems, 5, 021015

[602] Heilmann, R. K. et al., 2016, in *Proc. SPIE*, *Society of Photo-Optical Instrumentation Engineers (SPIE) Conference Series*, vol. 9905, 99051X

[603] Heilmann, R. K. et al., 2017, in *Proc. SPIE*, *Society of Photo-Optical Instrumentation Engineers (SPIE) Conference Series*, vol. 10399, 1039914

[604] Heilmann, R. K. et al., 2018, in *Proc. SPIE*, *Society of Photo-Optical Instrumentation Engineers (SPIE) Conference Series*, vol. 10699, 106996D

[605] Heilmann, R. K. et al., 2019, Appl. Opt., 58, no. 5, 1223

[606] Günther, H. M. & Heilmann, R. K., 2019, Journal of Astronomical Telescopes, Instruments, and Systems, 5, 021003

[607] Canizares, C. R., Schattenburg, M. L. & Smith, H. I., 1986, in J. L. Culhane, ed., *Proc. SPIE*, *Society of Photo-Optical Instrumentation Engineers (SPIE) Conference Series*, vol. 597, 253–260

[608] McEntaffer, R. L., 2019, Journal of Astronomical Telescopes, Instruments, and Systems, 5, 021002

[609] Miles, D. M. et al., 2018, ApJ, 869, no. 2, 95

[610] Miles, D. M. et al., 2018, in *Proc. SPIE*, *Society of Photo-Optical Instrumentation Engineers (SPIE) Conference Series*, vol. 10699, 106996K

[611] Donovan, B. D. et al., 2018, in *Proc. SPIE*, *Society of Photo-Optical Instrumentation Engineers (SPIE) Conference Series*, vol. 10699, 106993U

[612] Bandler, S. R. et al., 2019, Journal of Astronomical Telescopes, Instruments, and Systems, 5, 021017

[613] Smith, S. J. et al., 2019, Journal of Low Temperature Physics, submitted, arXiv:1908.02687

[614] Mates, J. A. B. et al., 2017, Applied Physics Letters, 111, no. 6, 062601

[615] Yoon, W. et al., 2018, Journal of Low Temperature Physics, 193, no. 3-4, 258

[616] Bennett, D. A. et al., 2019, Journal of Astronomical Telescopes, Instruments, and Systems, 5, 021007

[617] Jackson, B. D. et al., 2016, in *Proc. SPIE*, *Society of Photo-Optical Instrumentation Engineers (SPIE) Conference Series*, vol. 9905, 99052I

[618] Eckart, M. E. et al., 2019, Journal of Astronomical Telescopes, Instruments, and Systems, 5, 021020

[619] Smith, S. J. et al., 2019, Journal of Astronomical Telescopes, Instruments, and Systems, 5, 021008

[620] Bitten, R. E., Shinn, S. A. & Emmons, D. L., 2019, in *2019 IEEE Aerospace Conference*, 1–13

[621] Arenberg, J. W., 2019, Journal of Astronomical Telescopes, Instruments, and Systems, 5, 021016

[622] Arenberg, J. & Zhang, W., 2019, in *AAS/High Energy Astrophysics Division*, AAS/High Energy Astrophysics Division, 109.45

[623] Prince, A., 2017, ICEAA Professional Development & Training Workshop

[624] 2019, Journal of Astronomical Telescopes, Instruments, and Systems, 5, `https://tinyurl.com/yxrd6w38`

[625] Kelly, E. V., 2009, PMI Global Congress 2009, `https://tinyurl.com/yxjwtlso`

[626] Cole, S. K. et al., 2013, Technology Estimating: A Process to Determine the Cost and Schedule of Space Technology Research and Development, `https://tinyurl.com/yxrcvyxz`

[627] Hogg, D. W., 2001, AJ, 121, no. 2, 1207

[628] Condon, J. J., 1974, ApJ, 188, 279

[629] Lehmer, B. D. et al., 2012, ApJ, 752, no. 1, 46

[630] Bouwens, R. J. et al., 2004, ApJ, 611, no. 1, L1

[631] Lehmer, B. D. et al., 2010, ApJ, 724, no. 1, 559

[632] Mineo, S. et al., 2014, MNRAS, 437, no. 2, 1698

[633] Prestwich, A. H. et al., 2013, ApJ, 769, 92

[634] Basu-Zych, A. R. et al., 2013, ApJ, 774, 152

[635] Douna, V. M. et al., 2015, A&A, 579, A44

[636] Basu-Zych, A. R. et al., 2016, ApJ, 818, 140

[637] Brorby, M. et al., 2016, MNRAS, 457, 4081

[638] Kennicutt, R. C., Jr., 1998, ARA&A, 36, 189

[639] Yukita, M. et al., 2016, ApJ, 824, no. 2, 107

[640] Hickox, R. C. & Markevitch, M., 2007, ApJ, 661, no. 2, L117

[641] von Kienlin, A. et al., 2018, in *Proc. SPIE*, *Society of Photo-Optical Instrumentation Engineers (SPIE) Conference Series*, vol. 10699, 106991I

[642] Snowden, S. L. et al., 1997, ApJ, 485, no. 1, 125

[643] Galeazzi, M. et al., 2007, ApJ, 658, no. 2, 1081

[644] Vikhlinin, A. et al., 1995, ApJ, 451, 542

[645] Freeman, P. E. et al., 2002, ApJS, 138, no. 1, 185

[646] Neyman, J., Pearson, E. S. & Pearson, K., 1931, Phil. Trans. of the Royal Society of London, Series A, 231, 289

[647] Pratt, W. K., 1978, *Digital Image Processing* (Wiley)

[648] Mahony, E. K. et al., 2010, MNRAS, 401, no. 2, 1151

[649] Klypin, A. A., Trujillo-Gomez, S. & Primack, J., 2011, ApJ, 740, no. 2, 102

SCIENCE WORKING GROUP MEMBERS

Working Group co-chairs are listed in ***Bold***

Cycles of Baryons In *&* Out *of* Galaxies

Joel Bregman
Juna Kollmeier
Andrey Kravtsov
Mehmet Alpaslan
Gabriella Alvarez
Camille Avestruz
Akos Bogdan
Massimiliano Bonamente
Lia Corrales
Massimiliano Galeazzi
Oleg Gnedin
Li Jiangtao
Dong-Woo Kim
Ralph Kraft
Fabrizio Nicastro
Susan Nulsen
Benjamin Oppenheimer
Frits Paerels
Scott Randall
Mateusz Ruszkowski
Kosuke Sato
Grant Tremblay
Eugenio Ursino
Lynne Valencic
Alexey Vikhlinin
Norbert Werner
Noriko Yamasaki

First Accretion Light

Niel Brandt
Piero Madau
Daniel Stern
James Aird
Nico Cappelluti
Francesca Civano
Andrea Comastri
Paolo Coppi
Anastasia Fialkov
Francesca Fornasini
Elena Gallo
Mélanie Habouzit
Zoltan Haiman
Philip Kaaret
Demosthenes Kazanas
Ildar Khabibullin
Joseph Lazio
Bin Luo
Mar Mezcua
Takamitsu Miyaji
Dan Schwartz
Ohad Shemmer
Benny Trakhtenbrot
Cristian Vignali
Fabio Vito
Marta Volonteri

Evolution of Structure *&* AGN Populations

Steven Allen
Ryan Hickox
Tesla Jeltema
Daniel Stern
James Aird
Felipe Andrade-Santos
Camille Avestruz
David Ballantyne
Elizabeth Blanton
Rebecca Canning
Chien-Ting Chen
Francesca Civano
Ashkbiz Danehkar
Abraham Falcone
Francesca Fornasini
Elena Gallo
Danielle Gurgew
Demosthenes Kazanas
Michael Koss
Erwin Lau
Adam Mantz
Kyoko Matsushita
Michael McDonald
Beatriz Mingo
Takamitsu Miyaji
Daisuke Nagai
Ming Sun
Benny Trakhtenbrot
Sara Turriziani
Panayiotis Tzanavaris
Stephen Walker
Reinout van Weeren
Cristian Vignali

X-rays *in the* Multiwavelength/Messenger Era

Robert Petre
Randall Smith
Vallia Antoniou
Esra Bulbul
Becky Canning
Chien-Ting Chen
Valerie Connaughton
Ashkbiz Danehkar
Yuichiro Ezoe
Abe Falcone
Federico Fraschetti
Suvi Gezari
Richard Griffiths
Hans Guenther
David Kieda
Albert Kong
Michael Koss
Peter Maksym
Adam Mantz
Herman Marshall
Michael McCollough
Patrick Motl
Frits Paerels
Alberto Sadun
Marcos Santander
Gregory Sivakoff
Francesco Tombesi
Grant Tremblay
Eleonora Troja
Sara Turriziani
Tonia Venters

SCIENCE WORKING GROUP MEMBERS

continued from previous page

Physics *of* Feedback

Megan Donahue
Christopher Reynolds
Nahum Arav
Elizabeth Blanton
Laura Brenneman
Teddy Cheung
Ashkbiz Danehkar
Massimo Gaspari
Oleg Gnedin
Martin Hardcastle
Sebastian Heinz
Julie Hlavacek-Larrondo
Edmund Hodges-Kluck
Chritine Jones
Alvaro Labiano
Sibasish Laha
Peter Maksym
Alex Markowitz
Herman Marshall
Francesco Massaro
Eileen Meyer
Jon Miller
Brian Morsony
Emanuele Nardini
Joey Neilsen
Paul Nulsen
Scott Randall
Mateusz Ruszkowski
Eric Schlegel
Norbert Schulz
Dan Schwartz
Paul Sell
Aneta Siemiginowska
Gregory Sivakoff
Lukasz Stawarz
Douglas Swartz
Makoto Tashiro
Francesco Tombesi
Grant Tremblay
Norbert Werner
Dan Wilkins
Mihoko Yukita
Shuo Zhang
Irina Zhuravleva

Physics *of* High Density Matter *&* Accretion

Feryal Özel
Frits Paerels
Christopher Reynolds
Frederick Baganoff
Slavko Bogdanov
Laura Brenneman
Deepto Chakrabarty
Filippo D'Ammando
Keigo Fukumura
Massimiliano Galeazzi
Javier Garcia
Hans Guenther
Sebastien Guillot
Craig Heinke
Paul Hemphill
Jeroen Homan
Erin Kara
Oleg Kargaltsev
Denis Leahy
Simin Mahmoodifar
Peter Maksym
Herman Marshall
Michael McCollough
Jon Miller
Cole Miller
Patrick Motl
Emanuele Nardini
Joey Neilsen
Eric Perlman
David Pooley
Bettina Posselt
Dimitrios Psaltis
Roger Romani
Norbert Schulz
Gregory Sivakoff
James Steiner
Francesco Tombesi
John Tomsick
Eleonora Troja
Giacomo Vianello
Dan Wilkins
Shuo Zhang
Michael Zingale

Stellar Lifecycles

Laura Lopez
Rachel Osten
Dave Pooley
Andy Ptak
Jeff Andrews
Vallia Antoniou
Frederick Baganoff
Aya Bamba
Arash Bodaghee
Slavko Bogdanov
Daniel Castro
Robin Corbet
Lia Corrales
Federico Fraschetti
Hans Guenther
Kenji Hamaguchi
Craig Heinke
David Huenemoerder
Margarita Karovska
Vinay Kashyap
Albert Kong
Denis Leahy
Maurice Leutenegger
Michael McCollough
Rodolfo Montez
Lidia Oskinova
Thomas Pannuti
Dan Patnaude
Sangwook Park
Paul Plucinsky
Katja Pottschmidt
Samar Safi-Harb
Manami Sasaki
Eric Schlegel
Norbert Schulz
Paul Sell
Gregory Sivakoff
Pat Slane
Douglas Swartz
John Tomsick
Eleonora Troja
Panayiotis Tzanavaris
Maureen van den Berg
Brad Wargelin
Ben Williams
Brian Williams
Scott Wolk
Andreas Zezas

LYNX SCIENCE SUPPORT OFFICE

GRANT **TREMBLAY**
Science Support Office Lead

JOHN **ZuHONE** FRANCESCA **CIVANO**
ERIC **MANDEL** BENJAMIN **OPPENHEIMER** DAN **PATNAUDE**
Center *for* Astrophysics | Harvard *&* Smithsonian

MICHAEL **McDONALD** DAVID **PRINCIPE** HANS MORITZ **GÜNTHER**
MIT Kavli Institute *for* Astrophysics *&* Space Research, Massachusetts Institute *of* Technology

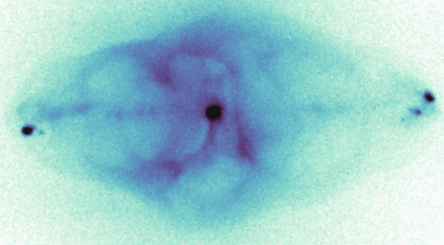

ADDITIONAL CONTRIBUTORS

Tom Alcroft
Julián David Alvarado-Gómez
Marcelo Alvarez
Jonathan Arenberg
Antara Basu–Zych
Roger Brissenden
Akos Bogdan
Slavko Bogdanov
Herve Bourdin
Laura Brenneman
Nancy Brickhouse
Esra Bulbul
Rebecca Canning
Eugene Churazov
Jason Conry
Lia Corrales
Romeel Davé
Larry David
Jeremy Drake
William Dunn
Ian Evans
Clarke Esmerian
Giuseppina Fabbiano
Anastasia Fialkov
Elena Gallo
Julie Hlavacek-Larrondo
Edmund Hodges-Kluck
Una Hwang
Ildar Khabibullin
Sibasish Laha
Martin Laming
Bret Lehmer
Andrew MacFadyen
W. Peter Maksym
Adam Mantz
Maxim Markevitch
Alex Markowitz
Jonathan McDowell
Andrei Mesinger
Joey Neilsen
Paul Nulsen
Salvatore Orlando
Fabio Paccuci
Paul Plucinsky
Katja Poppenhauger
Scott Randall
Arnold Rots
Mateusz Ruszkowski
Evan Schneider
Pat Slane
Bradford Snios
Emanuele Sobacchi
Mattia Sormani
Nicholas Stone
Ming Sun
Yike Tang
Francesco Tombesi
Lynne Valencic
Reinout Van Weeren
Eli Visbal
Fabio Vito
Stephen Walker
Rainer Weinberger
Nastasha Wijers
Belinda Wilkes
Scott Wolk
Andreas Zezas
Irina Zhuravleva

LYNX ENGINEERING SUPPORT TEAM

ALEX **DOMINGUEZ**
Team Lead

RANDY **HOPKINS**
Team Lead

ANDREW **SCHNELL**
Team Lead

MICHAEL **ALLISON** JEFF **APPLE** MIKE **BAYSINGER**
TYRONE **BOSWELL** JENNIFER **BRACKEN** TERESA **BROWN**
TERRY **BROWN** PETE **CAPIZZO** BILL **COOKE**
LEO **FABISINSKI** ALEX **FEW** JAY **GARCIA**
ERIC **GILLIGAN** LEVIN **GUILLERMO** JIM **HOWARD**
J. BRENT **KNIGHT** JOE **MINNOW** EMILY **MITCHELL** JACK **MULQUEEN**
BEN **NEIGHBORS** RACHEL **RIVERA** MITCHELL **RODRIGUEZ**
JUSTIN **ROWE** IAN **SMALL** JAMES **STURM**
ROB **SUGGS** STEVE **SUTHERLIN**

NASA Marshall Space Flight Center | Advanced Concepts Office

Lynx Mirror Assembly Trade Team (LMAT)

Gary Blackwood
Lynn Allen
Jon Arenberg
Charlie Atkinson
Jaya Bajpayee
Chip Barnes
Terri Brandt
David Broadway
Vadim Burwitz
Marta Civitani
Lester Cohen
Casey DeRoo
Daniel Evans
Mark Freeman
Jessica Gaskin
Karen Gelmis
Paul Glenn
Jennifer Gregory
Ryan Hickox
Steve Jordan
Gabe Karparti
Bernard Kelly
Kiran Kilaru
Gary Matthews
Ryan McClelland
Ted Mooney
John Nousek
Feryal Özel
Frits Paerels
Robert Petre
Denise Podolski
Bill Purcell
Paul Reid
Rita Sambruna
Mark Schattenburg
Eric Schwartz
Peter Solly
Daniel Stern
Doug Swartz
Alexey Vikhlinin
Dave Windt
William Zhang

Model-Based Systems Engineering Team

Marc Gethers
Ashleigh Lynch
Elizabeth Patterson
Isabeta Rountree
Dale Thomas

Technology Assessment & Roadmap Team

Robert Bitten
Angie Buckley
Frank Curran
Brett Drake
Linda Herrel
Mark Skinner

Cost & Technical Evaluation Team

Hank Apgar
Patrick Malone

INDUSTRY PARTNERS & REVIEW TEAMS

LOCKHEED MARTIN CORPORATION
Greg Feller, David Frank, Allison Nordt, & Jeff Olson

NORTHROP GRUMMAN CORPORATION
Jonathan Arenberg, Charlie Atkinson, Mike McEachen, & Perry Knollenberg

BALL AEROSPACE & TECHNOLOGIES CORP.
Steve Jordan, Mark Kilpatrick, & Bill Purcell

HARRIS CORPORATION
Keith Havey, Ted Mooney, & Lynn Allen

LUXEL, INC.
Ben Zeiger

HYPRES, INC.
Deepnarayan Gupta

CREARE, INC.
Mark Zagarola

ORBITAL ATK
Mike McEachen

NATIONAL INSTITUTE *for* STANDARDS & TECHNOLOGY
Charles Tarrio

LABORATORY *for* ATMOSPHERIC & SPACE SCIENCES
Andrew Jones

LYNX RED TEAM

CHRYSSA **KOUVELIOTOU**
Chair

JAYA **BAJPAYEE** VADIM **BURWITZ** JAN-WILLEM **DEN HERDER**
DIETER **HARTMANN** GABE **KARPATI** PATRICK **MALONE**
JOHN **NOUSEK** WILT **SANDERS** LEISA **TOWNSLEY** DAVID **WEINBERG**

LYNX STUDY OFFICE COSTING & SCHEDULE

ROBBIE **HOLCOMBE**
Lead

TERESA **BROWN** GREGG **GELMIS** SPENCER **HILL**
ANDY **PRINCE** AMBERLY **STAPLER** VIRGINIA **TICKLES**
NASA Marshall Space Flight Center

LYNX INSTRUMENT & OPTICS WORKING GROUP MEMBERS

Instrument Working Group

Mark Bautz
Ryan Allured
Simon Bandler
Douglas Bennett
Akos Bogdan
Casey DeRoo
Michael DiPirro
Benjamin Donovan
Megan Eckart
Abraham Falcone
Enectali Figueroa-Feliciano
Hans Moritz Günther
Ralf Heilmann
Kent Irwin
Ralph Kraft
Benjamin Mates
Dan McCammon
Randy McEntaffer
Drew Miles
Jeffrey Olson
Kevin Ryu
Kazuhiro Sakai
Dan Schwartz
Stephen Smith
Vyshnavi Suntharalingam
Doug Swartz
Daniel Swetz
James Tutt
Joel Ullom
Wonsik Yoon
Ben Zeiger
Thomas Stevenson
James Chervenak

Optics Working Group

Lester Cohen
Mark Schattenburg
Ryan Allured
Carolyn Atkins
Stefano Basso
Wayne Baumgartner
Michael Biskach
Stephen Bongiorno
Jay Bookbinder
David Broadway
Brandon Chalifoux
Kai-Wing Chan
Marta Civitani
Daneile Cocco
Vincenzo Cotroneo
Jaqueline Davis
Casey DeRoo
Manel Errando
Daniel Evans
Abe Falcone
Charly Feldman
Mark Freeman
Terry Gaetz
Mauro Ghigo
Hans Guenther
Danielle Gurgew
Ralf Heilmann
Mourad Idir
Anders Jakobsen
Diab Jerius
Kiranmayee Kilaru
Jeff Kolodziejczak
Vladimir Kradinov
Ralph Kraft
Herman Marshall
James Mazzarella
Ryan McCelland
Steve O'Dell
Takashi Okajima
Howard Padmore
Giovanni Pareschi
Giancarlo Parodi
Kurt Ponsor
Lisa Poyneer
Brian Ramsey
Paul Reid
Raul Riveros
Oliver Roberts
Timo Saha
Timo Saha
Bianca Salmaso
Dan Schwartz
Eric Schwartz
Peter Solly
Harvey Tananbaum
Susan Trolier-McKinstry
James Tutt
Mel Ulmer
Gabriele Vecchi
David Windt
Youwei Yao
William Zhang

Calibration Working Group

Wayne Baumgartner
Larry David
Jeremy Drake
Megan Eckart
Jessica Gaskin
Dale Graessle
Diab Jerius
Jeff Kegely
Ralph Kraft
Paul Plucinsky
Dan Schwartz
Doug Swartz

LAYOUT, ARTWORK, & BRANDING

Report Manager
Jared Austin

Report Layout
Jennie Mitchell, Jared Austin, Alexey Vikhlinin, Jessica Gaskin, Karen Gelmis, & Grant Tremblay

Technical Writing Support
Jared Austin, Troy Farsoun, Kay Glover, & Eric Mandel

***Lynx* Communications Working Group**
Samantha Johnson, **David Pooley**, Terri Brandt, Megan Donahue, Antonella Fruscione, Jessica Gaskin, Karen Gelmis, Bernard Kelly, Rodolfo Montez, & Grant Tremblay

***Lynx* Branding & Graphic Design Lead**
Grant Tremblay

***Lynx* Wordmark Design**
Tanya Borman-Voit | Design Five Seven

Artwork & Graphic Contributors
Seán Doran, Niko Maisuradze, David O. Miller, Jennie Mitchell, Michael Tremmel, & Evan Schneider

Credits for additional artwork used on our website and promotional materials can be found at
WWW.LYNXOBSERVATORY.ORG / CREDITS

X-RAY OBSERVATORY
LYNX
WWW.HIDDENCOSMOS.ORG

ACKNOWLEDGMENTS & THANKS

Lynx, our vision for a new epoch of discovery, is the joint achievement of a large international community whose expertise spans the disciplines of physics, astrophysics, optics, and aerospace engineering. This concept study has involved thousands of hours of community effort to provide scientific insight and engineering design solutions that exceed the most rigorous standards.

Lynx is possible only because NASA continues to encourage bold dreams, assiduously planning for discoveries that will be made by future generations. *Lynx* is one of four Large Mission Concept Studies funded by NASA for the 2020 Decadal Survey. The *Lynx* Team appreciates the opportunity afforded by NASA to design a reference mission concept for a New Great Observatory, alongside our friends and colleagues on the *LUVOIR*, *HabEx*, and *Origins Space Telescope* teams.

The history of NASA astrophysics has shown that Large Missions become something more than a pursuit of important but defined science goals: they become discovery platforms for the questions we have not yet thought to ask. To that end, we are honored to present our vision of a revolutionary X-ray observatory that will accelerate the expansion of discovery.


WWW.LYNXOBSERVATORY.ORG